In-Situ Energy Performance Analysis of A Hybrid-Fuel Heating System in A Net-Zero Ready Duplex

by

Wanrui Qu

A thesis submitted in partial fulfillment of the requirements for the degree of

Master of Science

in

Civil (Cross-disciplinary)

Department of Civil and Environmental Engineering
University of Alberta

ABSTRACT

The growing global population and increase in energy usage have led to a rise in greenhouse gas (GHG) emissions. The residential sector in Canada accounts for 17% of total secondary energy consumption and 14% of GHG emissions. To reduce energy consumption, operational costs, and GHG emissions, there is a need to promote the use of renewable energy and energy-efficient heating systems. One potential solution is a hybrid-fuel space and domestic hot water heating system that combines a conventional air-source heat pump (ASHP) with a natural-gas tankless water heater (TWH). This system can operate alternately between the ASHP and the TWH or use both based on system efficiency and time-sensitive energy cost, offering benefits such as a reduction in peak electric power demand on the grid and improved resilience during power outages. While laboratory experiments in existing literature have shown the advantages of this system, there is a lack of in-situ performance evaluations. Moreover, software tools for energy performance of buildings and their systems such as HOT2000 rely on default software values, such as system operation schedule. As a result, the prediction may not reflect in-situ performance and has not been reported in literature. This study presents an analysis of the in-situ energy performance of a duplex and their hybrid-energy heating systems, covering building energy consumption assessment, system space heating hourly output, lessons learned about building operations, and heating performance of the system. The study proposes an economical control strategy based on in-situ data or manufacturers specifications. Using the ANN model, the study proposes an approach to compare the energy performance between in-situ results and HOT2000 simulations. The life-cycle costs and energy performance of the hybrid energy heating system with other conventional heating systems are also compared. The study presents a comprehensive study of a hybrid-energy heating system and the results show potential for improvement in the system's energy efficiency.

PREFACE

The design and implementation of the monitoring system in Chapter 3 was conducted by Dr. Yuxiang Chen, the rest of the thesis is an original work by Wanrui Qu.

A journal paper based on this thesis will be submitted to journal Sustainability (ISSN 2071-1050, IF 3.889) Special issue “Advances in Thermal Performance and Energy Efficiency of Buildings in Various Regions.

ACKNOWLEDGMENTS

I would like to express my deepest gratitude to the following individuals and groups for their invaluable contributions and support throughout the completion of this thesis.

First and foremost, I would like to express my sincere appreciation to my supervisor, Dr. Yuxiang Chen, for his guidance, support, continuous patience and encouragement throughout my graduate studies at the University of Alberta. Thanks Dr. Chen for giving me this opportunity to join the field of building engineering. His insightful feedback and enlightenment not only inspired the direction of my academic life, but also widened my experience and knowledge.

I would also like to thank the members of my thesis committee for their valuable feedback and thoughtful suggestions for improving this work.

I extend my appreciation to the Landmarks Homes who provide research filed, resources, and financial support for this work, without their sponsor, this project cannot be possible. Thanks Dr. Haitao Yu from the Landmarks Homes, his participation and cooperation have enriched the finding and strengthened the validity of this thesis.

I would like to thank my colleagues in our research group: Alexander Jordan, Bowen Yang, Charlie Shields, Marzieh Mohammadi, Maysoun Ismaiel, Mohammad Rezvanpour, Vahid Zamani, Xiao Han, for their guidance and suggestions.

Lasty, I would like to express my thank to my family and friends. It is impossible for me to finish my graduate study without the supports from my parents. I would like to thank my boyfriend Xiaoyu Liu, who always support me and never ceased to back me up. I would also like to thank my friends Weijia Gao and Yifan Bian, and their cat Van Gogh, who always provide emotional support throughout my graduate studies.

TABLE OF CONTENTS

LIST OF TABLES

LIST OF FIGURES

CHAPTER 1 INTRODUCTION

1.1 Background

As the global population grows and energy usage increases, the consumption of fossil fuels has led to a corresponding increase in greenhouse gas (GHG) emissions. This has contributed to both the energy crisis and global warming, prompting researchers to explore alternative energy sources. In Canada, the residential sector consumes approximately 17% of the country's total secondary energy consumption, followed closely by the industrial and transportation sectors. Additionally, the residential sector accounts for 14% of GHG emissions (Natural Resources Canada, 2016), with household water and space heating representing a significant portion of total housing energy consumption (Natural Resources Canada, 2017b). In order to conserve energy, reduce utility costs, and curb GHG emissions, it is essential to promote the use of clean energy (e.g., electricity produced from renewable sources) and energy-efficient heating systems.

Conventional electric heat pumps are widely used due to their energy efficiency, but their performance can be adversely affected by low ambient temperatures. A hybrid energy source system that incorporates an air-source heat pump (ASHP) and a natural gas boiler is a potential solution for increasing the efficiency of heating systems in cold climates. This system can provide space and water heating and alternate its operation between the ASHP (electricity) and the boiler (natural gas) based on system efficiency and energy cost considerations. The benefits of this hybrid energy source system include: 1. The ability to install a smaller and more cost-effective heat pump due to the gas boiler's ability to handle cold peaks. 2. A reduction in peak demand on the grid compared to heat pump-only installations. 3. Improved resilience over heat pump-only systems during power outages, as the gas boiler can supply heat with only fan power if the home is equipped

with a small battery backup. 4. Easy retrofitting in conjunction with existing natural gas furnace or boiler systems.

While laboratory experiments and simulations have demonstrated the advantages of a hybrid heat pump and natural gas boiler system (Klein et al., 2014; G. Li, 2018; G. Li & Du, 2018; Park et al., 2014), there is a lack of in-situ performance results and lessons learned from the implementation of this system in cold climate residential buildings. Therefore, intentional study of such systems and building energy performance is necessary to bridge the gap between simulation results and actual monitored energy performance. Predicting building energy performance is essential to improve energy efficiency and reduce environmental impact. However, predicting building energy performance can be difficult due to the numerous factors that can affect energy consumption.

Several approaches have been proposed to predict building energy performance, which can be broadly classified into three categories: engineering methods that use thermal dynamic functions and specialized software such as EnergyPlus, statistical methods that apply regression models to correlate energy consumption with various factors, and artificial intelligence methods such as artificial neural networks (ANN) or support vector machines (SVM) (Zhao & Magoulès, 2012).

Software tools are among the most commonly used methods for building energy prediction. In Canada, HOT2000 is a popular energy simulation modeling software that has been extensively used and developed by Natural Resources Canada (Government of Canada, 2021). However, the use of HOT2000 for energy prediction requires numerous inputs, and the calculations may rely on default software values, such as climate conditions and system operation methods. As a result, the simulation results may be relatively imprecise and incomparable with the monitored results. Therefore, it is necessary to investigate methodologies for precisely comparing software-modeled

results with monitoring results. This investigation can lead to future improvements of the default values used in the software and enhance the accuracy of the building energy prediction.

1.2 Project Description

The hybrid energy heating system under study has been installed in both units of a residential duplex house situated in Edmonton, Canada. This duplex house is designed to be energy-efficient and net-zero ready. The occupied left unit of the duplex house has a main floor area of 2011 sq ft, while the right unit of the duplex house serves as a show house and has a main floor area of 1898 sq ft. The floor plan of the duplex house can be found in Appendix 1 Floor Plans of the Project House.

The hybrid heating system is composed of an electric air-source heat pump and a natural gas tankless water heater (TWH), as shown in Figure 1. This system provides both space heating and domestic hot water for users. The air handling unit (AHU) receives return air from the house, which is heated by either the heat pump or the natural gas TWH. The heat pump has a heating capacity of 11.2 kW, while the TWH has 32.8 kW of space heating capacity. The system was designed to ensure that both the heat pump and TWH can independently meet the space heating demands of the house. Further details about the specifications of the AHU, heat pump, and TWH are provided in Appendix 2 Specifications of the Hybrid Energy Heating System.

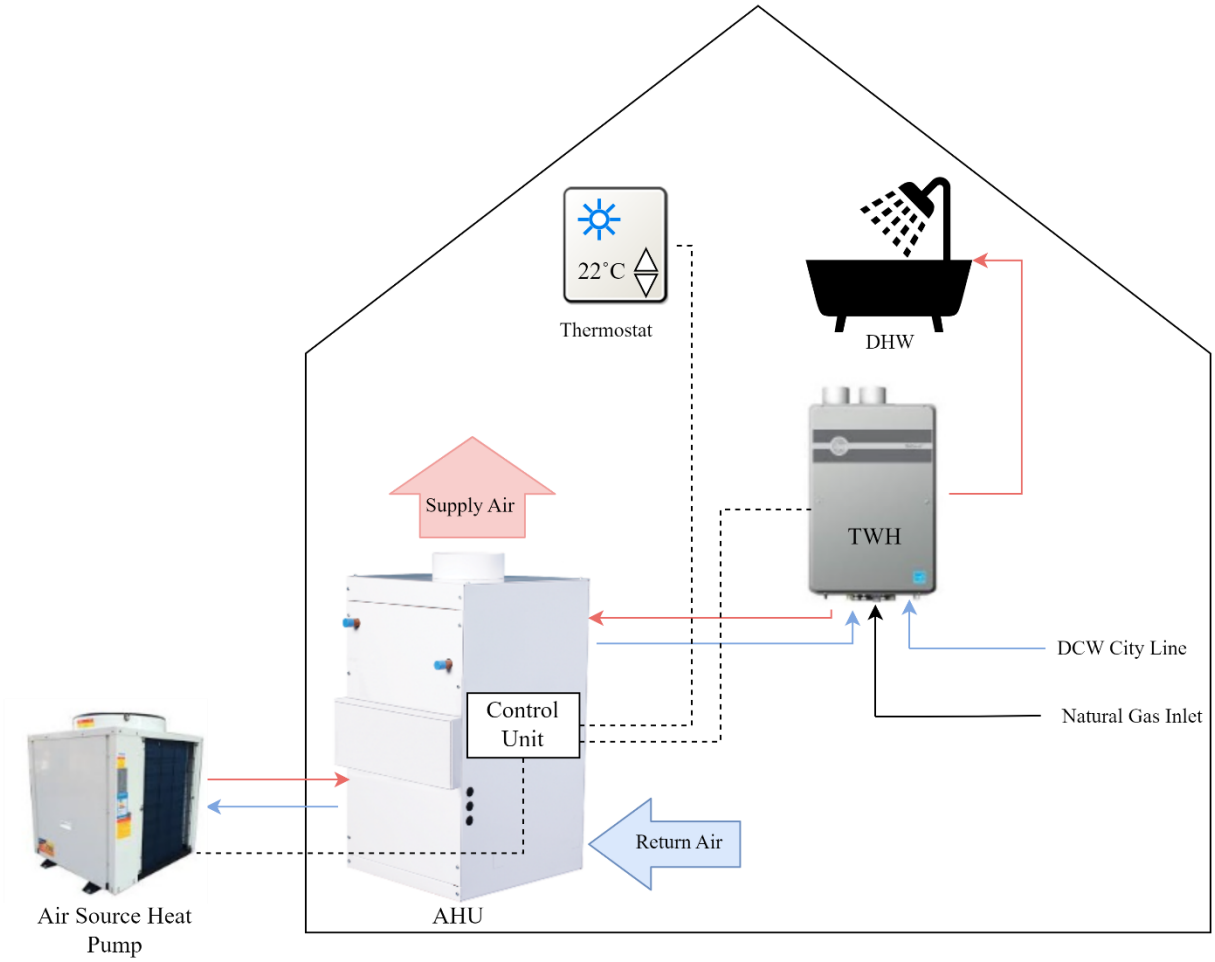

Figure 1. Schematics of the hybrid energy heating system.

The current control strategy of the heating system employs a time delay mechanism to regulate the operation of the heat pump and TWH. Specifically, the system initiates the heat pump for space heating. If the target temperature is not achieved within seven minutes, the system infers that the coefficient of performance (COP) of the heat pump is insufficient and shifts to the TWH to enhance the overall efficiency of the system.

The average wintertime ambient temperature in Edmonton, where the residence is located, is approximately -14 degrees Celsius. The benefits of using a hybrid energy electric heat pump and natural gas TWH heating system in cold climates have been demonstrated in various literature

sources, and will be explored in detail in CHAPTER 2. In addition to the enhanced heating energy efficiency, when the heating efficiency of the electric heat pump and natural gas TWH are equivalent, the cost of operating the TWH for space heating is significantly lower than that of the heat pump, which is powered by electricity. Thus, the benefits of this hybrid energy heating system motivated the collaborative builder to integrate the system into real residential buildings, and attracted researchers to initiate this project.

1.3 Research Objective

The aim of this study is to evaluate the in-situ performance of a hybrid energy heating system, while identifying any practical challenges that may compromise its performance, and to determine the differences between actual performance and current energy modelling results. Additionally, compare the performance and cost of the hybrid energy system with other residential energy systems.

To achieve these aims, the study has the following objectives:

1. To analyze the energy performance of the hybrid heating system and the duplex house.
2. To propose an economically efficient control strategy for the hybrid heating system.
3. To compare hybrid system and building energy performance based on HOT2000 simulation with results predicted by ANN.
4. To compare the monthly and life cycle energy and cost of the hybrid energy system with other residential energy systems via HOT2000 modelling.

This study will provide valuable insights into the in-situ performance of hybrid energy heating systems, as well as contribute to the improvement of energy modelling results.

1.4 Thesis Organization

The upcoming chapters of this thesis are structured as follows: Chapter 2 provides a review of the need for renewable energy heating systems, current technologies for hybrid energy source heating systems, building energy modeling, and research gaps in existing literature. Chapter 3 presents the building energy consumption assessment, including an analysis of monthly energy consumption, lessons learned, and the heating performance of the hybrid energy heating system. Chapter 4 develops an ANN model to predict the energy performance of the hybrid energy heating system under HOT2000 default weather conditions and compares the predicted performance with HOT2000 energy modeling results. Additionally, a comparison of monthly energy and life cycle cost analysis between different heating systems will be conducted. Finally, Chapter 5 summarizes the research findings, contributions, and outlines future study opportunities.

CHAPTER 2 LITERATURE REVIEW

This chapter provides an overview of the current state of renewable energy in residential heating and presents research findings on various renewable energy-based heating systems. Additionally, this chapter reviews methods for predicting building energy consumption and summarizes the challenges and research gaps identified in existing literature.

2.1 Situation of Renewable Energy and Residential Heating Energy

In recent years, the two major global drivers for increased adoption of clean energy and electrification have been reducing greenhouse gas (GHG) emissions and saving fossil fuel storage. The combustion of fossil fuels for heating or transportation produces GHG emission and air pollutants. Electrifying these sectors with clean energy can help to mitigate air pollution and reduce reliance on fossil fuels. Clean energy are commonly referred as renewable energy that originates from natural processes and is replenished at a rate that is equal to or greater than its consumption (U.S EIA, 2022). Renewable energy sources include biomass, liquid biofuels, as well as energy generated from the sun, wind, geothermal, hydropower, and ocean resources (Natural Resources Canada, 2017a). As of 2020, renewable energy sources contributed 15% to the global primary energy consumption source, with the U.S. EIA (2021) predicting that this share would grow to 27% by 2050. Due to its large landmass and diverse geology, Canada is well positioned to play an important role in renewable energy production. In fact, Canada is a global leader in generating and utilizing energy from renewable resources, with 18.9% of its total primary energy supply coming from renewable sources. (Natural Resources Canada, 2017a). Hydroelectricity is the most significant source of renewable energy in Canada, accounting for 59.3% of the country's electricity generation (Natural Resources Canada, 2017a).

However, despite the increasing trend of renewable energy use, there is still a significant disparity between the production and consumption of renewable energy due to the increase in global energy demand. In Canada, the residential sector accounts for approximately 17% of the total secondary energy consumption and 14% of greenhouse gas emissions (Natural Resources Canada, 2016). Due to a growth in the number of households, appliances/electronics, living space, and air conditioning use (Natural Resources Canada, 2017b). Household water and space heating account for a large portion of the total residential energy consumption due to Canada's cold environment. As shown in Figure 2, as of 2017, residential water heating and space heating accounted for 19.3% and 61.6% of the total energy use, respectively, while space cooling, lighting, and other appliances accounted for the remaining 19.1% (Natural Resources Canada, 2017b). Therefore, the residential sector has significant potential for reducing secondary energy consumption and greenhouse gas emissions by implementing electrified and energy-efficient heating systems.

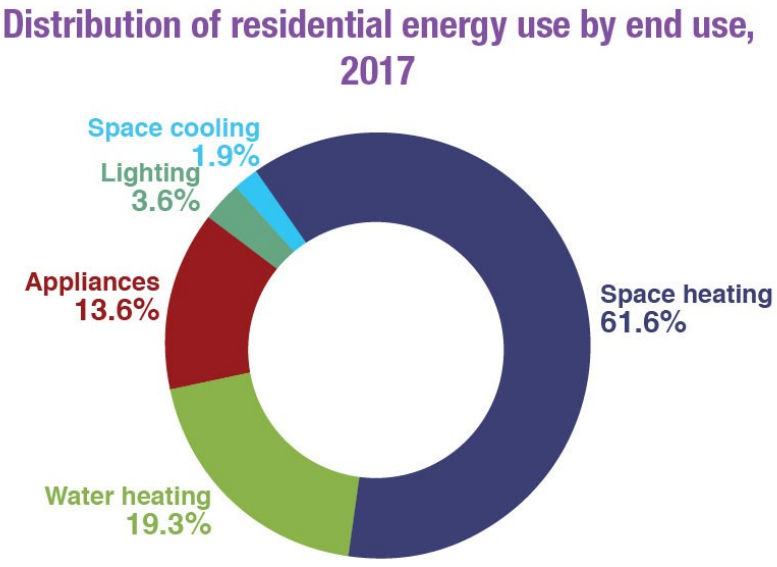

Figure 2. Distribution of residential energy use by end-use (Natural Resources Canada, 2017b).

2.2 Existing Hybrid Energy Source Heating Systems

Conventional electric heat pumps can provide energy-efficient space and domestic hot water heating; however, they exhibit lower energy efficiency in wintertime due to low outdoor temperatures. To address this issue, extensive research has been conducted on the hybrid energy source heating systems that integrate renewable energy source with the conventional heat pump to enhance the efficiency and economic benefits of the heat pump system and also reduce the GHG emission. This section reviews various hybrid heating systems, including solar energy combined heat pumps, wind power integrated heat pumps, and heat pump and natural gas boiler systems. Based on this review, suitable heating systems for Alberta, Canada are proposed.

2.2.1 Solar Energy Combined Heat Pump

The utilization of solar energy combined heat pump can be broadly categorized into two types: direct expansion solar assisted heat pump (DX-SAHP) and indirect expansion solar assisted heat pumps (IDX-SAHP) (Chen & Yu, 2017). An example of DX-SAHP system can be found in Figure 3, where the solar collector functions as the evaporator for the heat pump unit. The system directly acquires the solar heat source, which can be disadvantageous during periods of insufficient solar radiation. In such cases, the DX-SAHP may not be able to collect enough heat from the air resource to supplement the solar energy, leading to a significant reduction in system performance (Facão & Carvalho, 2014).

Numerous studies have been conducted to analyze the thermodynamic performance of direct expansion solar-assisted heat pumps (DX-SAHP). Y. W. Li et al. (2007) evaluated the performance of a DX-SAHP water heater using experimental setups and found that its coefficient of performance (COP) ranges between 3.11 to 6.11, depending on ambient temperature, solar

radiation intensity, and water temperature. Similarly, Huang and Lee (2007) developed a simple linear correlation to evaluate the performance of different solar-assisted heat pump water heaters. Kong et al. (2011) analyzed the performance of DX-SAHPWH using simulation models based on a lumped and distributed parameter approach, and the results were consistent with the experimental measurements. Sun et al. (2015) conducted a numerical study on DX-SAHPWH's performance under different conditions and found that the system's COP was significantly influenced by solar radiation intensity and ambient temperature. Although the DX-SAHP had a higher COP than the conventional air source heat pump water heater (ASHPWH) in clear winter days, its performance was inferior during the night due to the solar collector/evaporator's low convectional heat exchanging performance and radiative heat loss to the night sky. Chyng et al. (2003) simulated the performance of a similar DX-SAHP system using a quasi-steady state operation of all components and determined that the daily total COP ranges from 1.7 to 2.5 year-round for the system, depending on season and weather conditions. To effectively utilize both solar and air energy, Chen and Yu (2017) proposed a new DX-SEHPC cycle for water heating. The DX-SEHPC system operates in two modes, alternating between solar and air energy depending on solar radiation conditions, consistently maintaining high performance under all operational circumstances, and increasing the COP by up to an average of 13.78% and 25.07% under the given operation circumstances while greatly reducing the amount of energy used for water heating. Similarly, Huang et al. (2005) combined the DX-SAHP system with a solar heat pipe collector and found that the COP of the combination of hybrid mode operation could achieve 3.32 and increase 28.7% compared to conventional heat pump operation. Deng and Yu (2016) improved the COP by 14.1% by adding an additional air source evaporator in parallel to the conventional DX-SAHPWH, thereby reducing the heating time at low solar radiation conditions. Zhu et al. (2014) proposed a

dual nozzle ejector-enhanced cycle for the DX-SAHP system, which theoretically enhanced the heating COP and volumetric heating capacity. D. Zhang et al. (2014) studied the system performance of DX-SAHP under various structural parameters and recommended using copper as the material for manufacturing solar collectors to increase the thermodynamic performance of DX-SAHP due to its higher thermal conductivity. Research also proposed that corresponding refrigerant could be employed under certain outdoor temperature to optimize the performance of the DX-SAHP, they found that R744 had a better increasing order of COP when the ambient temperature was below 13 ˚C, while R134a showed a better increasing order of COP when the ambient temperature was above 13 ˚C (S. Li et al., 2015).

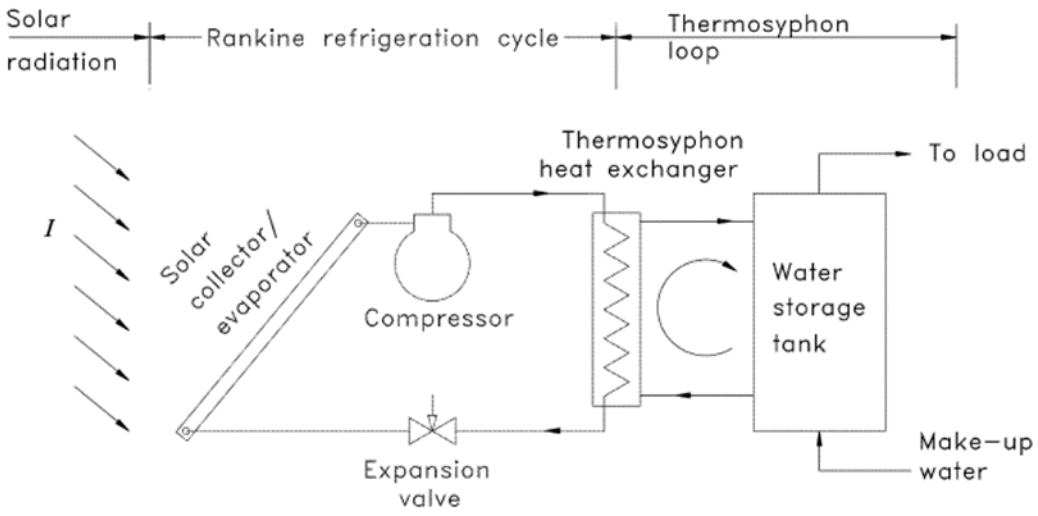

Figure 3. Schematic diagram of a DX-SAHP (Chyng et al., 2003).

According to Yang et al. (2021), the IDX-SAHP can be categorized into two types: serial and dual-source systems. In a serial system, solar radiation heats the water flowing through the solar collector, which is then stored in a water tank. The heated water is then transferred to the heat pump evaporator as the sole source of heat for the heat pump. On the other hand, in a dual-source system, the IDX-SAHP uses either ambient air or solar energy, whichever is more efficient, as the

heat source. Heat pumps in dual-source systems can operate independently of solar energy sources. Compared to the DX-SAHP, the IDX-SAHP can store solar radiation energy into heat storage, thereby enhancing system performance during nighttime. However, the configuration of the IDX-SAHP system is more complex than that of the DX-SAHP system.

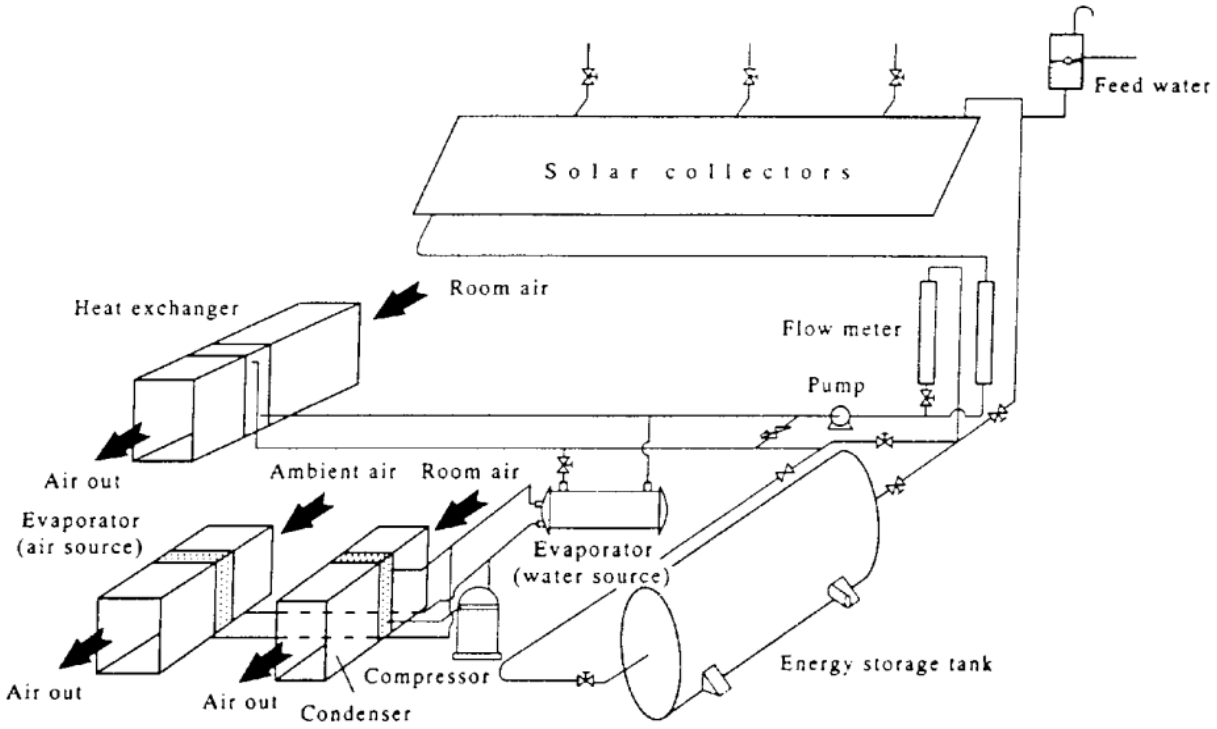

Figure 4. Schematic diagram of a serial IDX-SAHP (Kaygusuz, 1999a).

Figure 4 illustrates a serial IDX-SAHP system, which has been shown to outperform conventional heat pumps in terms of energy efficiency and cost-effectiveness in a simulation study by Abou-Ziyan et al. (1997). Experimental testing in a relatively cold climate in Turkey demonstrated that the low-temperature thermal requirements of a heat pump make it an excellent match for low-temperature solar energy. The system achieved an average COP of 3.8 for the heat pump and 2.9 for the whole system, while meeting residential heating demand (Bakirci & Yuksel, 2011). Banister and Collins (2015) proposed a dual-tank serial IDX-SAHP with multiple modes

of operation to minimize electricity consumption. Their simulation results indicated that the proposed system provides significant energy and cost savings compared to traditional solar domestic hot water and standard electric domestic hot water systems. The performance of the serial IDX-SAHP is highly dependent on the number of solar collectors, as demonstrated in a simulation study by Kaygusuz (1999b), where increasing the number of collectors from 10 to 20 resulted in a 37% increase in the maximum COP, but a 65% increase in investment. In a study conducted by Treichel and Cruickshank (2021b), the energy performance of heat pump water heaters and IDX-SAHP water heaters was compared across different climate conditions in Canada and the United States using an empirical model. The SAHP water heater was found to decrease the space heating load by 2% in the climate zone of Alberta. Treichel and Cruickshank (2021a) also analyzed the economic feasibility of the IDX-SAHP under the same climate conditions and found that heat pump water heaters were typically more feasible than SAHP water heaters, except in locations with high electricity rates or long heating seasons.

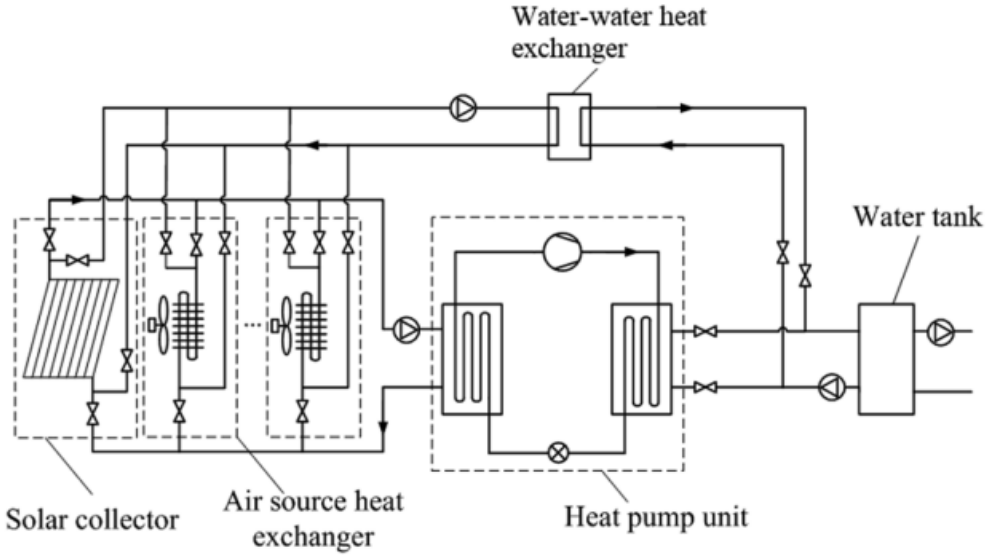

Figure 5. Schematic diagram of a dual-source IDX-SAHP(Ran et al., 2020).

The schematic diagram of a dual-source IDX-SAHP system, which can utilize both a solar collector and air source heat exchanger as heating sources, is presented in Figure 5. The parallel configuration of the solar collector and ASHP enables the system to operate in different modes, including solar only, solar and air dual-source, and air source only, depending on the working conditions. C. Zhang et al. (2011) conducted a mathematical simulation study on the optimal operation mode of the dual-source IDX-SAHP, suggesting that the solar-air dual-source mode should be prioritized when heating capacity is the primary concern, while the solar-only mode should be preferred when the heating capacity decreases. Ran et al. (2020) evaluated the system's performance when solar intensity is insufficient and found that the solar-air dual-source mode can still produce a considerable amount of heat (about 22%-15%, depending on the climate location) and effectively utilize weak solar radiation. Liu et al. (2016) conducted an experimental study on the three working modes and found that during low ambient temperature conditions (-15 ˚C), the solar and air dual-source mode increased heat capacity and COP by 62% and 59%, respectively, compared to the air-only mode. Moreover, when the temperature difference of combined heat transfer was 5 ˚C, the solar and air dual-source mode increased heat capacity and COP by 51% and 49%, respectively, compared to the air source only mode. Youssef et al. (2017) designed a new dual-source IDX-SAHP system that integrates a phase change material storage heat exchanger tank to improve system performance. They evaluated the system performance under different weather conditions and found that the PCM tank could increase the average COP of the IDX-SAHP system by 6.1% and 14.0% on sunny and cloudy days, respectively, compared to systems without PCM tank integration. In terms of GHG emissions, da Cunha and Eames (2018) developed a numerical model to assess the replacement of conventional gas fire boilers with a dual-source

IDX-SAHP system, predicting a reduction in yearly CO2 emissions by an average of 58% when heat pump operation is offset from peak electrical demand periods.

2.2.2 Wind Power Integrated Heat Pump Systems

A wind power integrated heat pump system is a hybrid heat pump system that combines wind turbines and a heat pump to reduce the amount of energy required from the grid and lower energy costs. However, the intermittent nature of wind energy can lead to significant thermal discomfort (H. Li et al., 2018), and thus additional energy sources are needed to fulfill the heat demand of the building. An example of such a system is presented in Figure 6, proposed by Q.-Y. Li et al. (2013) and implemented on a 2-storey building in Beijing, China. The wind power system provides power to the heat pumps, solar thermal system, air source heat pump for domestic hot water heating, and a water source heat pump for room heating and cooling. The system's exergy efficiency increases significantly when the wind speed is high enough to generate power for domestic applications, and the wind power can provide about 7.6% of the annual power requirement. Ozgener (2010) investigated solar-assisted geothermal heat pump and small wind turbine systems and concluded that the studied system can be economically preferable to conventional space heating systems used in agricultural and residential building heating applications in regions with good wind resources. Using an appropriate control strategy can further improve the energy and cost savings of the wind power integrated heat pump system. Sichilalu et al. (2016) developed an optimal control model of a wind and solar-powered heat pump water heater based on time-of-use electricity tariffs, and the results yielded a maximum energy saving of 85.67% and the possibility of achieving a net zero-energy building.

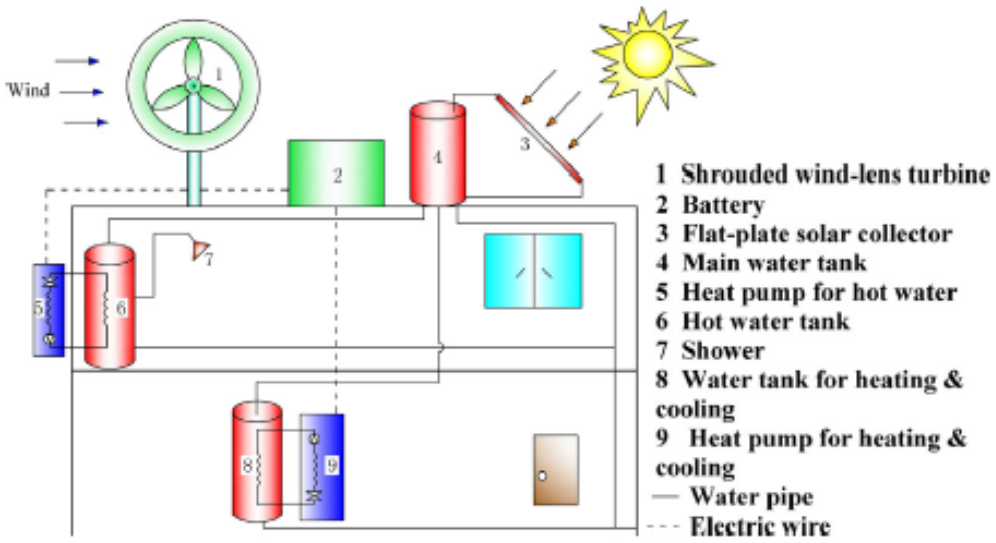

Figure 6. Schematic of a wind solar hybrid heat pump system (Q.-Y. Li et al., 2013).

2.2.3 Heat Pump and Natural Gas Boiler Systems

The hybrid heating system, composed of a heat pump and a natural gas boiler, utilizes the gas boiler as an auxiliary heating source to meet the peak heating demand. The system operates either independently or in conjunction with the shared water line, as illustrated in Figure 7, the energy savings achieved by this system heavily depend on the method of operation and the outdoor temperature. Compared to conventional water heaters, the system's efficiency is 2% to 30% higher, resulting in an annual cost savings of 8.9% in the United States. In regions with lower electricity and gas costs, this system has the potential to generate even greater savings (Park et al., 2014).

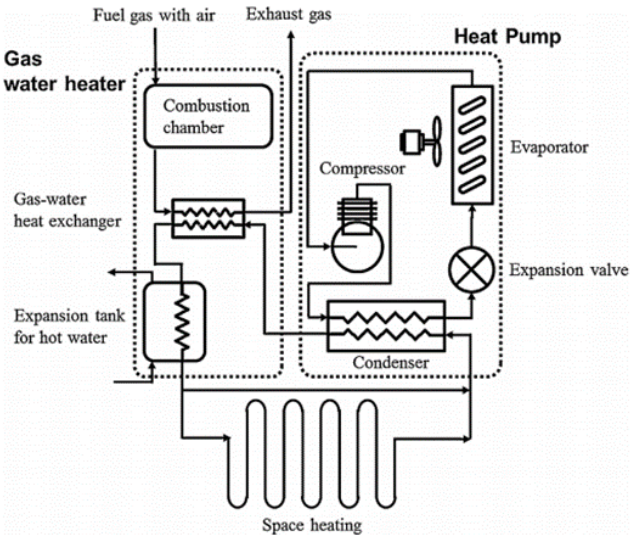

Figure 7. The schematic diagram of the heat pump-gas fired water heater hybrid system (Park et al., 2014).

Numerous studies have demonstrated the advantages of using a hybrid heat pump and natural gas heating system for achieving energy and cost savings. F. Li et al. (2013) developed a model for the hybrid gas boilers-centrifugal heat pumps heating system, suggesting a constant water flow rate in the system, and found that the hybrid heating system consumes much less energy than the conventional coal-fired boiler heating system and has significant energy-saving potential. Klein et al. (2014) conducted research on hybrid heat pump systems comprising an electrically driven air-to-water compression heat pump and a condensing gas boiler in full-year dynamic numerical simulations, resulting in considerable primary energy savings (12%-26%) compared to conventional boiler systems. Wang et, al. (2020) concluded that the hybrid gas boiler and electric heating system provided a more economical heating solution for smart homes, leading to operating energy cost savings of 22.6% and 21.9% compared to pure electricity and pure gas solutions, respectively. G. Li and Du (2018) conducted an experiment on a heat pump gas water heater and space heating hybrid system under two control strategies with different operation modes, resulting

in energy cost savings of about 20% to 65% compared to the gas water heater from -5 ˚C to 20 ˚C ambient temperatures, and hourly energy cost savings of about 6% to 70% compared to gas heaters from -15 ˚C to 20 ˚C ambient temperature in space heating applications. G. Li (2018) proposed a parallel loop configuration for the hybrid heating system as a new economic-based control strategy that can yield a 10% to 60% system operating economic benefits for -12 ˚C to 20 ˚C ambient temperatures. He also suggested that raising water flow rates could increase system efficiency and that the fuel price ratio could strongly affect the saving potential.

2.2.4 Suitable Heating System for Cold Climate Regions

Three different renewable energy-integrated heat pump systems have been evaluated and their respective advantages and disadvantages have been discussed. Research has demonstrated that all three systems have the potential to achieve substantial energy savings and reductions in GHG emissions.

The solar-assisted heat pump (SAHP) uses solar thermal energy to preheat the working fluid in the heat pump, which enhances the overall system efficiency. Additionally, the dual-source IDX-SAHP has shown promising results for cold climates. However, the SAHP system relies heavily on the availability of sunlight, and in Alberta's high latitude location, the average solar power output decreases by 20% to 50% during winter, resulting in insufficient solar energy (Solar Eenergy Maps Canada, 2020).

The wind power-integrated heat pump system utilizes wind power to generate electricity for the heat pump, thus reducing energy costs during peak demand. However, the main issue with this system is the requirement of a suitable location with adequate wind to generate electricity. The wind energy capacity in Alberta is relatively low (Wind Energy in Canada, 2019), and the

minimum energy savings may result in a longer payback period, which is not economically efficient.

The heat pump and natural gas boiler system use natural gas as a backup heating source when the ambient temperature drops too low for the heat pump to operate effectively, ensuring the heating system's efficiency. Natural gas is a relatively inexpensive and widely available energy source, and it is the most commonly used energy source for residential space and water heating in Canada. Natural gas shared for over half (55.0%) of the energy used for space heating, followed by electricity (27.2%) (Natural Resources Canada, 2019a). Similarly, most of the Canadian household use natural gas (69.7%) and electricity (26.1%) for domestic hot water heating (Natural Resources Canada, 2019b). Therefore, the heat pump and natural gas boiler system is an easy retrofit with existing heating systems, making it an ideal choice for Alberta to increase heating efficiency while maintaining reliability.

In summary, the hybrid heat pump and natural gas boiler system is the most suitable choice for heating systems in Alberta as it offers increased efficiency and reliability while utilizing readily available and relatively inexpensive energy sources.

2.3 Building Energy Consumption Prediction

The enhancement of building energy efficiency is contingent on the precise forecasting of building energy usage. Predicting the energy consumption of a building is a complex task as it is impacted by multiple factors including the characteristics of the building envelope, climate conditions, occupancy schedule, and mechanical systems. To address this issue, various methods have been developed to predict building energy consumption, which can be categorized into three main groups: engineering methods, statistical methods, and artificial intelligence methods (Ahmad

et al., 2014). This section provides an overview of the applications, advantages, and limitations of these methods.

2.3.1 Engineering Methods

Engineering methods are used to analyze building energy performance by employing thermal dynamic functions. These analyses can be complex and time-consuming and are usually conducted through building energy simulation software. In Canada, commonly used simulation software includes EnergyPlus, HOT2000, and Can-Quest. While these software can provide accurate results, they require detailed input of building information such as building envelope details, climate conditions, mechanical system information, and occupancy schedules (Al-Homoud, 2001). However, some of this information may be unavailable during the design phase, which can lead to inaccurate results.

Numerical modeling techniques, such as the finite element method and resistor-capacitor network (RC) model, are widely used by researchers for energy demand estimation. Deru et al. (2002) developed a three-dimensional finite-element heat-transfer computer program to investigate ground-coupled heat transfer from buildings, which provided improved analysis of the ground-coupled heat transfer process. De Rosa et al. (2019) presented an iterative methodology to reduce the complexity of building simulation models while identifying potential trade-offs between computational requirements and energy estimation accuracy, which resulted in good agreement between experimental and numerical results.

To further simplify the require inputs and calculations of the prediction model, many other techniques has been proposed. One such method is the heating and cooling degree day method, which correlates building energy demand with a climatic indicator. However, this method is not

very accurate and does not take into account different building characteristics. De Rosa et al. (2014) developed a simple dynamic model for building energy consumption simulation based on degree days that takes into account some other important factors, such as solar irradiation. The equivalent full load hours (EFLH) method is another commonly used simplified energy estimation approach. This method provides a simple and direct way to assess the effectiveness of energy efficiency programs, but requires knowledge of EFLH data for a specific area (Spandagos & Ng, 2017). Papakostas et al. (2009) introduced a new approach for computing the EFLH for heating and cooling systems using hourly dry-bulb temperature bin data and various other factors. Barnaby and Spitler (2005) developed the residential load factor (RLF) to estimate heating and cooling loads of residential buildings, which is tractable by hand or can be straightforwardly implemented using spreadsheet software. The RLF calculation is based on the idea of the sum of independent load components.

2.3.2 Statistical Methods

Statistical method utilize historical performance data to develop regression models that can establish correlations between energy consumption or energy index and the influencing variables (Zhao & Magoulès, 2012). While these methods are typically less complex than engineering or artificial intelligence approaches, they may not always yield as comprehensive or precise results.

Ciulla and D'Amico (2019) proposed a reliable linear regression model to determine the energy requirements of buildings, utilizing multiple linear regression to establish simple relationships based on a few well-known parameters. Statistical analysis of the main error indices showed a high level of reliability in the results. Bauer and Scartezzini (1998) introduced a straightforward correlation method to compare energy performance and HVAC control system

efficiency in buildings with both heating and cooling loads, considering internal and solar gains and calculating utilization factors for free gains in the heating and cooling periods. Westergren et al. (1999) used climate data for a "normal" year and a regression equation to determine the average annual energy use of a single-family house. Korolija et al. (2013) developed a highly accurate regression model that can predict the annual heating, cooling, and auxiliary energy needs of office buildings with diverse HVAC systems. The model is a function of the heating and cooling demands of the building and demonstrated that single or bivariate regression models can adequately predict the energy requirements of HVAC systems for typical office buildings in the United Kingdom. Bilous et al. (2018) developed a nonlinear regression model for internal air temperature prediction, based on external climatic factors and internal building properties factors, as part of their building energy performance analysis. The validation results indicated a high level of accuracy for the obtained multivariate nonlinear regression.

2.3.3 Artificial Intelligence Methods

In the context of forecasting building energy consumption, artificial intelligence methods are widely used, particularly the artificial neural network (ANN) and support vector machine (SVM) algorithms, due to their effectiveness in solving nonlinear problems (Amasyali & El-Gohary, 2018). In a comparative study by Ahmad et al. (2014) both ANN and SVM demonstrated strong forecasting performance, with SVM even outperforming ANN in certain circumstances. However, both methods require ample historical data, and their models can be excessively intricate (Zhao & Magoulès, 2012).

Artificial neural network (ANN) was first proposed by McCulloch and Pitts (1943), as a computational technique inspired by biological neural networks. ANNs are composed of

interconnected layers of neurons that employ various functions. Z. Li et al. (2014) reviewed twelve methods for benchmarking building energy consumption and suggested that ANNs are well-suited for predicting space heating load and total energy consumption. Bagnasco et al. (2015) applied a backpropagation algorithm-based multi-layer perceptron ANN to forecast day-ahead load consumption for a large facility, yielding satisfactory results with reasonable error. Esen et al. (2015) developed an ANN model to assess the performance of a solar ground source heat pump, which produced a successful forecast with an R-square value of 0.9627. González and Zamarreño (2005) proposed a novel approach for predicting short-term building load using a feedback neural network trained with a hybrid algorithm. Their method showed precise predictions with only atmospheric temperature and electric power measurements as inputs. Hou et al. (2006) integrated rough sets and ANN using a data-fusion technique to forecast the cooling load of an air-conditioning system. Kwok et al. (2011) investigated the modeling of building cooling load using an MLP-based ANN that considers building occupancy rate. The results demonstrate the importance of occupancy data in predicting building cooling load using ANN.

SVM was introduced in 1995 by Vapnik and has since been widely used for various analyses such as regression, classification, and non-linear function approximation (Ahmad et al., 2014). Xing-Ping and Rui (2007) used SVM with a Gaussian radial basis function as the kernel function to forecast electrical energy consumption from 1994 to 2006, and the results showed that multivariable SVM was effective in forecasting electrical energy consumption in China. Solomon et al. (2011) applied SVM to forecast the building energy consumption without the requirement of physical properties, using a regression model purely based on historical data of the building. They created feature vectors for SVM training using time-delay coordinate and predicted a week of future energy usage based on past energy, temperature, and dew point temperature data. Jain et al.

(2014) developed a sensor-based forecasting model using SVM and applied it to an empirical data-set from a multi-family residential building in New York City. They examined the impact of temporal and spatial granularity on the model's predictive power and found that the model can be extended to multi-family residential buildings, and the optimal monitoring granularity occurs at the by-floor level in hourly intervals.

2.4 Research Gap

In conclusion, the heat pump and natural gas boiler system is a suitable option for residential homes in Alberta, Canada, with evidence of its advantages in cold climates through simulations. However, there is a limited amount of research on the actual performance of such hybrid energy systems and their integration with net-zero energy residential buildings. Additionally, there is a lack of monitoring data and lessons learned from the implementation of such systems in cold climates. Furthermore, current residential building energy modeling methods lack a comparison between the monitored results and the software simulation results. The use of HOT2000 for energy prediction relies heavily on the input parameters, such as indoor settings, climate conditions and system operation methods, this information can be unknown during the design state and relies on the default files of the HOT2000, which may result in imprecise and non-comparable results. Therefore, a method for precise comparison between the software modeled results and the monitored results is necessary to investigate and may lead to future improvements in the default values of the software.

CHAPTER 3 HYBRID SYSTEM IN-SITU ENERGY PERFORMANCE

This chapter assesses building energy consumption, analyzing monthly usage, hybrid energy system space heating output, lessons learned, heating performance of the hybrid energy system using a heat pump and natural gas tankless water heater, and an economically efficient control strategy. The purpose of this analysis is to provide a comprehensive understanding of the actual performance of the hybrid energy system in residential units, identify any realistic issues, and present practical energy performance results that can be used in subsequent chapters and further studies.

3.1 Methodology

A flow chart illustrating the methodology of this chapter can be found in Figure 8. The original data used in this study was obtained through a monitoring system installed in the duplex. The energy performance of both units was analyzed, and the heating performance of the hybrid system were determined from the right unit only. To assess the in-situ performance of the hybrid energy heating system, it was necessary to gather information on both the system's energy consumption and the building's electrical and heating load. Therefore, specific monitoring parameters were selected to ensure that the system's performance could be evaluated accurately. Appendix 3 Information of the monitoring devices and Appendix 4 Raw Data Examples provide detailed information on the monitoring parameters and raw data file used in this study.

Once the raw data was collected, it underwent a processing stage before any calculations could be made. In order to ensure data quality, any missing values were either removed or filled in as appropriate. Additionally, suitable subsets of data were extracted from the original data set for use

in various calculations. To examine the in-situ performance of the hybrid energy system, the space heating output, heat pump performance, and TWH performance were evaluated. From the heating performance, A correlation between the energy cost ratio and the switching temperature of the ASHP and TWH were determined. The data processing and analysis for this chapter were carried out using MATLAB 2022a.

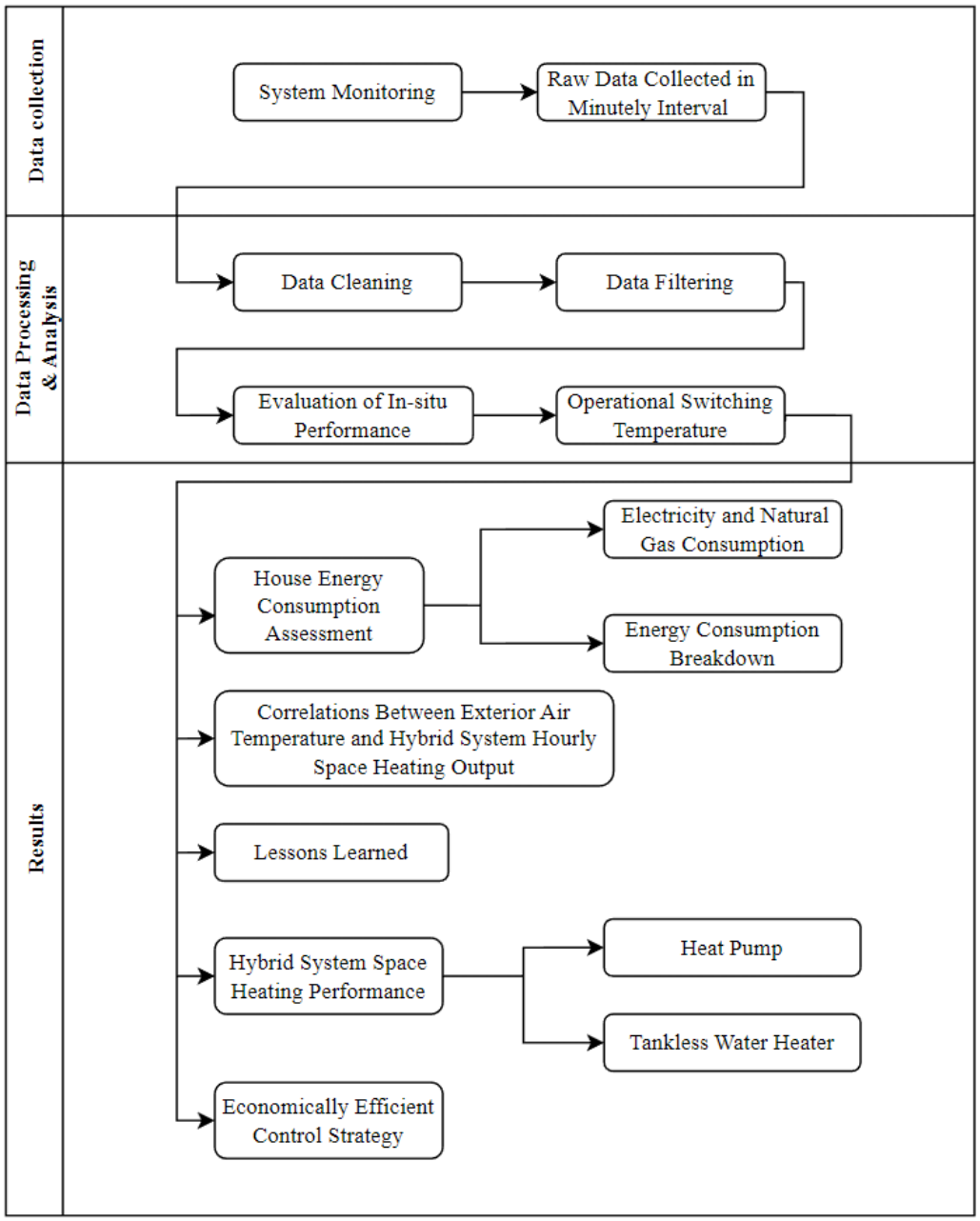

Figure 8. Flow chart of Chapter 3 methodology.

The system's performance was demonstrated by means of several key indicators. Firstly, the house energy consumption was assessed, including both monthly and annual total electricity and natural gas consumption, as well as a breakdown of energy consumption. Secondly, the correlations between the exterior air temperature and the hybrid energy system's hourly space heating output were examined. Thirdly, the lessons learned during the analyzation and investigation of both the building and the system were highlighted. Finally, the hybrid energy system's space heating performance was evaluated, while the system operating the heat pump or TWH. Furthermore, an economically efficient control strategy has been proposed, complemented by a switching temperature selection chart. With flex energy prices, the proposed control strategy guarantees optimal energy cost for the system's operation.

Based on the actual monitoring data and energy consumption assessment presented in this chapter, the proposed method highlights the benefits of hybrid energy systems as an energy-saving system. Furthermore, the impact of the operation method and the potential for improvement through the lessons learned are demonstrated. The analysis of the hybrid energy system's space heating performance also yields practical results on energy performance.

3.1.1 Monitoring System Description

Table 1. Monitoring system measurement.

Device	Measurement
Current transformer	Whole house electricity consumption
	AHU electricity consumption
	Mechanical room electricity consumption
	Heat pump electricity consumption
Gas meter	TWH natural gas consumption
Humidity sensor	Return air humidity
Thermocouple	Temperature of return air
	Temperature of air between the HP and TWH coil
	Temperature of supply air
Airflow sensor	Return air flow rate
Thermal (BTU) meter	Energy provided by the TWH for space heating

A commercial monitoring system was deployed in both units of the duplex house to measure the relevant parameters. The measured parameters of the hybrid energy system are presented in Table 1 , while the location of the sensors and the connections between the monitoring devices are depicted in Figure 9 and Figure 10.

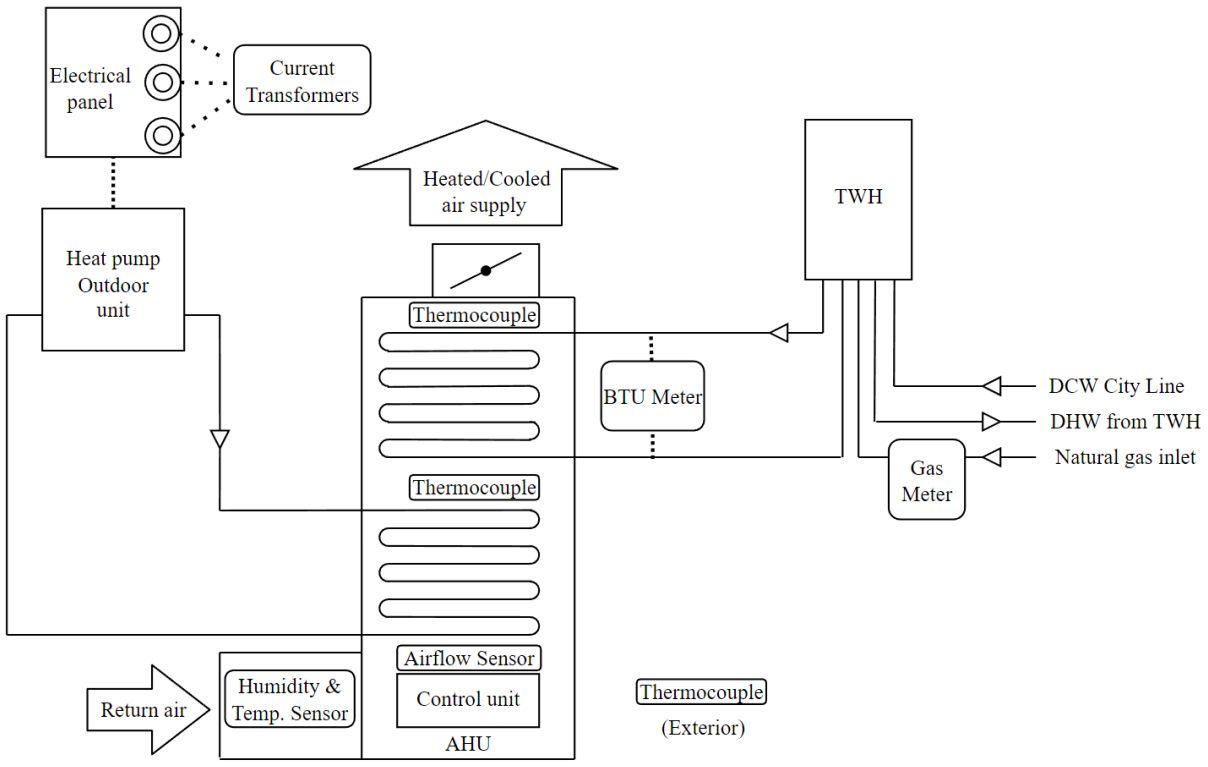

Figure 9. Location of the monitoring sensors.

To measure the electricity consumption of the house, AHU, mechanical room, and heat pump unit, current transformers in the panel circuits were utilized. The natural gas consumption of the TWH was collected using the natural gas meter, while the return air's relative humidity and temperature, the temperature of the air across the heat pump coil and the TWH coil, and the temperature of the supply air were used to determine the amount of heating energy required. In one of the houses, a BTU meter was installed to differentiate between domestic hot water consumption and space heating consumption, thus allowing for a more accurate determination of the amount of space heating energy provided by the TWH. Climate data of the exterior air temperature, retrieved every hour from nearby meteorological stations, was also included in the dataset. The data was collected in minutely intervals and stored in the gateway, which then

uploaded the data packages to the cloud server every five minutes through the cellular network. The raw monitoring data could then be downloaded to the laboratory computer for further analysis.

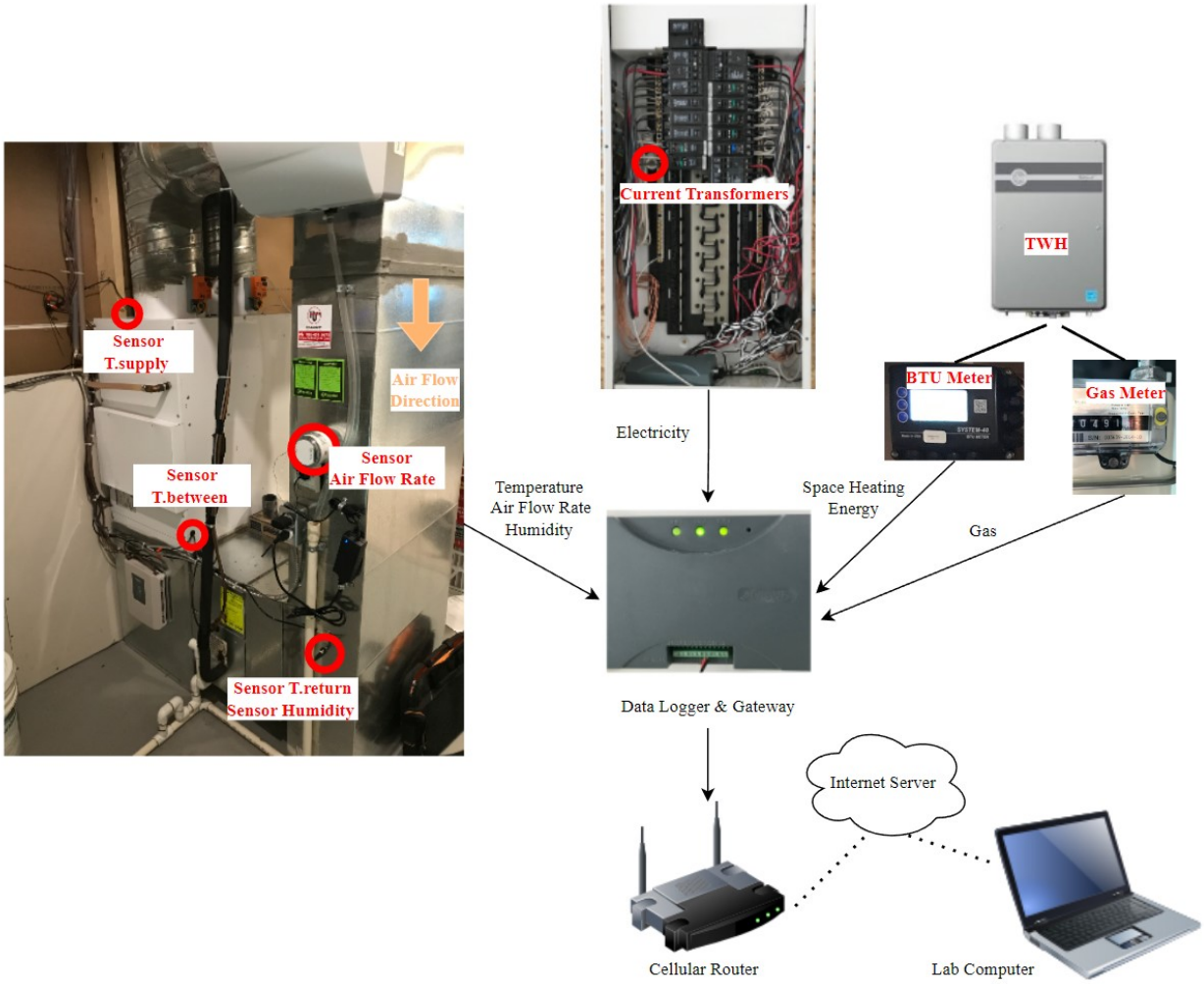

Figure 10. Monitoring system devices and connection.

3.1.2 Data Processing

The data may be missing from time to time, as indicated in Appendix 5 Data Availability Timeline, which provides details on the monitoring timeline and available data. Data cleaning and processing are crucial for analyzing the system's performance, as specific data points need to be filtered out.

3.1.2.1 Data Cleaning

A sample raw data table can be found in Appendix 4 Raw Data Examples. The minutely data set was used for this section. Appendix 6.1 Data interpolation and replacement shows the example of MATLAB code of this section. All on-site monitored data except the natural gas consumption was the averaged value over one minute, each time the gas meter indicated an increment of cubic feet, natural gas consumption data was recorded, and the exterior air temperature was only collected once every hour. Volume of the natural gas consumption data has been converted into energy form for comparison purposes using Eq. (3.1)

$$Ng_{MJ} = Ng_{cf} \times \frac{1.06MJ}{1\ cf\ of\ natual\ gas} \tag{3.1}$$

Where

Ng_{MJ}: Energy of the natural gas in *MJ*.

Ng_{cf}: Volume of the natural gas in *cf*.

In order to maintain consistency of units, the air flow sensor collects data in feet per minute (FPM), which is subsequently converted to meters per second (m/s). This conversion is carried out using the following equation:

$$\dot{v}_{air} = \dot{v}_{air_{FPM}} \times \frac{5.08 \times 10^{-3} \frac{m}{s}}{1FPM} \tag{3.2}$$

Where

$\dot{v}_{air}$: Return air flow rate in m/s.

$\dot{v}_{air_{FPM}}$: Return air flow rate in FPM.

In the event of a glitch or disconnection in the monitoring system, missing values and outliers may occur. To address missing data points within a five-minute interval, the moving median method with a window length of five (Eq. (3.3)) was used to replace the missing values. This method is robust and helpful in identifying trends in the data set and is less sensitive to outliers (Justusson, 1981). An example of filling in missing data using the moving median method is provided in Table 2. Data points that were missing for more than or equal to five minutes were removed from the data set. To address outliers and abnormal data, the data points were replaced with the average of the previous and next non-missing values in the array.

$$P_t = Median\{P_{t-2}, P_{t-1}, P_{t+1}, P_{t+2},\} \tag{3.3}$$

Where

P: An array of data.

t: The index of the array.

Table 2. Example of moving median method filled in missing values.

Time	Original data	Filled in value
2021-01-01 23:58	123.7	
2021-01-01 23:59	101.6	
2021-01-02 0:00		101.6
2021-01-02 0:01		82.1
2021-01-02 0:02	82.1	
2021-01-02 0:03	80.3	

The exterior air temperature was collected only once per hour from nearby meteorological stations, unlike other data, which were collected at minute intervals. Therefore, it was necessary to interpolate the temperature readings to meet the analysis requirements. Linear interpolation was used to approximate the temperature changes over time. The linear interpolation method is represented by Eq. (3.4). Figure 11 shows an example of the results obtained from interpolating the temperature data.

$$T = T_1 + \frac{t - t_1}{t_2 - t_1}(T_2 - T_1) \tag{3.4}$$

Where

T: Estimated exterior temperature.

t: Time value corresponds to T.

T_1, T_2: Nearest available exterior temperatures.

t_1, t_2: Time values correspond to T_1 and T_2.

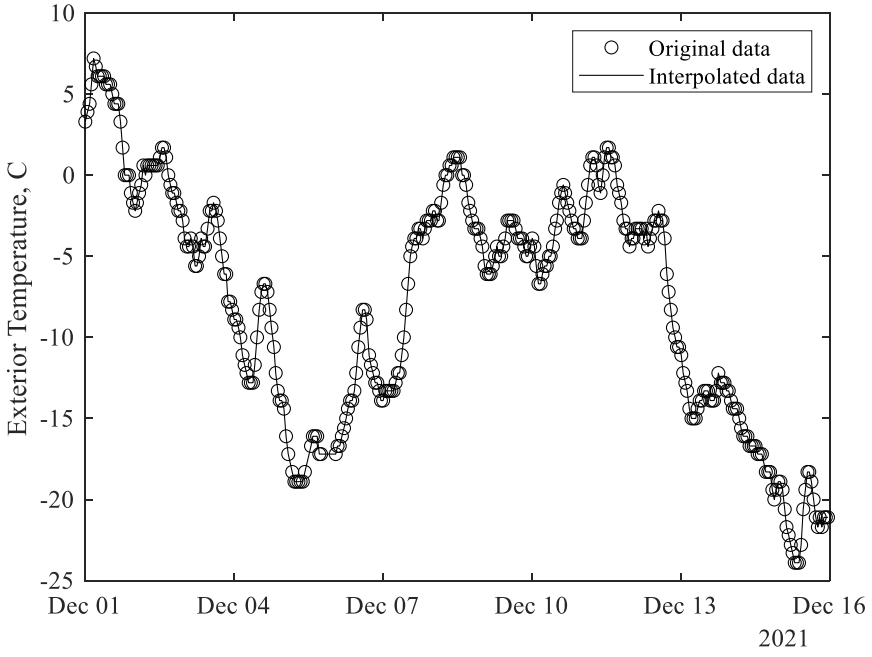

Figure 11. Example of the interpolated temperature data.

3.1.2.2 Data Filtering

After the data has been cleaned initially and given that this study only focuses on the heating performance of the hybrid system, the dataset needs to be filtered and classified to facilitate the evaluation of its heating performance. The air source heat pump operates at a variable speed, and it can also provide both space heating and cooling. Figure 12 illustrates the heat pump power consumption during the monitoring, when the heat pump starts to operate, there will be a "stating-state" that the heat pump runs on full capacity to reach the desire temperature first, after that, it operates more slowly to maintain a constant output. To approach the objective of this study, which is the assessment of the hybrid energy systems components' performance and aid in the development of appropriate system control strategies, the "steady-state" space heating operation data was extracted from the data set to evaluate the performance of the system while operating the air source heat pump. The records of the power consumption of the heat pump and the thermocouples installed inside the AHU were utilized to identify the desired data: a stable power consumption records indicates the heat pump is running at "steady-state", the positive temperature difference across the heat pump coil indicates the heating pump is providing space heating. Moreover, the natural gas TWH can provide both space heating and domestic hot water (DHW), the space heating records need to be separated for TWH space heating performance evaluation. For the right house unit, the BTU meter installed on the working fluid pipe would help to identify the space heating natural gas consumption. For both units, the positive temperature difference across the TWH coil indicates the TWH is providing space heating. Detail of the filter algorithm MATLAB code can be found in Appendix 6.2 Data filtering and analyzation (Heat pump performance) and Appendix 6.3 Data filtering and analyzation (TWH performance) for heat pump and TWH, respectively.

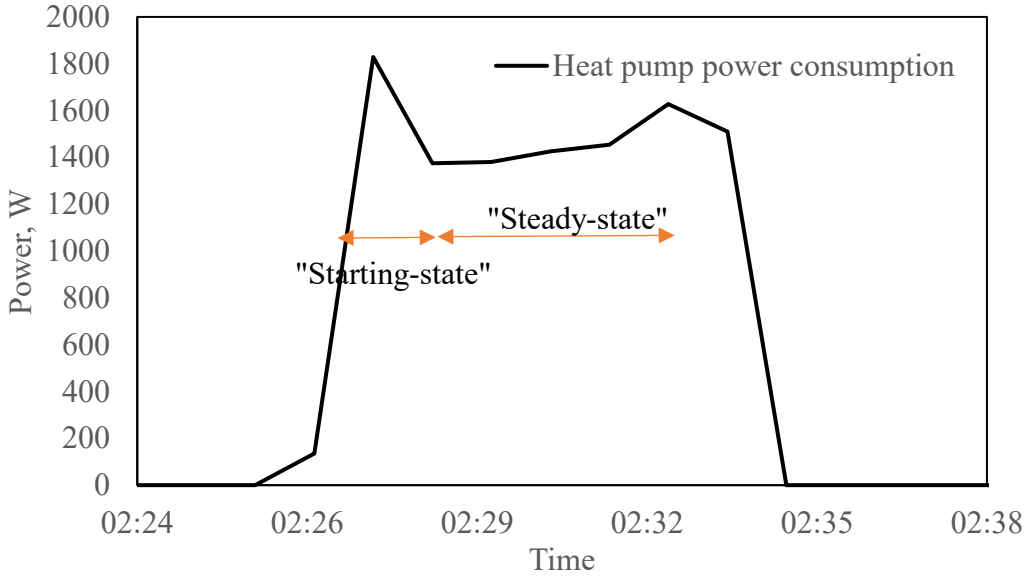

Figure 12. Example of heat pump power consumption.

3.1.3 Evaluation of In-Situ Performance

In this study, the focus was on investigating the space heating performance of the hybrid energy system, as it was designed to address cold weather conditions. Therefore, the space cooling function of the heat pump, which is similar to a conventional air conditioning system, was not analyzed. The performance of the system was evaluated by developing a hybrid energy system on site and subjecting it to various exterior air temperature conditions. The heating coefficient of performance (COP) was used to measure the efficiency of the system when running the heat pump, while the efficiency of the natural gas TWH operation was also evaluated to determine its ability to convert natural gas into useful heat.

The heating load of the house, Q_{hl}, is expressed as:

$$Q_{hl} = t\,\dot{v}_{air} A_d \rho_{air} c_{p,air} \left(T_{supply} - T_{return}\right) \tag{3.5}$$

Where

t: Corresponding time of the required heating load.

$\dot{v}_{air}$: Return air flow rate in m/s.

A_d: Cross-sectional area of the return air duct in m^2.

ρ_{air} : Density of air in kg/m^3.

$c_{p,air}$: Specific heat of air in kJ/kgK.

T_{supply}: Supply air temperature in $^{\circ}C$.

T_{reutrn}: Return air temperature in $^{\circ}C$.

The system performance while using electricity heat pump for space heating, $COP_{sys,HP}$, is calculated by:

$$COP_{sys,HP} = \frac{Q_{HP}}{W_{HP}} \tag{3.6}$$

Where

W_{HP}: Work input to the heat pump in kJ

Q_{HP}: Heating energy provided by the system while operating heat pump in kJ, which can be determined by:

$$Q_{HP} = t\dot{v}_{air}A_d\rho_{air}c_{p,air}(T_{between} - T_{return}) \tag{3.7}$$

Where

t: Corresponding time of the required heating output.

$\dot{v}_{air}$: Return air flow rate in m/s.

A_d: Cross-sectional area of the return air duct in m^2.

ρ_{air} : Density of air in kg/m^3.

$c_{p,air}$: Specific heat of air in kJ/kgK.

$T_{between}$: Temperature of air between the heat pump coil and TWH coil in $^{\circ}C$.

T_{return}: Return air temperature in $^{\circ}C$.

The system efficiency while using natural gas TWH for space heating, $\eta_{sys,TWH}$, was defined as:

$$\eta_{sys,TWH} = \frac{Q_{TWH}}{E_{NG}} \tag{3.8}$$

Where

E_{NG}: Amount of energy of consumed natural gas in *kJ*.

Q_{TWH}: Heating energy provided by the system while operating TWH in *kJ*, and can be estimated using the BTU meter.

Base load of each unit was determined for all other electricity usage (e.g., lighting, electric appliance) except the HVAC system electricity consumption, and was estimated as:

$$E_{bl} = E_{total} - E_{HP} - E_{AHU} - E_{MR} \tag{3.9}$$

Where

E_{bl}: Base load electricity consumption.

E_{total}: Whole house electricity consumption.

E_{HP}: Air source heat pump electricity consumption.

E_{AHU}: Air handling unit electricity consumption,

E_{MR}: Electricity consumption of all other HVAC components in the mechanical room.

3.1.4 Operational switching temperature

The economical efficient control strategy is proposed in this chapter, this control strategy decides the hybrid energy system switches between the ASHP and TWH whenever the cost of operating the corresponding components is lower than the other. Based on Eq. (3.5), the space heating load of the studied unit can be determined, and a correlation between the space heating load and the exterior air temperature, $Q_{hl}(T)$, can be found in section 3.2.1. Based on Eq (3.6) and (3.8) the in-situ performance of the ASHP and TWH ($\eta_{sys,TWH}$) can be evaluated, and a correlation between the COP of the ASHP and the exterior air temperature, $COP_{sys,HP}(T)$, can also be obtained, detailed can be found in section 3.2.3.

The cost of operating ASHP, C_{ASHP}, and the cost of operating TWH, C_{TWH}, can then be calculated using Eq (3.11) and (3.12), respectively:

$$C_{ASHP} = C_{elec} \frac{Q_{hl}\,(T)}{COP_{sys,HP}(T)} \tag{3.10}$$

$$C_{TWH} = C_{ng} \frac{Q_{hl}\,(T)}{\eta_{sys,TWH}} \tag{3.11}$$

Where:

C_{elec}: Electricity price.

C_{ng}: Natural gas price.

T: Exterior air temperature in $^{\circ}C$.

Hence, with the known exterior air temperature, if $C_{ASHP} > C_{TWH}$, then the system operates with TWH only, otherwise, if $C_{ASHP} \leq C_{TWH}$, the system operates with heat pump only.

From the above, a relationship between the energy prices and the system performances can be determined, at the operational "switching temperature" of the system, $C_{ASHP} = C_{TWH}$, which is:

$$C_{elec} \frac{Q_{hl}\,(T)}{COP_{sys,HP}(T)} = C_{ng} \frac{Q_{hl}\,(T)}{\eta_{sys,TWH}} \tag{3.12}$$

The above equation can then be simplified to:

$$\frac{C_{elec}}{C_{ng}} = \frac{COP_{sys,HP}(T)}{\eta_{sys,TWH}} \tag{3.13}$$

By using this relationship, the operational "switching temperature" can be solved with the known energy prices.

3.2 Results and Discussion

3.2.1 House Energy Consumption Assessment

Within this section, the data that has been monitored on a daily and minute-by-minute basis is utilized to conduct a comprehensive analysis of the energy performance of the two duplex house units and the hybrid energy heating system. This analysis involves an examination of the monthly total energy consumption, as well as a fuel type energy consumption breakdown of the right unit. A thorough understanding of the energy performance of the units will aid in the identification of the problem with the building energy system and will assist in the development of building energy models and simulations in both present study and future studies.

Figure 13 and Figure 14 show the monthly total energy consumption of the right and left units of the duplex house, respectively, over the period spanning from October 2020 to September 2021. Based on the figures, a decrease in the average exterior air temperature correlates with an increase in natural gas consumption for both units, suggesting that the heating system is functioning as intended. In periods of low exterior air temperatures, natural gas is primarily utilized for space heating. Furthermore, electricity consumption in the right unit is significantly higher during the cold winter season compared to other seasons, while the trend for the left unit is relatively stable. It is important to note that as a show house, the right unit has consumed significantly more electricity for lighting and electric appliances due to occupants' preferences.

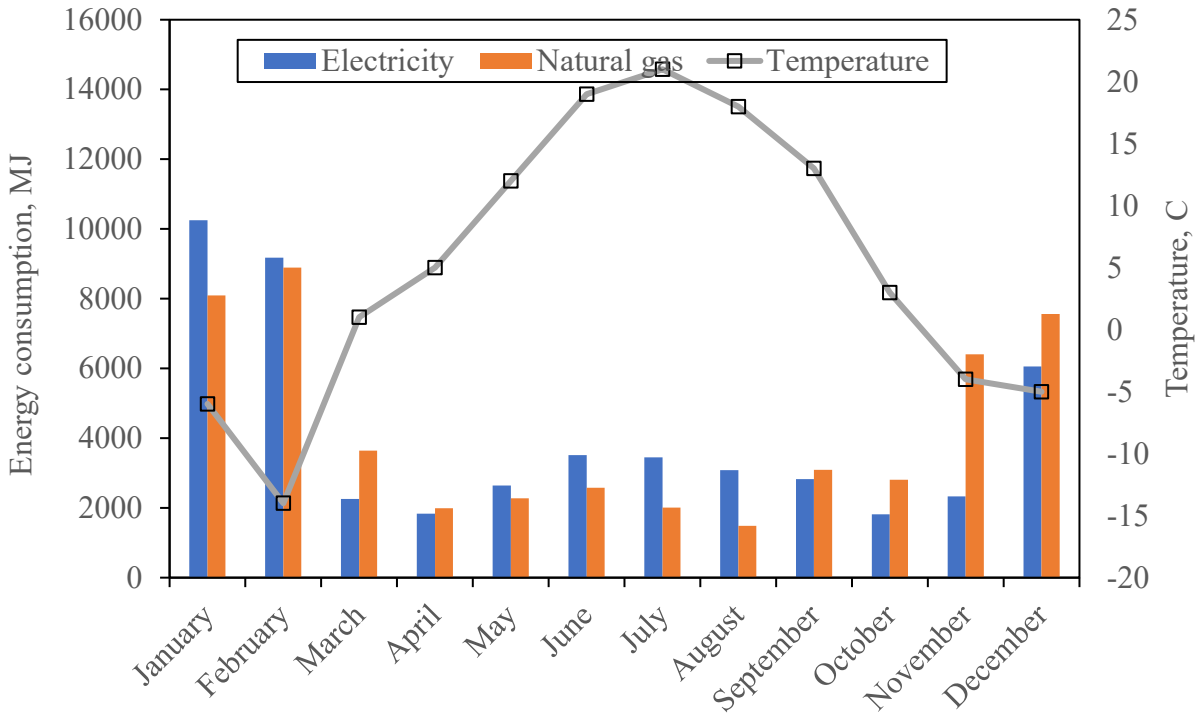

Figure 13. Monthly energy consumption the right unit.

Table 3 displays the annual energy consumption for both the left and right units under investigation, alongside the average annual energy consumption for duplex households in Alberta (Statistics Canada, 2022). As observed in the table, both units utilizing the hybrid energy heating system consume more electricity and less natural gas compared to the Alberta average. With regard to total energy consumption, there is a notable discrepancy between the two studied units and the average household. Given that the majority of Albertans rely on natural gas for space heating, the utilization of a hybrid heating system incorporating an electric heat pump to supplement conventional natural gas space heating has the potential to yield considerable energy savings.

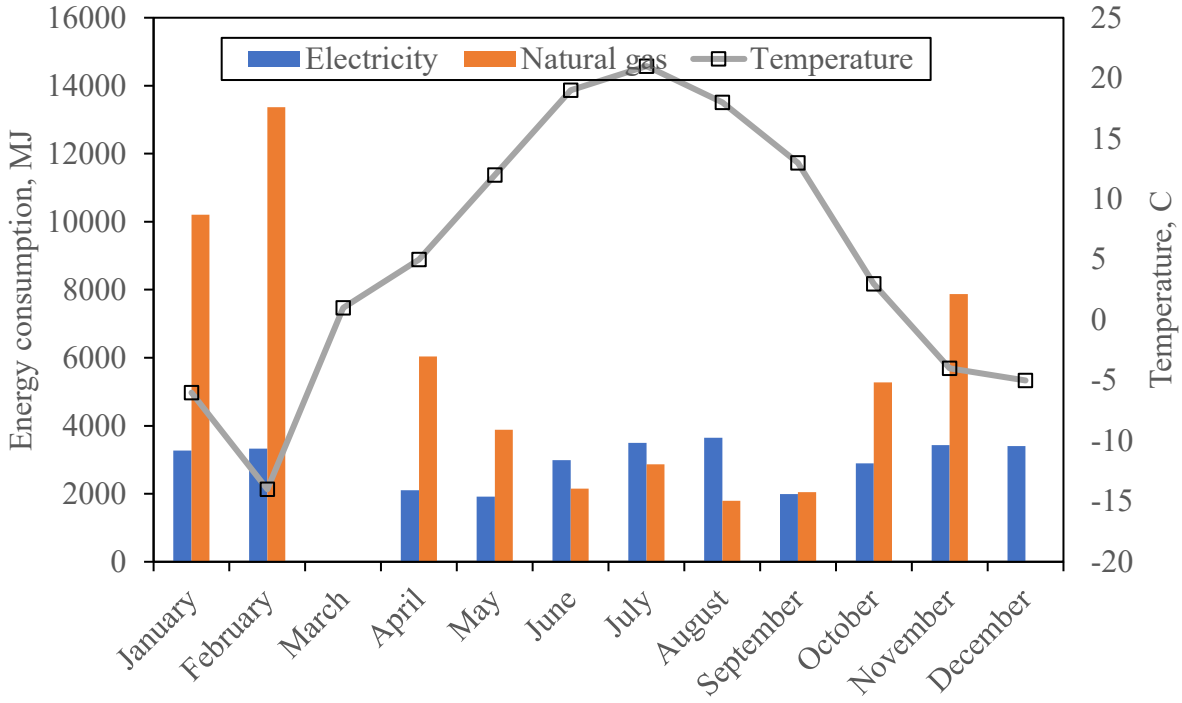

Figure 14. Monthly energy consumption of the left unit (due to a disconnected sensor, data regarding natural gas consumption for the left unit in December 2020 and electricity and natural gas consumption for March 2021 cannot be obtained).

Table 3: Annual energy consumption (*MJ*).

	Total energy	Electricity	Natural gas
Right Unit	84048.01	42952.79	41095.55
Left Unit[1]	94165.99	30840.44	63325.55
Average of Alberta Duplex Household[2]	116502.12	20620.87	95881.25

Note: 1 - Due to missing data during March and December, the annual energy consumption of the left unit was approximated by the monthly average of energy consumption x 12.

2- Obtained from Statistic Canada (2022)

Table 4 displays the total monthly energy consumption and heating energy consumption for representative months of the right unit, while the corresponding breakdown of energy usage can be found in Figure 15 to Figure 16. This section of the results is based on available data sets from 2021, four typical months selected to represent the four seasons, Figure 15 breaks down the electricity consumption into space heating, space cooling, air handling unit (AHU), mechanical room, and baseload (i.e., the residual electricity consumption). The right unit exhibited a significant baseload usage during January, which was attributed to occupancy behavior. Figure 16 illustrates the natural gas consumption of the right unit, with the natural gas usage broken down into space heating and domestic hot water (DHW), both of which are provided by the tankless water heater (TWH). From the figure, the majority of natural gas consumption was used towards space heating, with only a small portion used for DHW. January was the month with the highest natural gas consumption, as it was comparatively colder than other months, which caused the heat pump to be less effective in assisting space heating within certain temperature ranges, leading to a higher overall space heating demand. It should be noted that the natural gas TWH performs a self-test for space heating every day, resulting in a small amount of TWH space heating consumption during the summer months.

Table 4. The monthly heating energy consumption for typical months (*MJ*).

	January	April	July	October
Total Electricity	10252	1839.74	3449.34	2236.57
Total NG	8221.39	2017.19	2041.27	2839.90
Total Energy Consumption for Space Heating	9052.81	2227.62	1931.69	3247.11

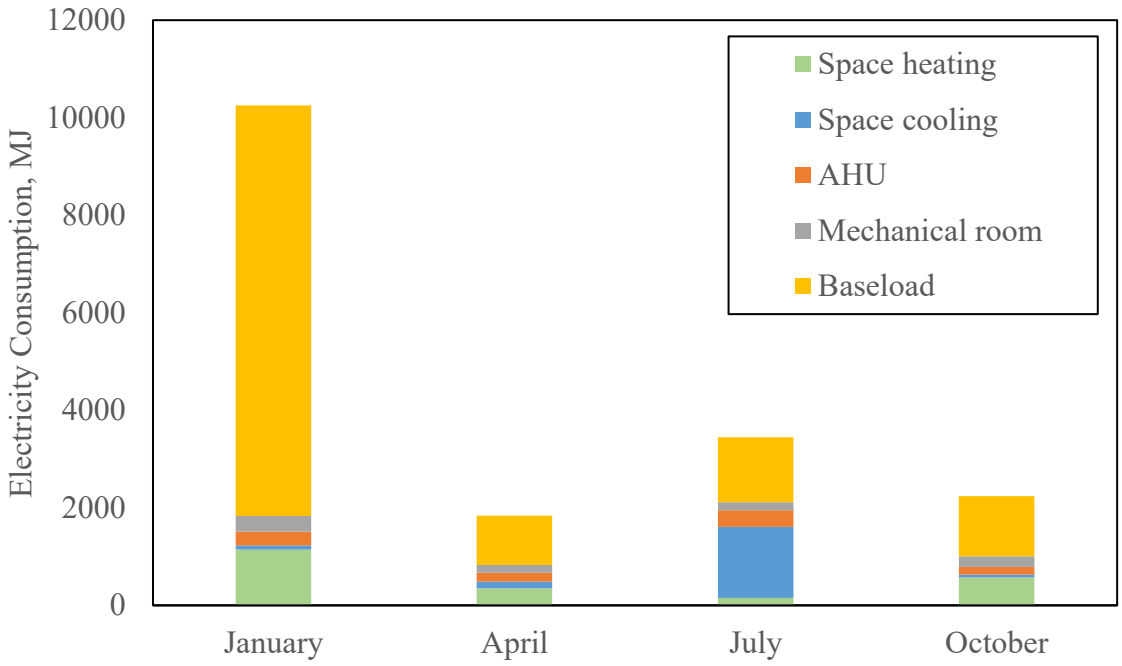

Figure 15. Electricity consumption breakdown of the right unit.

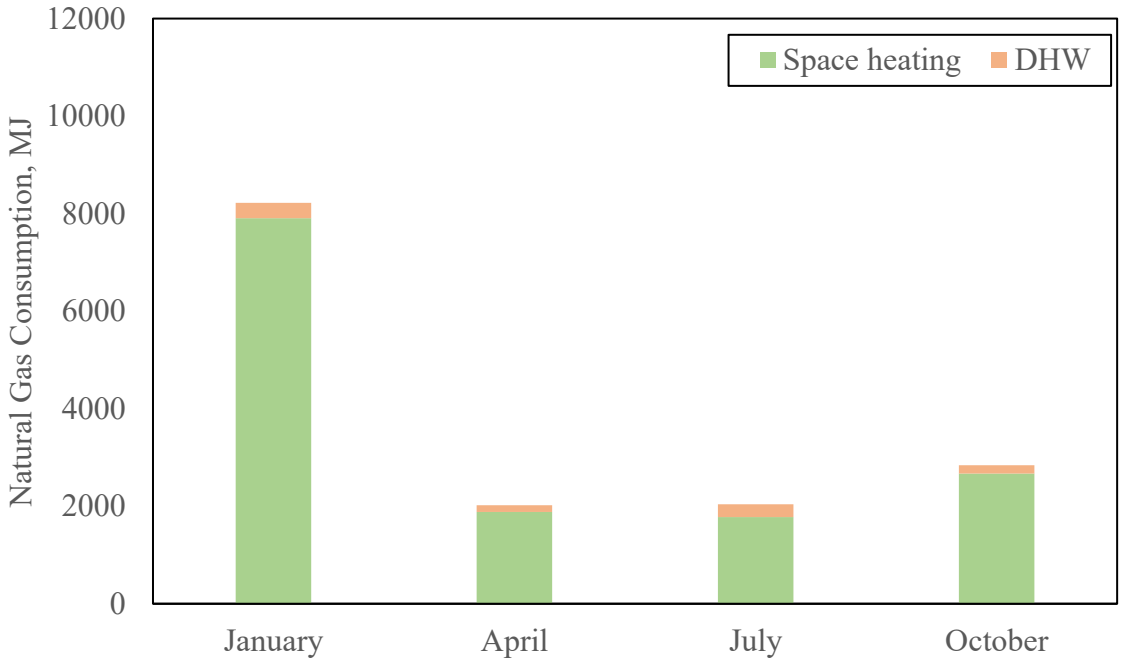

Figure 16. Natural gas consumption breakdown of the right unit.

In general, the hybrid heating system exhibited higher energy consumption for heating during the cold winter months, such as January, and lower energy consumption for heating during the summer months, such as July. The heating energy consumption for the months of April and October fell in between the two extremes.

The hourly space heating load of the right unit is presented in Figure 17. The result was achieved by adding the space heating energy supplied by the hybrid energy system over hourly intervals and computing the average hourly heating energy provided by the system for the corresponding exterior air temperature. The space heating output of the hybrid energy system is assumed to be the same as the heating load of the house on an hourly basis. The result was based on minutely monitoring data from September to December 2021. The figures illustrate that the studied unit requires space heating when the exterior air temperature drops below 20°C, and a linear relationship exists between the hybrid energy heating system's hourly heating output and the outside air temperature. When the exterior air temperature drops to -25°C, the space heating load of the studied unit is approximately 20 MJ per hour.

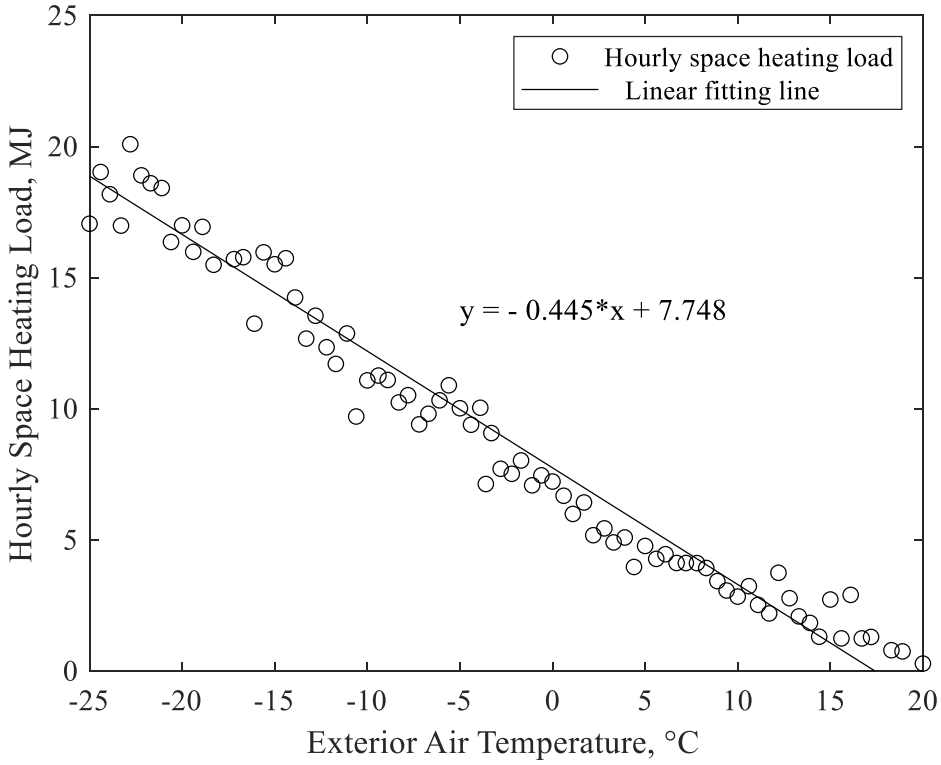

Figure 17. Right unit hourly space heating load.

3.2.2 Lessons Learned

There exists a high discrepancy in the energy consumption of the two units. An investigation was conducted and several issues were identified. These issues not only provide insights into the actual performance of the house units but also help identify deficiencies in the operation of the hybrid heating system, which can be addressed to improve its performance in future.

During the summer of 2022, the occupant of the right unit (formerly the show house) reported feeling hot on the main floor, despite the thermostat being set to a relatively low temperature. In order to investigate the issue, the energy consumption of the house was analyzed under various conditions to determine the cause of the excessive heat in the right unit. A high-level comparison of the entire house's electricity consumption was conducted between the left and right units to

determine if there was any unknown electricity consumption that could be responsible for the excessive heat within the right unit. Figure 18 shows the consumption of electric power for the right and left units of the duplex house for one common period during August 5th, 2022, without the heating and cooling systems operating. The results indicate that the right unit consumes more electricity than the left unit, especially during the daytime. During the early morning hours between 3:00 and 5:00 AM, when there were likely no occupational activities in either unit, the maximum power consumption of the left unit in this time period was 1276 W, with a minimum power consumption of 217 W. The right unit had a maximum power consumption of 911 W, with a minimum consumption of 276 W. It should be noted that the fan coil within the AHU may operate cyclically for indoor air circulation and have a capacity of 530 W, hence the power fluctuations during this period might be related to the fan's operation. Moreover, the minimum power profiles of the two units are similar.

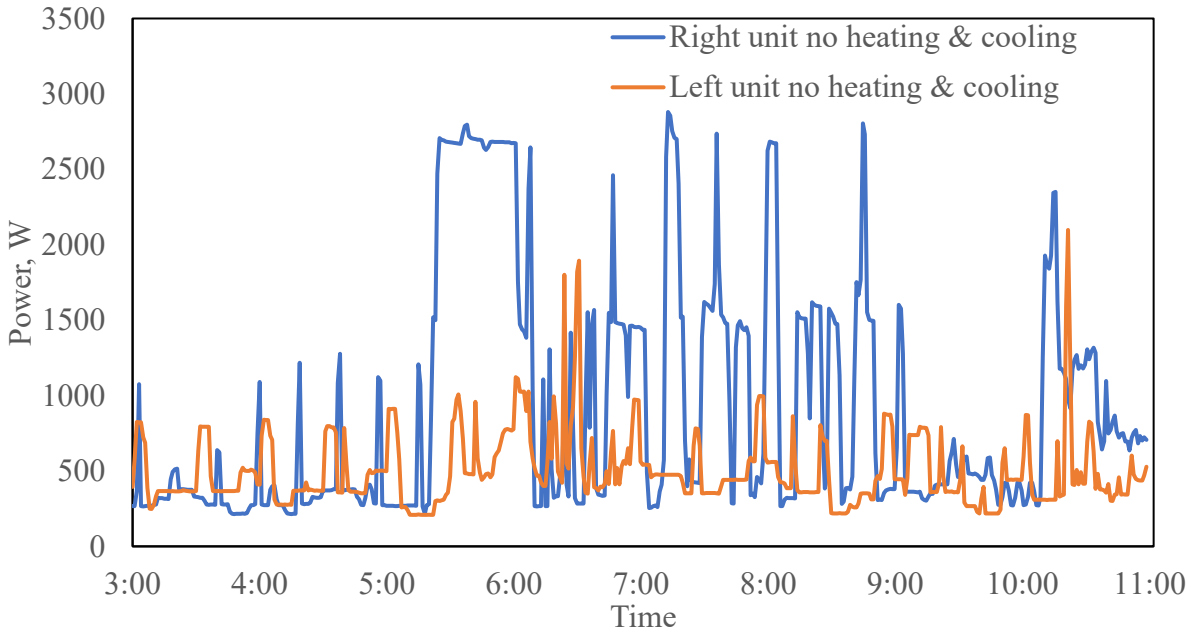

Figure 18. Power consumption of the two units when both heating and cooling were off (August 5th, 2022).

In order to investigate if there was an additional heating source that caused the occupant of the right unit to feel hot during the summer of 2022, the heating and cooling outputs of the hybrid energy system in both units were analyzed. Figure 19 and Figure 20 display the supply and return air temperature during cooling for the left and right unit, respectively. It was observed that the right unit had a lower supply air temperature, but similar return air temperature compared to the left unit.

Table 5 compare the space heating and cooling energy output of the hybrid energy system for both units on November 24th, 2021 (average exterior air temperature at -14°C), which is an example of a cold day when the system provides only space heating, and on July 28th, 2022 (average exterior air temperature at 28°C), which is an example of a hot day when the system provides only space cooling. The results indicate that the right unit had a higher cooling energy output than the left unit, suggesting the presence of an additional heat source. However, the right unit also demanded greater heating output than the left unit. It is reasonable to speculate that:

1. There is no evidence of electrical heat related to circuit problems since the minimum power consumption of both units is similar and no unusual power consumption was observed.
2. The AHU fan in the right unit may have a higher energy consumption or capacity than those in the left unit, and high-power electrical appliances may contribute to excess heat in the right unit.
3. The higher cooling and heating demand in the right unit may indicate a problem with the thermal resistance of the building envelope. Alternatively, the excess heat only occurs during hot weather conditions and may be considered as "phantom heat."

Table 5. Heating and cooling output during specific time range.

Unit	Heating output of Nov 24th (MJ)	Cooling output of July 28th (MJ)
Right unit	351.79	151.49
Left unit	169.42	86.94

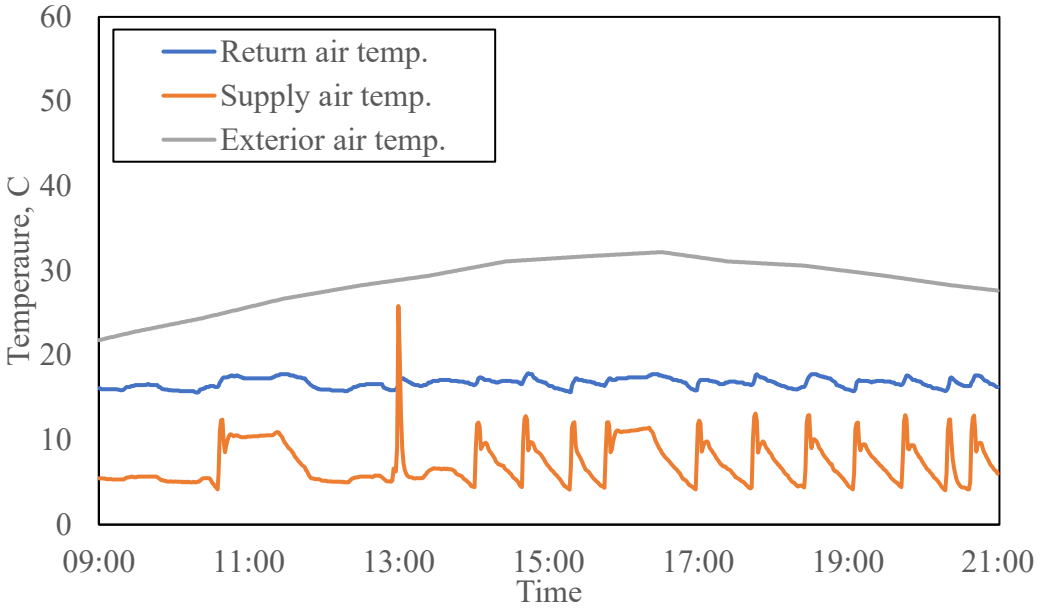

Figure 19. Cooling return and supply air temperature of the right unit (July 28th,2022).

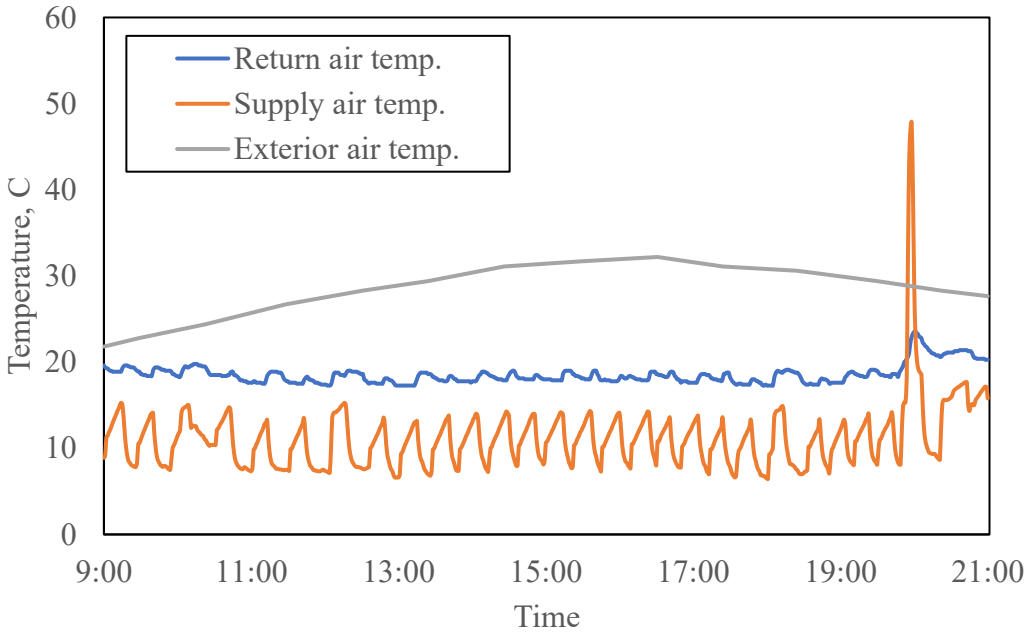

Figure 20. Cooling return and supply air temperature of the left unit (July 28th,2022).

During the investigation into the phenomenon of phantom heat within the right unit, an issue was uncovered in the room temperature conditioning process. As shown in Figure 21, the system engages in cyclic heating and cooling during hot summer weather, resulting in an increase in heat on the main floor, which can cause discomfort to the residents. Upon visiting the right unit and cross-referencing with the operation of the AHU, an interesting issue was identified concerning the thermostat settings. The units have a two-zone HVAC system, with one air duct supplying air to the main floor and the other to the basement. Modulating dampers in the AHU and thermostats on both floors are used to control air temperature corresponding to each floor. The two-zone HVAC system is intended to maximize energy efficiency, for instance, by providing heating/cooling to a single zone when required, or to customize indoor comfort for occupants who may prefer different temperatures in different zones (Sookoor et al., 2013). In the right unit, for example, when cooling is required on the main floor during hot summer weather, the HVAC system functions to supply cold air to the main floor. The occupants set both thermostats to the same setpoints. In the summer, the basement setpoint was higher than that of the main floor because the basement feels cooler due to a lower mean radiant temperature and the main floor feels warmer due to a significant amount of solar radiation from the south-oriented windows. Furthermore, the stairwell is close the basement thermostat. Due to the difference in density, the cold air is more likely to descend to the basement, which activates the heating system of the basement's thermostat automatically. Subsequently, as the HVAC system begins to supply hot air to the basement, the warm air will impact the air temperature on the upper floors, leading to discomfort for the occupants, and causing the HVAC system to cycle between space cooling and space heating. To address this cyclic issue, the researchers and technicians proposed several solutions:

1. One possible solution is to maintain a set point temperature on the main floor that is at least 2˚C higher than that of the basement, as this can increase the tolerance of the basement thermostat to changes in air temperature.
2. Additionally, it is recommended to keep the circulation fan running during hot weather to help maintain a uniform indoor air temperature. During summertime, the basement typically has a lower temperature due to the coolness of the soil and reduced exposure to sunlight. Circulating and mixing air from both floors can help to decrease the air temperature on the main floor and increase the temperature in the basement.

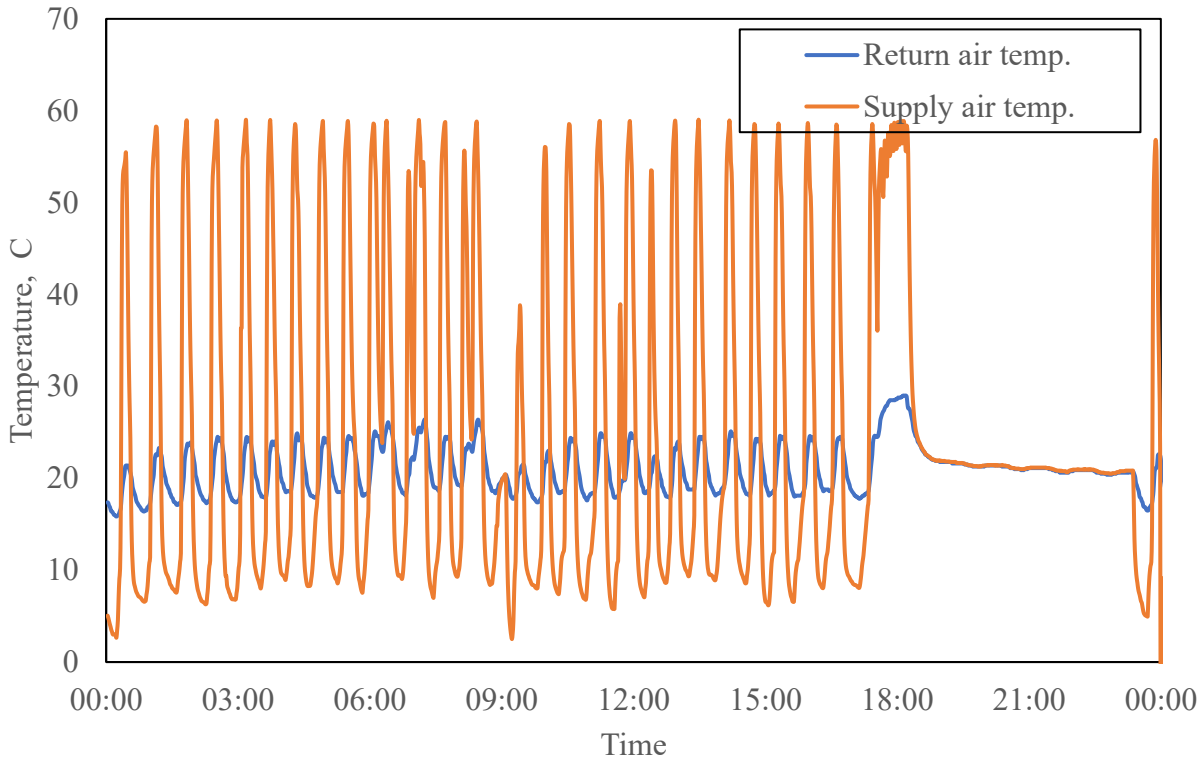

Figure 21. An example of cyclic heating and cooling during May 5th, 2022.

A refrigerant leak was detected in the ASHP unit of the left system in August 2021. As a result, the ASHP continued to consume electricity but was unable to provide space heating. The hybrid

system is designed to activate the TWH when the ASHP's heating output is insufficient. However, there was no specific temperature range setting that limited the TWH's operation. Consequently, when the refrigerant leak occurred, the TWH operated independently for space heating without the assistance of the ASHP. The occupant remained unaware of this situation until they required space cooling in the summer of 2022, as the ASHP is the only device capable of providing cooling. This issue has prompted the need for further investigation into improving the operation and maintenance procedures of the hybrid energy system. Future studies will focus on exploring suitable failure detection methods and alternative operation strategies.

3.2.3 Hybrid System Energy Performance

This section presents an analysis of the in-situ **heating performance** of the hybrid energy system, which involves operating both the air source heat pump unit and the natural gas tankless water heater unit. The analysis is based on the data collected at a minutely time interval of the right unit.

The heating performance of the hybrid energy system of the right unit is determined with the available data from June to December 2021. Figure 22 illustrates the coefficient of performance (COP) of the system under various exterior air temperatures, revealing a quadratic relationship between them. The COP ranges from 1.2 to 5.5 as the temperature changes between -24 to 17 ˚C. The COP is adversely impacted by lower exterior air temperatures as the heat capacity of the heat pump decreases. Therefore, the system consumes more energy for space heating in cold weather in provide the same amount of heat. The results are further illustrated in Figure 23, which displays a box plot showing a decrease in the variability of COP at lower exterior air temperatures. The box plot illustrates the distribution of data with the central line representing the median. The bottom

and top lines of the box indicate the 25th and 75th percentiles, respectively. The whiskers extend to the most extreme data points, and any outliers are shown as individual data points outside the whiskers. This variability may be due to the temperature difference between the hot (interior sink) and cold (exterior source) temperatures. A lower set point temperature improves the system's efficiency compared to higher set points, as shown in the figure. However, when temperature drop below -10 ˚C, the difference in hot temperatures does not significantly affect the system's efficiency. In Figure 24, the residuals plot shows the vertical deviations between the regression line and the observed data points, and the goodness of fit of the regression model, the residuals of COP versus exterior air temperature appear to be symmetric across the line and do not show any obvious shapes. Accordingly, the residual plots reveal a satisfactory fit. The residual values between the observed and predicted values of the study are mainly based on:

1. The measurement resolutions of the sensors used in this study are shown in Appendix 3 Information of the monitoring devices, and these resolutions contribute to the overall uncertainties as uncertainties in the independent variables.

2. The uncertainties associated with the airflow rate: Additionally, there are various operational air speeds depending on the heating/cooling demand and target zone within the house. The system's performance may also be correlated with the airflow rate, but the airflow condition inside the air duct is turbulent and unpredictable due to the structure of the air duct, resulting in a significant amount of noise in the data.

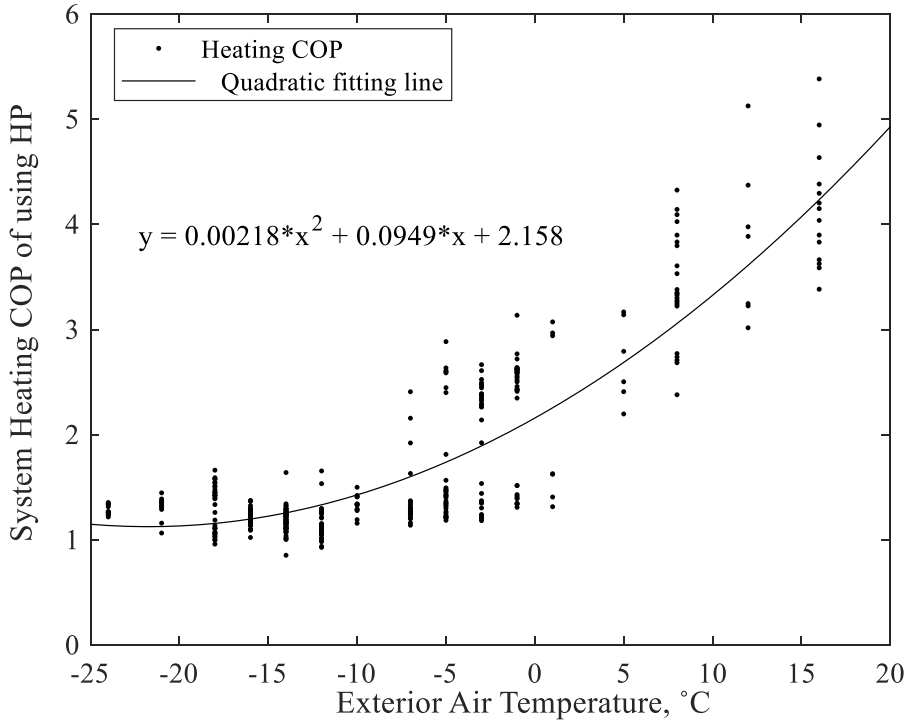

Figure 22. Hybrid energy system heating performance of operating heat pump.

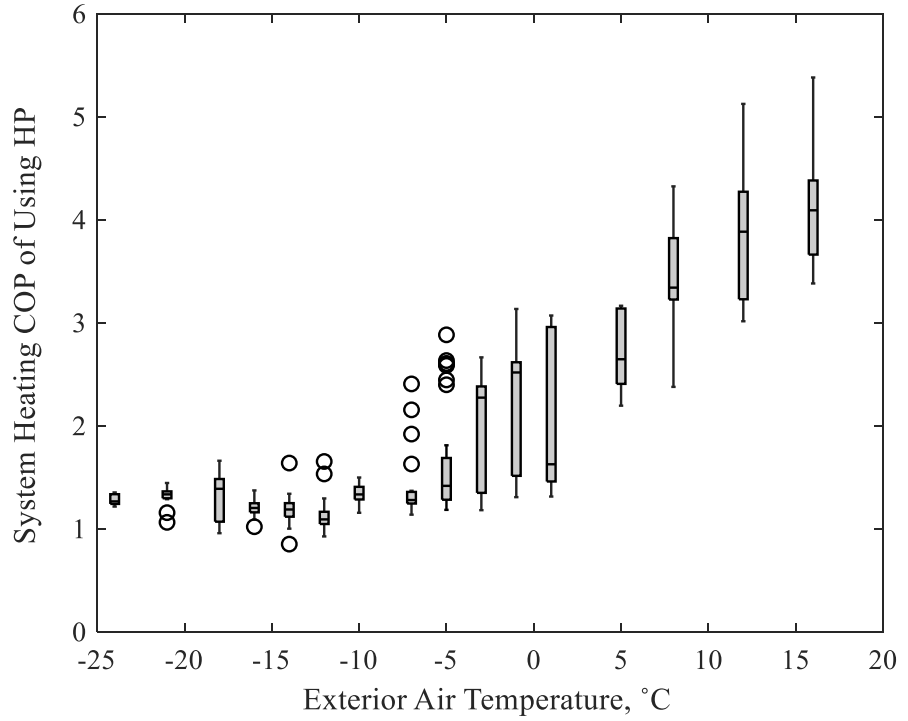

Figure 23. Box plot of the hybrid energy system heating performance of operating heat pump.

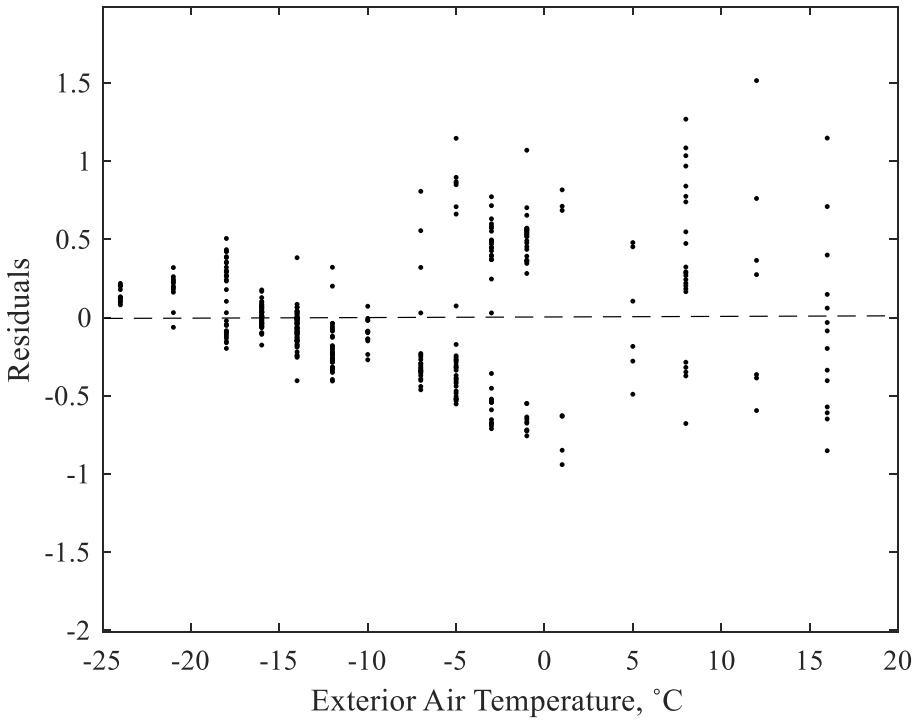

Figure 24. Residual plot of COP vs. Exterior air temperature.

Table 6 provide an analysis of the space heating performance of the natural gas tankless water heater (TWH) system. The data was collected in minute intervals, however, the TWH performance was estimated on a monthly basis due to the limitations of the natural gas meter, which records data only when there is an increment in one cubic foot of natural gas. The energy consumption for domestic hot water was determined by calculating the difference between the total household natural gas consumption and the space heating natural gas consumption. The results indicate that the system space heating performance while operating TWH varies from 0.6917 to 0.7569, with an average of 0.7305. However, the performance falls short of the annual fuel utilization rate (AFUR) for TWH on Appendix 2 Specifications of the Hybrid Energy Heating System, which is 95%, indicating that approximately 22% of energy is lost to the mechanical room during the process of heat transfer to the supply air. This could lead to the creation of a localized "hot zone"

within the residential house, which may negatively impact occupational comfort. Improving the effectiveness of the heat exchanger at the TWH ends could significantly enhance energy efficiency.

Table 6. Hybrid energy system heating performance of operating TWH.

Month	DHW natural gas consumption	TWH space heating output	TWH space heating natural gas consumption	System space heating performance
-	MJ	MJ	MJ	-
May	178.08	1278.6	1848.6	0.6917
Jun	328.6	1648.3	2280.1	0.7229
Jul	266.06	1266.4	1776.6	0.7128
Aug	253.34	950.18	1257.2	0.7558
Sep	286.2	2074.7	2741.2	0.7569
Oct	166.42	1947.9	2672.3	0.7289
Nov	242.74	4071.4	5470.7	0.7442
			Average	0.7305

3.2.4 Economical Control Strategy

Figure 25 illustrates the switching temperature selection chart of the hybrid energy system. The space heating load for the unit under investigation was determined in Figure 17 of section 3.2.1, while the heating capacity of the ASHP was provided by the manufacturer's specifications. By considering the heating performances of the system and using Eq. (3.13), the cost ratio curve can be derived as follows:

$$CR(T) = \frac{C_{elec}}{C_{ng}} = \frac{0.00218T^2 + 0.0949T + 2.158}{0.7305} \tag{3.14}$$

The purpose of this cost ratio curve is to determine the corresponding cost ratio, C_{elec}/C_{ng}, between electricity and natural gas prices for the hybrid energy heating system to determine when it should switch between the ASHP and the TWH based on the exterior air temperature, T. In the

same way, by using the known energy prices, the switching temperature can be easily obtained from the figure.

At the intersection of the space heating load and the heating capacity of the air source heat pump (ASHP), the cutoff temperature is determined. When the exterior air temperature falls below this point, the ASHP cannot provide enough heat to the house, additional heating source (TWH) will be required. In this case, the cut off temperature is observed at -22 ˚C.

The cost ratio curve obtained using the manufacturer specification is also shown in Figure 25. Additional details regarding these specifications can be found in specification can be found in Appendix 2 Specifications of the Hybrid Energy Heating System. The coefficient of determination, R^2, between these two cost ratio curves is 0.9768 within the exterior air temperature range of -22 ˚C to 8 ˚C, Indicating a significant similarity between two curves. Therefore, in the absence of comprehensive system monitoring and performance analysis, the switching temperature can be reasonably approximated using the manufacturer's specifications.

Figure 26 presents the flow chart outlining the proposed economically efficient control strategy of the hybrid heating system. Initially, the cut off temperature (T_{cut}) is identified, and the exterior air temperature (T_{ext}), current electricity and natural gas prices (C_{elec}, C_{ng}) are provided. The exterior air temperature should be then compared with the cut off temperatures using the following condition. If:

$$T_{ext} < T_{cut} \tag{3.15}$$

This condition signifies that the ASHP cannot generate sufficient heat to meet the heating requirements of the house during this period. Consequently, the system should operates the TWH for space heating.

Otherwise, if the condition is not met, the cost ratio corresponding to current exterior air temperature should be determined using Eq. (3.14), which is expressed as follows:

$$CR(T_{ext}) = \frac{0.00218{T_{ext}}^2 + 0.0949T_{ext} + 2.158}{0.7305} \tag{3.16}$$

The calculated $CR(T_{ext})$ represents the desired energy cost ratio that should be achieved if the heating system should switch between the ASHP and TWH at the given exterior air temperature, T_{ext} . Then, this desired switching temperature cost ratio should be compared with the current operating cost ratio, C_{elec}/C_{ng}, as follows:

$$\frac{C_{elec}}{C_{ng}} > CR(T_{ext}) \tag{3.17}$$

This indicates that the current cost ratio is higher than the switching cost ratio. In other words, the electricity prices are considerably higher compared to the natural gas prices. As a result, the heating system should operate TWH for space heating. Else, when the current cost ratio is less than or equal to the switching cost ratio, the system should operate ASHP for space heating.

The proposed economical control strategy can ensure the system operated with the most favorable operational energy cost. However, feasibility analysis of this control strategy is not inside the scope of this thesis and can be done in future studies; the proposed control strategy can be simulated using the monitored data of the house and compare the monthly energy cost with the existing utility bills.

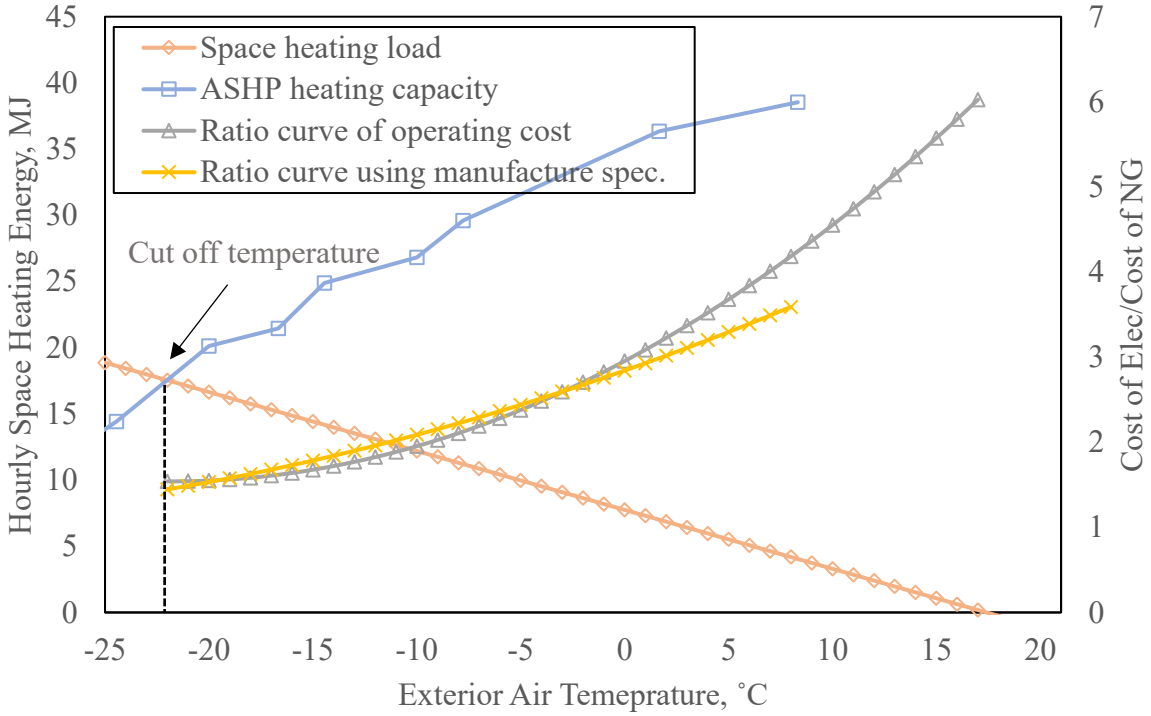

Figure 25. Switching temperature of the hybrid energy system.

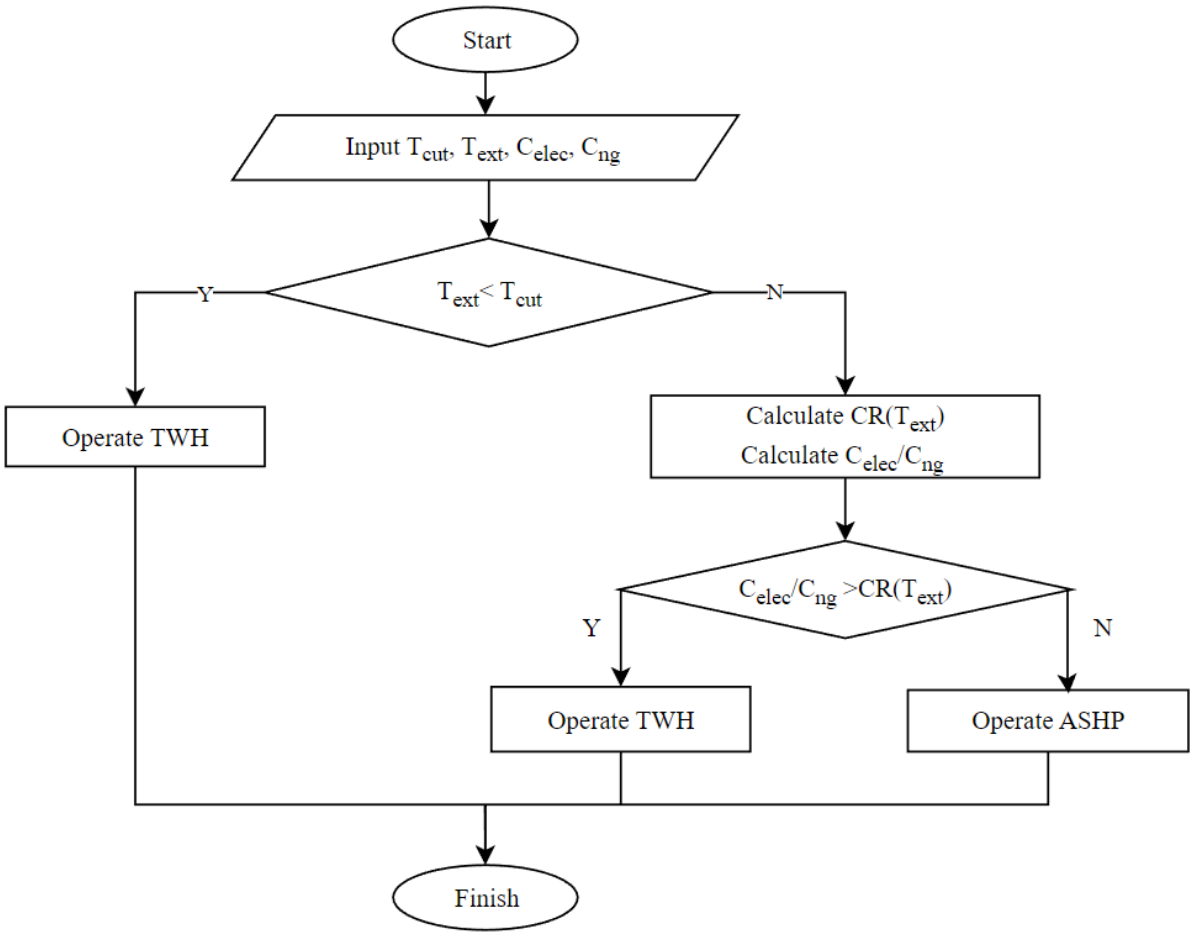

Figure 26. Flow chart of the economic efficient control strategy.

3.3 Summary

This chapter presents an analysis of the in-situ energy performance of a hybrid energy heating system. The analysis covers building energy consumption assessment, system space heating hourly output, lessons learned during monitoring, and the heating performance of the system operating both a heat pump and natural gas TWH. The hybrid energy heating system exhibits expected behavior, with lower energy consumption during summer and higher consumption during winter. Natural gas consumption for heating varies significantly with temperature changes, while

electricity consumption has relatively less variability. The monitoring also revealed issues such as phantom heat, cyclic heating and cooling, and refrigerant leakage, which necessitated operational recommendations and system improvement suggestions for increased energy efficiency and improved operation. The heating performance of the hybrid system was analyzed using monitored data. The heating COP of the heat pump ranges from 1.2 to 5.5 in the temperature range of -24 ˚C to 17 ˚C, and the average system heating efficiency for the operating natural gas TWH is 0.7305. Various factors that affect system performance are identified and discussed, and the results show potential for improvement. Moreover, an economically efficient control strategy has been proposed. The strategy takes into account the heating performance of the system and incorporates a cost ratio curve that combines the relationship between energy prices and the "switching temperature" of the system. By using the proposed curve and control strategy, the system can consistently operate with the lowest possible energy cost for the process.

CHAPTER 4 ENERGY MODELLING AND COMPARISION

The objective of this chapter is to enhance the accuracy of energy modeling outcomes by analyzing the disparities between observed energy performance and prevailing energy modeling outcomes. To achieve this goal, an artificial neural network (ANN) model of a hybrid energy heating system has been formulated by using monitoring data to forecast the real energy performance, and examines hybrid energy system performance by contrasting the results generated by HOT2000 with the practical outcomes predicted by ANN. Moreover, a comparative analysis has been performed on the monthly energy consumption and the 30-year life cycle cost of a hybrid energy system and two distinct residential energy systems.

4.1 Methodology

The following paragraphs and Figure 27 explain the methodology employed in this chapter in detail. To evaluate the accuracy of the energy modelling software (HOT2000) against actual performance, ANN models were trained with the actual performance data of the hybrid energy heating system for each duplex unit. HOT2000 software was used to perform building energy modeling by inputting the building's construction information and indoor settings. Using the temperature data from the HOT2000 weather file as input, the correlations between exterior air temperature and space heating load presented in Section 3.2.1 was employed to forecast the system's space heating output in the HOT2000 default environment. The resulted space heating output and the temperature data were then input into the trained ANN model to forecast energy performance. The results obtained from the ANN model and HOT2000 were compared to determine any differences. In addition, monthly energy consumption and life cycle cost analysis

of the hybrid energy system and two other residential energy systems were conducted using the HOT2000 model.

As part of the study conducted in this chapter, the collected data of one month for each duplex unit were cleaned to ensure the quality of the data. To train the ANN prediction model, suitable data were selected from pre-cleaned data set. ANN models were trained for each unit using the prepared data to predict the energy consumption of the hybrid energy heating system (presented in section 4.1.1). A normal distribution of the training data can make the ANN model be more effective and produce more accurate results. To achieve that, the training data has been normalized and transformed, normalization involves transforming the data within the range of 0 to 1, and transformation involves using logarithm to modify the distribution closer to a normal distribution. The optimal number of neurons in the hidden layer of the ANN model was determined using a sensitivity analysis. To advance to the next step, the models were trained for ten times and the best performing model for each unit was selected. MATLAB 2020 was used to process data and model ANNs in this chapter.

Building energy simulation was carried out using HOT2000 software, where building envelope details, mechanical and ventilation system specifications, indoor setpoint temperatures, and baseload, among other factors, were analyzed. Utilizing the input parameters and default climate data, HOT2000 determined the monthly space heating loads and energy consumption of the HVAC systems selected in HOT2000. To predict the energy consumption of the hybrid systems installed in the duplex house, while maintaining the same operating conditions, including interior and exterior conditions as used in HOT2000, a linear regression model was employed. This model was established in section 3.2.1 and used to determine the building's space heating load. The

resulting space heating output and temperature data were subsequently fed into the trained ANN model.

The ANN model resulted in the actual performance of the hybrid heating system under the same operating condition used in HOT2000, and then compare with the HOT2000 modeled results and the monitored data. Since the outcomes were based on different weather, to facilitate the comparison, the results were normalized by heating degree days. The monitored, HOT2000, and ANN data on natural gas and electricity consumption of the hybrid heating system, as well as the space heating output, were presented.

In addition, a comparison was made between the monthly energy consumption and life-cycle cost of the hybrid energy system and commonly used residential heating systems. Two additional heating systems, namely the conventional and combi boiler system, were simulated using HOT2000 software. The simulation considered using the Right Unit’s building's construction information and indoor settings, with the only difference being the heating systems used. The resulting energy consumption of the three different systems was compared. Using the Alberta average energy cost, the energy cost was determined, and along with the equipment, labor, and maintenance cost, a life-cycle cost analysis of the three different heating systems was presented.

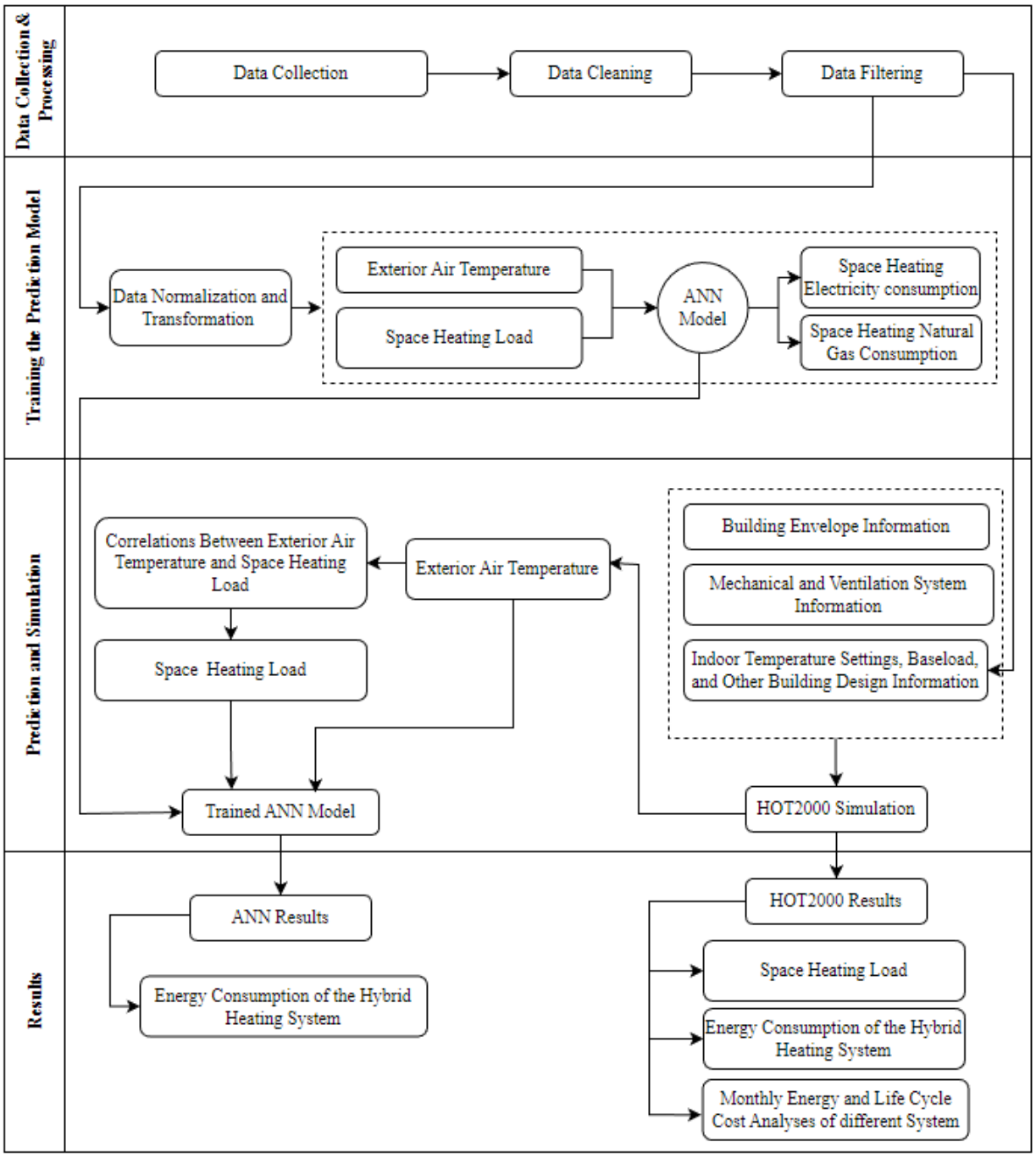

Figure 27. Flow chart of Chapter 4 methodology.

4.1.1 Data-Driven Heating Energy Consumption Prediction

4.1.1.1 Artificial Neural Network (ANN)

Artificial neural network (ANN) is a computational method inspired by biological neural networks. It was first developed by McCulloch and Pitts (1943), and has been widely used in many fields of studies due to its advantages in building non-linear relationship between the input and output variables. A fully connected feed forward network is one of the most commonly used ANN models in the case of predicting building energy consumption. The general structure of the fully connected, feed forward network is shown in Figure 28, the network is composed of an input layer, a hidden layer and an output layer, each layer contains a number of neurons. During the training process of the neural network, the synaptic weights and bias will be adjusted to generalize the targeting outputs (Da Silva et al., 2017). The relationship between input and output k-th neurons are as follows:

$$Y_k = G\left(\sum_{m=1}^{z} X_m W_{km} + b_k\right) \tag{4.1}$$

Where

Y_k: Output of the *k*-th neuron.

G: Activation function.

X_m: Input of the *m*-th neuron.

W_{km}: The weight of the connection between the m-th neuron of the input layer and k-th neuron of the hidden layer.

b_k: The bias for the k-th neuron of the hidden layer.

G: Activation function.

The activation function, G was selected as tangent sigmoid, which is a commonly used activation function, and also a default activation function in MATLAB:

$$G(x) = \frac{2}{1 + e^{-2x}} - 1 \tag{4.2}$$

The activation function plays an important role in the performance of an ANN model as it allows for the incorporation of non-linearity into the decision-making process of the network, thus enabling it to solve complex problems. The tangent sigmoid function is often utilized as it confines any input values within the range of -1 to 1. The training algorithm utilized in this study was the Levenberg-Marquardt algorithm, which has demonstrated to be the most efficient technique for training MLP networks (Hagan & Menhaj, 1994).

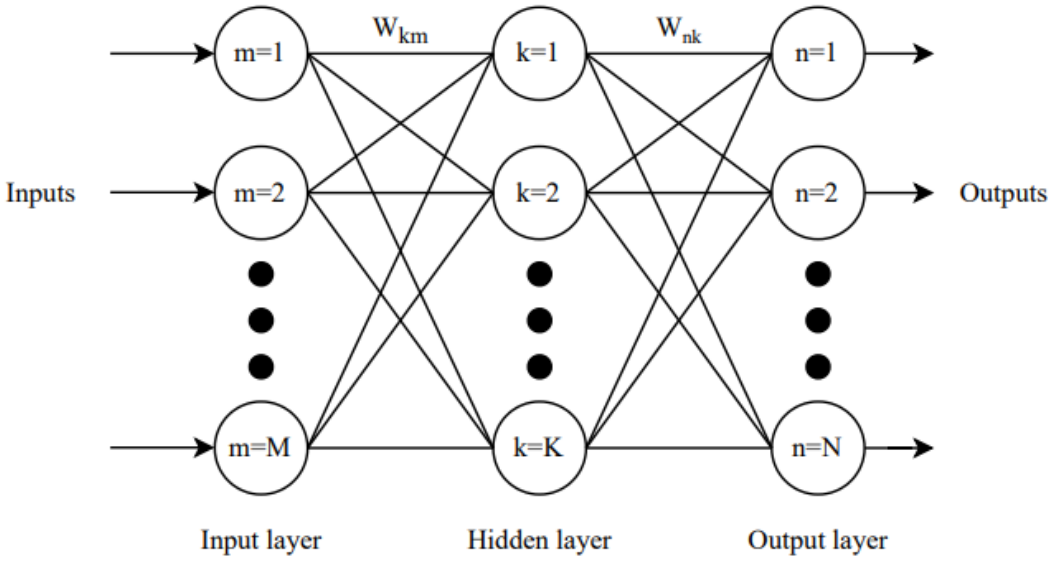

Figure 28. The structure artificial neural network.

4.1.1.2 Data Selection

The baseline model for the studied unit was developed utilizing minutely data collected during November 2021. The dataset was selected based on the availability of space heating data and its coverage of exterior air temperature ranges as extensively as possible. The original dataset was subjected to cleaning and then converted into hourly intervals to facilitate training of the MLP model, since the hourly prediction are more computationally efficient than minute-by minute predictions, while providing sufficient granularity and accuracy. The dataset prepared for training comprised hourly space heating load, space heating electricity consumption (from the air source heat pump), space heating natural gas consumption (from TWH), and exterior air temperature. The return air temperature sensor was located downstream of the heat recovery ventilator, where the return air was already mixed with fresh air from the exterior. As a result, the return air temperature in this study was not included as a significant input variable for energy consumption prediction models. Statistical information regarding the dataset is presented in Table 7, with the total number of data points available for training being 719.

Table 7. Data statistic of the right unit.

Variables	Unit	Mean	Median	Minimum	Maximum	Standard Error
Electricity Consumption of Heat Pump for Space Heating	MJ	1.74	1.63	0.00	8.39	4.171E-02
Natural Gas Consumption of TWH for Space Heating	MJ	7.09	6.89	0.00	22.26	1.41E-01
Space Heating Load	MJ	11.21	11.51	0.41	28.24	1.98E-01
Exterior Air Temperature	$^{\circ}C$	-1.60	-1.10	-16.70	10.60	1.87E-01

4.1.1.3 Data Processing

Data processing conducted for this chapter involved cleaning missing data and filling in the gaps utilizing the same methodology outlined in Section 3.1.2. Space cooling load and natural gas usage for domestic hot water were removed as it is not part of the model, and data transformation and normalization were executed. A sample code for data transformation and training of the ANN model is provided in Appendix 6.4 Training the ANN model..

The data set analyzed in this chapter contained only a small number of missing records. To fill in these gaps, the moving medium method was employed, as described in Section 3.1.2.1 The space heating load of the studied unit was calculated using Eq. (3.5), and any negative values were substituted with zeros indicating space cooling. Furthermore, the space heating natural gas consumption of the TWH and electricity consumption of the ASHP were determined from the data set using the same methodology presented in Section 3.1.2.2. The minutely data set was then transformed into an hourly interval after the cleaning process was completed.

By using the equation below, the hybrid energy system space heating output and exterior air temperature were normalized within the range of 0-1.

$$X^* = \frac{X_i - x_{min}}{x_{max} - x_{min}} \tag{4.3}$$

Heat pump space heating electricity consumption was transformed using logarithm to have the data distributed normally:

$$y^* = \log(1 + y) \tag{4.4}$$

TWH space heating natural gas consumption remained unchanged since it was already being distributed normally.

4.1.1.4 Model Structure

The ANN models were implemented using the neural network toolbox integrated in MATLAB R2022a. To facilitate comparison with HOT2000, the selection of input parameters was limited to the available default parameters of HOT2000 while ensuring acceptable performance of the ANN model. Therefore, the input layer comprised hourly system space heating output and exterior air temperature, while the output layer included hourly natural gas consumption of TWH for space heating and hourly electricity consumption of heat pump for space heating. Thus, the neural network had 2 input neurons and 2 output neurons. Based on sensitivity analysis, the ANN models were designed with 6 hidden neurons. The models were trained with various numbers of hidden neurons ranging from 1 to 30, and each configuration was run 10 times to obtain the average mean square error (MSE). Figure 29 display the average MSE of the training set and validation set for different numbers of hidden neurons for the right and left unit, respectively. MSE can be estimated by:

$$MSE = \frac{1}{n}\sum_{i=1}^{n}(\hat{y}_i - y_i)^2 \tag{4.5}$$

Where

$\hat{y}_i$: The predicted energy consumption value of the model.

y_i: The measured energy consumption value.

n: The total number of observations.

Based on the figures, it was observed that increasing the number of hidden neurons resulted in a decrease in the mean square error (MSE) of the training set and an increase in the MSE of the validation set. This indicates that the model tends to overfit as more hidden neurons are added. The optimal performance of the network was determined based on the smallest MSE of the validation set, which was achieved with 6 hidden neurons. A convergence criterion of 10^{-5} was set for the model. Within the data set, 70% of randomly selected data were used for training the baseline ANN model, and the rest of 30% of data were used to validate the accuracy of the model.

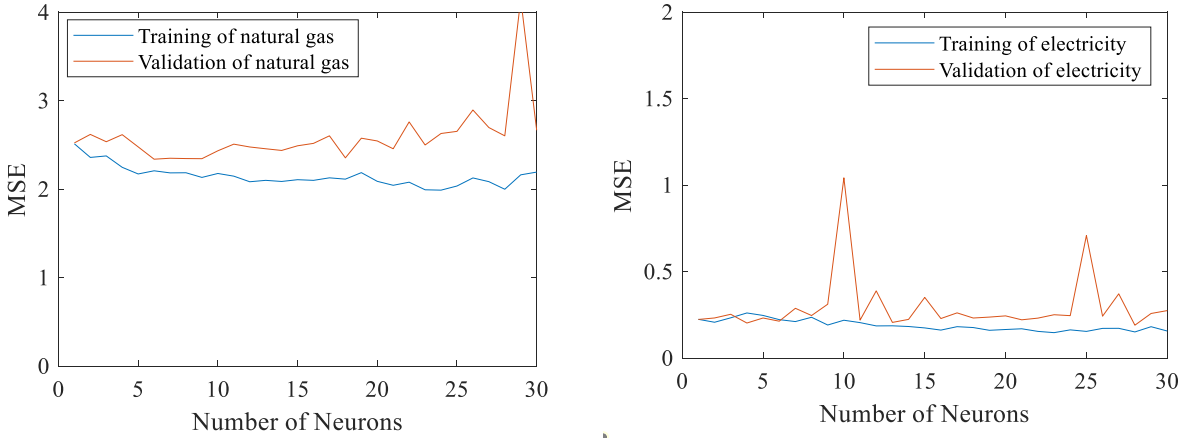

(a) (b)

Figure 29. Results of sensitivity analysis of ANN model. (a) Natural gas and (b) Electricity consumption of the system in the right unit.

4.1.1.5 Performance Evaluation

The selected ANN models were trained 10 times, and the best-trained model was chosen for comparison with the HOT2000 model, which will be discussed in Section 4.1.2. To evaluate the performance of the model, the Coefficient of Variation of the Root Mean Square Error (CVRMSE) was used. This measure is widely used to evaluate energy prediction models, as it indicates the

relative variability of the model's error compared to the mean of the measured data. The CVRMSE can be calculated using the following formula:

$$RMSE = \sqrt{\frac{1}{n}\sum_{i=1}^{n}(\hat{y}_i - y_i)^2} \tag{4.6}$$

$$CVRMSE(\%) = \frac{\sqrt{RMSE}}{\bar{y}_i} \times 100 \tag{4.7}$$

Where

$\hat{y}_i$: The predicted energy consumption value of the model.

y_i: The measured energy consumption value.

$\bar{y}_i$: The average energy consumption value.

n: The total number of observations.

4.1.2 Building Energy Simulation with HOT2000

HOT2000 is an energy simulation modeling software that has been widely used in Canada for various programs (Government of Canada, 2021), such as Home Energy Rating system, Energy Star program, and the R-2000 residential energy efficiency program (Government of Canada, 2021). The simulation of building energy consumption in this study was performed using HOT2000 version 11.10b19. The software simulates energy requirements based on building envelope information, indoor set point temperature, baseloads, air change rate, ventilation, heating and cooling system, and domestic hot water. Details of the building envelope for the studied unit

are presented in Table 9, the floor plan of the duplex house can also be found in Appendix 1 Floor Plans of the Project House.

Table 8. Building mechanical system information.

Set point temperature	22.5 C
Baseload	Right unit: 11.52 kWh/day Left unit: 14.04 kWh/day
Air change rate	Right unit: 1.09 ACH @ 50 Pa. Left unit: 0.89 ACH @ 50 Pa.
Whole-house ventilation	193 cfm
Heating system	Type 1: Combo heating/DHW, 95% AFUE Type 2: Air source heat pump, 3.4 COP@8.3 C
Domestic hot water	Controlled by combo heating system

Table 9. Building envelope information.

	Components	Structure information		Area m^2	RSI Km^2/W
Ceiling	Ceiling	Flat ceiling, heel height 0.61 m		176.3	12.51
Main walls	Exterior wall	Total length of 37.41 m		114.9	2.98
	Garage party wall	Total length of 7.15 m		21.97	3.08
	Interior party wall	Total length of 15.7 m		48.23	3.75
Exposed floors	MF overhang			2.23	4.88
Foundations	Foundation wall	Wall height 2.9 m Depth below grade 2.39 m		174.4	5.65
	Foundation header	Header height: 0.23 m		13.75	3.71
	Foundation slab			138.8	0.71
Windows	SE master living CSMT (2)	Triple glazing with single low e argon	2.29 m*2.51 m	11.5	0.73
	SE basement (2)		1.52 m*1.07 m	3.25	0.58
	SE patio (2)		1.83 m*2.62 m	9.57	0.62
	NW insert window P (1)		0.15 m*2.13 m	0.33	0.41
	NW CSMT (1)		2.26 m*2.29 m	5.17	0.72
	SW basement (2)		1.52 m*1.07 m	3.25	0.58
	SW ensuit P (1)		1.52 m*0.61 m	0.93	0.61
	SW laundry CSMT (1)		0.61 m*1.22 m	0.74	0.54
Doors	Front door	2.44 m* 0.91 m, facing NW		2.23	1.18
	Garage door	2.03 m*0.81 m, facing NW		1.65	0.88

Table 8 provides the input for the building mechanical system. The indoor thermostat set point temperature was assumed to be constant and was retrieved from the occupants of the house. The baseload was estimated using the monitored data and Eq. (3.9). The air change rate was based on the measured value. The whole house ventilation and heating system information were obtained from the homeowner information sheet and mechanical system specifications, respectively.

Other than comparing the monitored and ANN-predicted energy performance to that simulated by HOT2000, this study also compares the energy and economic efficiency of the hybrid energy system with other building energy systems based on HOT2000 simulations. We simulated three types of HVAC systems in HOT2000. The first system was the hybrid energy system studied in this research, which consisted of a TWH for space heating and DHW, and an ASHP for both space heating and cooling. The second system was a conventional energy system, consisting of a TWH for DHW, a natural gas furnace for space heating, and an AC for space cooling. The third system was a combi boiler system, which used a combi-boiler for both space heating and DHW, and an AC for space cooling. The building characteristics for the simulations were based on the right unit of the duplex house, with the same indoor HVAC settings (set point temperature, baseload, air change rate, and whole-house ventilation) as provided in Table 8. Additionally, the building envelope was identical to that shown in Table 9. The input parameters for the three different HVAC systems can be found in Table 10.

Table 10. HOT2000 HVAC system inputs of different types energy systems.

	Hybrid energy system	Conventional system	Combi-boiler system
Heating system	Type 1: Combo heating/DHW, 95% AFUE Type2: Air source heat pump, 3.4 COP@8.3 C	Natural gas furnace, 96% AFUE	Combo heating/DHW, 95% AFUE
Cooling system	Controlled by ASHP, 14 SEER	Air conditioning, 14 SEER	Air conditioning, 14 SEER
Domestic hot water	Same as the heating system	Natural gas tankless, 95% efficiency	Same as the heating system

4.1.3 Predict Hybrid System Energy Consumption under HOT2000 weather conditions

HOT2000 utilizes climate data from its weather file and user-defined building envelope thermal insulation and ventilation information to approximate the building's space heating loads. Based on mechanical system performance, the software then estimates the space heating energy consumption. To predict the practical hybrid system energy consumption within the HOT2000 framework, the weather data and corresponding space heating loads from HOT2000 were input into the best performing ANN model.

4.1.3.1 Input Processing

In section 4.1.1, an ANN model was proposed to predict the space heating energy consumption of the hybrid energy system using hourly exterior air temperature and the space heating load as inputs. HOT2000 software utilizes a 20-year average climate data from 1998 to 2017 for

simulations of houses situated in Edmonton, based on Canadian Weather Energy and Engineering Datasets (CWEEDS) (Natural Resources Canada, 2020). Thus, this 20-year average hourly exterior air temperature of November was used as one input to the ANN model, and the hourly space heating load was calculated using the regression model estimated in section 3.2.1, as follows:

$$Q_{hl} = -0.445\, T_{exterior} + 7.748 \tag{4.8}$$

Where

Q_{hl}: Space heating load of the studied unit in MJ.

$T_{exterior}$: 20-year hourly exterior air temperature of corresponding months in $^{\circ}C$.

4.1.3.2 Normalization of Energy Consumption

To facilitate comparison of the monitored, HOT2000 simulated, and ANN predicted energy consumption results, heating degree days (HDD) were used for normalization. HDD is an index of energy consumption and used in HVAC industries to quantify energy demands (D'Amico et al., 2019). The normalization based on HDD was done because the monitored data were obtained under a weather profile different from the HOT2000 weather profile. HDD is a measure of the value of the daily average temperature that falls below 18 ˚C. It can be estimated using the following equation:

$$HDD = \begin{cases} 18\,^{\circ}\mathrm{C} - \bar{T}_{exterior}, & \bar{T}_{exterior} < 18\,^{\circ}\mathrm{C} \\ 0, & \bar{T}_{exterior} \geq 18\,^{\circ}\mathrm{C} \end{cases} \tag{4.9}$$

Where

$\bar{T}_{exterior}$: Average daily exterior air temperature in $^{\circ}C$.

The space heating load and energy consumption results were normalized following Eq. (4.10):

$$E^{*} = \frac{E}{HDD} \tag{4.10}$$

Where

E: Space heating load or energy consumption in MJ.

E^{*}: Normalized space heating load or energy consumption using HDD.

4.2 Results and Discussion

4.2.1 Heating Energy Consumption Prediction

The ANN model in this study have been trained to predict the natural gas and electricity consumption of the hybrid energy space heating system using the space heating load and exterior air temperature as input.

The findings of the ANN model are presented in

Table 11 Table 11, after conducting 10 training runs with the optimal number of hidden neurons. The tables also include the CVRMSE value for the best performing model out of the 10 runs, which indicates the accuracy of the networks. Comparing the results to prior research in ANN models for building energy prediction, Edwards et al. (2012) achieved a CVRMSE of 24.32%-37.15% on heating energy consumption using hourly real data for model training, while Yun et al. (2012) achieved a CVRMSE of 23.0% - 23.3% in modeling heating energy consumption for a

residential building based on hourly data, the ANN model in this study reveal a satisfactory prediction.

Figure 30 shows a comparison between the actual and predicted natural gas and electricity consumption of the hybrid energy space heating system using the best performing model. The comparison was conducted for 100 hours. The figures indicate that the predicted values closely track the trend of the actual data, indicating a high degree of accuracy in the ANN model used in this study. Consequently, the model exhibits reliable performance.

Table 11. Results of the artificial neural networks.

		Natural gas consumption	Electricity consumption
After 10 runs	CV-RMSE(validation)	19.35%-23.05%	23.32%-34.39%
	CV-RMSE(Training)	17.89%-20.17%	23.92%-30.69%
Best performed model	CV-RMSE(validation)	19.89%	25.43%
	CV-RMSE(Training)	19.25%	23.92%

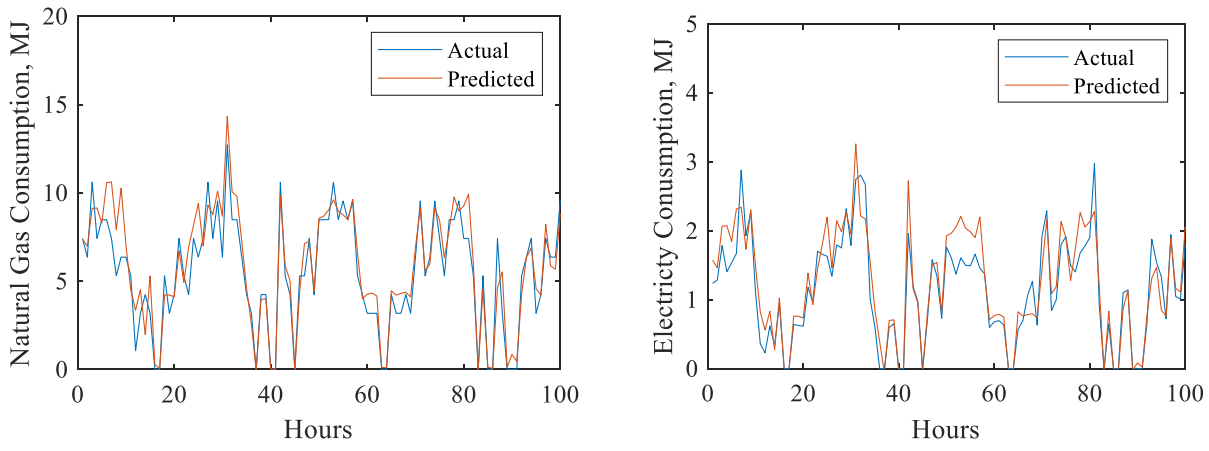

(a) (b)

Figure 30. Performance of the artificial neural network model.

4.2.2 Comparison of Modelled and Monitored Energy Performance

The temperature of the outdoor air, as recorded in the HOT2000 weather file, and the hourly space heating load, as determined by the linear regression model (Equation 4.8), were used as inputs in the most effective artificial neural network (ANN) model to anticipate the actual heating energy consumption within the HOT2000 environment. Moreover, a comparison was conducted among the energy consumption for space heating that was monitored, as well as those that were simulated by HOT2000 (referred to as "HOT2000" results in the following figures), and those produced by the ANN model (referred to as "ANN" results in the following figures).

Figure 31 display a comparison of the space heating energy consumption and space heating energy output of the studied unit among the monitored, ANN, and HOT2000 results. The monitored outcomes represent the actual performance of the system, obtained from the monitoring system. To compare the results under different weather conditions, heating degree days (HDD) with a base of 18 ˚C were used for normalization, since the monitored data was collected under different weather conditions than the ANN and HOT2000 simulations. Table 12 shows the heating degree days of the monitored weather data and HOT2000 weather data. The results were estimated based on the collected data and the 20-year average weather file of November.

Table 12. Heating degree days of monitored and HOT2000 weather file.

	Monitored weather file	HOT2000 weather file
Month	Nov	Nov
HDD	592.2	680.6

It can be seen from the figures that the HOT2000 simulated total energy consumption of the hybrid heating system is similar to the monitored energy consumption. However, the HOT2000 simulated system consumes more electricity and less natural gas. The HOT2000 simulated hybrid

heating system electricity consumption is 4.98 MJ/HDD (236.02%) more than the monitored electricity consumption, and the HOT2000 simulated hybrid heating system natural gas consumption is 5.46 MJ/HDD (59.09%) less than the monitored natural gas consumption. The HOT2000 simulated system space heating load also shows a substantial variation from the monitored result, which is 10.1 MJ/HDD (87.98%) more than the monitored result.

The above results demonstrate the difference between actual and HOT2000 simulated building energy consumption:

1. The HOT2000 simulated heating load of the house is significantly higher than the actual value, which could be attributed to uncertainties during monitoring and differences between the actual setting and HOT2000 input parameters. Furthermore, the monitoring system measures the temperature of the return and supply air to obtain the space heating output, while the heat loss from the mechanical room during fluid transfer can provide additional warmth to the house and cannot be measured. Moreover, the thermal settings may frequently change due to the occupants, and their schedules may differ from the HOT2000 input parameters.

2. The HOT2000 simulated results indicate a better system performance for the hybrid energy heating system, which diverges from the actual system. This is because the HOT2000 software uses the input manufacturer specifications for heating system components (ASHP and TWH) to calculate the energy consumption of the corresponding heating load, which performs better than the in-situ system performance (as shown in Chapter 3).

3. HOT2000 manages the operation between the heat pump and the TWH based on the heating capacity of the system. Space heating is primarily provided by the heat pump, and the TWH serves as a backup heating system to support the heat pump when it cannot meet the space heating load.

However, this mode of operation is not exactly the same as the actual system (which uses the time delay method). As a result, the TWH worked more than it was supposed to in reality, resulting in more electricity consumption and less natural gas consumption than the monitored system.

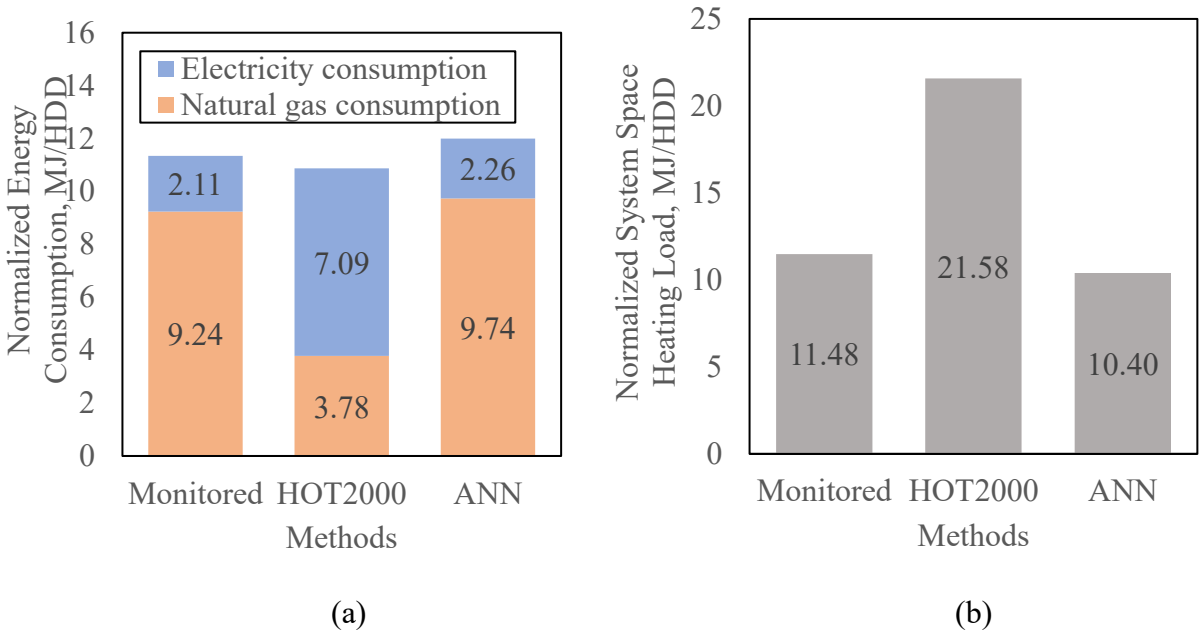

Figure 31. Comparison of monitored, HOT2000, and ANN (a) space heating energy consumption, and (b) space heating load of the studied unit.

From Figure 31, it can be observed that the total energy consumption and system space heating load predicted by the ANN model are in line with the monitored results, indicating the high accuracy of the ANN model. The electricity consumption of the hybrid heating system predicted by the ANN is slightly higher than the monitored result, by 0.15 MJ/HDD (7.11%). Similarly, the ANN predicted natural gas consumption is also slightly higher than the monitored result, by 0.5 MJ/HDD (5.41%).

The ANN's prediction for space heating load was derived from the linear regression model, which has demonstrated good performance. The ANN result differs by only 1.08 MJ/HDD (9.41%)

from the monitored results. The ANN's prediction of hybrid heating system energy consumption reveals a similar amount of normalized electricity and natural gas consumption, as well as normalized system space heating energy output. This suggests that the ANN model accurately predicts the practical energy consumption of the hybrid heating system, which optimizes the HOT2000 simulation results.

4.2.3 Monthly Energy and Life Cycle Cost Analyses Between Different Systems

This section presents a comparative analysis of three residential building energy systems modeled using HOT2000, based on their energy consumption and cost over the course of one year. The analysis takes into account both initial and operational costs and includes monitored outcomes of the hybrid energy system. The results demonstrate the superior energy efficiency of the hybrid system and provide cost comparisons with other energy systems, guiding optimal energy system selection for achieving both energy efficiency and cost savings.

Table 13. Initial costs of different types of energy systems.

	Equipment	Equipment cost CAD	Labour cost CAD	Total CAD
Hybrid energy system	TWH (combi-boiler)	4950.00	2600.00	19840.00
	ASHP	5850.00	1940.00	
	Ducting	2300.00	2200.00	
Conventional system	TWH	1500.00	450.00	13195.00
	Natural gas furnace	1500.00	2600.00	
	AC	2125.00	520.00	
	Ducting	2300.00	2200.00	
Combi-boiler system	TWH (combi-boiler)	4950.00	2600.00	14695.00
	AC	2125.00	520.00	
	Ducting	2300.00	2200.00	

Table 13 the estimated costs of three different energy systems for residential buildings, which were provided by Landmark Homes, the builder of the duplex house examined in this study. The hybrid energy system includes both a TWH and an ASHP, which can provide both space heating and DHW and space cooling, respectively. In contrast, the conventional energy system comprises a TWH for DHW, a natural gas furnace for space heating, and an AC for space cooling. The combi-boiler system utilizes a combi-boiler for space heating and DHW and an AC for space cooling, and the installation cost includes the cost of an AHU. According to the table, the installation of the hybrid energy system has the highest estimated initial cost of $19,840.00, followed by the combi-boiler system and the conventional system, respectively.

Table 14. Electricity and natural gas rates of Alberta (Government of Alberta, 2023).

	Electricity rate		Natural gas rate
	Cent/kWh	CAD/GJ	CAD/GJ
January	16.406	45.572	3.893
February	15.972	44.367	4.842
March	10.732	29.811	4.758
April	10.825	30.069	5.281
May	10.722	29.783	6.399
June	12.066	33.517	8.037
July	15.093	41.925	8.324
August	17.345	48.181	5.797
September	16.202	45.006	6.146
October	19.501	54.169	4.595
November	17.700	49.167	5.641
December	24.208	67.244	6.14

Table 14 displays the electricity and natural gas rates in Alberta (Government of Alberta, 2023). The table indicates that the electricity rates range from 29.811 CAD/GJ in March to 67.244 CAD/GJ in December, with lower rates in the spring and higher rates in the winter months. On the

other hand, the natural gas prices are lower during winter and higher during summer, showing an opposite trend to electricity rates. It is important to note that electricity prices are generally higher than natural gas prices, and both are subject to seasonal fluctuations, which can significantly impact the energy costs incurred by end-users.

Figure 32 presents a comparison of the monthly normalized electricity and natural gas consumption, along with the associated operating costs of various space heating systems. The "Monitored hybrid" category shows the observed results of the hybrid energy system in the right unit of the duplex house, while the "Hybrid" represents the simulated results of the hybrid energy system using HOT2000. Furthermore, the "Conventional" and "Combi-boiler" correspond to the simulated conventional and combi-boiler systems, respectively, also generated through HOT2000. These results are based on the monitored data of the right unit during November 2021. The total energy consumption of the hybrid energy system is lower than that of the conventional and combi-boiler systems. Based on the November energy rates, the operational costs of the conventional and combi-boiler systems are comparable, whereas the cost of operating the hybrid energy system is higher. It should be noted that the HOT2000 simulation may result in higher electricity and lower natural gas consumption than the monitored outcomes, and thus, with higher electricity prices, the "Hybrid" system may result in the highest normalized energy cost.

Figure 33 illustrates a comparison of monthly electricity and natural gas consumption for space heating, space cooling, and DHW, along with their operating costs for the three simulated energy systems. The results indicate that the hybrid energy system exhibits a significant advantage in terms of total energy consumption during the colder months, compared to the conventional and combi-boiler systems. However, during the warmer months from June to September, the energy consumption of all three systems becomes comparable. The combi-boiler system has a slightly

higher total energy consumption than the conventional system. In terms of energy costs, the simulated hybrid energy system incurs relatively higher energy costs as per the HOT2000 simulation, and only demonstrates benefits during the hottest months of June, July, and August, due to lower energy usage and relatively lower electricity prices. The total energy consumption and cost of the three different types of systems over one year are presented in Table 15.

The findings show that the hybrid energy system is more energy-efficient compared to the conventional and combi-boiler systems. However, the hybrid system requires a higher initial investment, and its operational costs may not be significantly lower due to the relatively high electricity rates and low natural gas rates in Alberta, Canada. As discussed in Section 3.2.3, the monitored performance of the hybrid energy system suggests that the coefficient of performance (COP) of the ASHP remains consistently higher than the TWH efficiency when the outdoor temperature drops below -24 ˚C. Therefore, the system can be primarily operated using the ASHP to achieve energy savings when the outdoor temperature is above -24 ˚C. Conversely, if cost savings are the priority, the system can be operated mainly using the boiler.

Table 15. Energy consumption and cost of different types of systems over one year.

	Energy consumption		Energy cost
	Electricity	Natural gas	
	MJ/year	MJ/year	CAD/year
Hybrid energy system	35828.30	42645.20	1863.44
Conventional system	6225.20	129765.30	939.96
Combi-boiler system	6250.30	131497.40	947.92

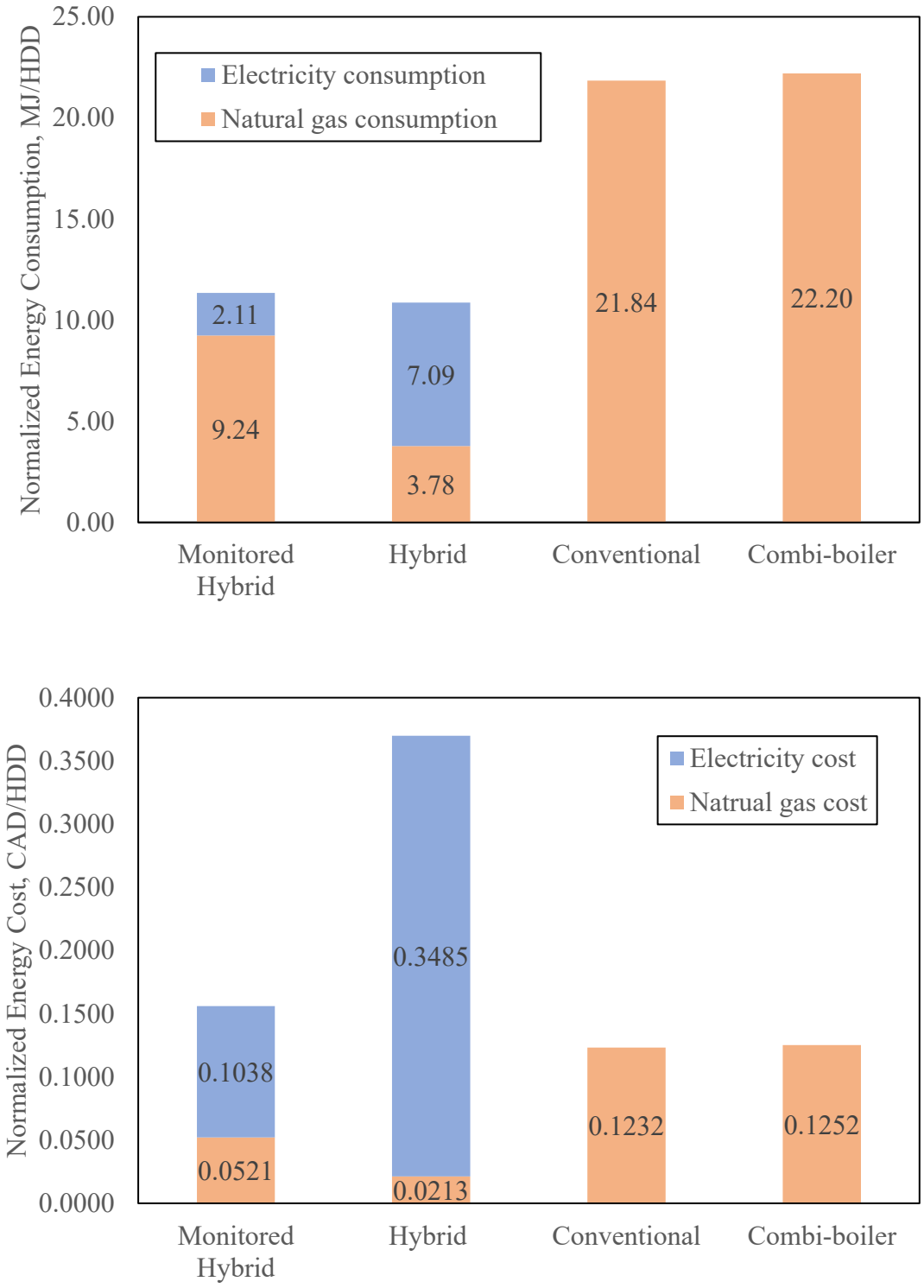

Figure 32. Normalized space heating energy consumption (top) and costs (bottom) of different systems.

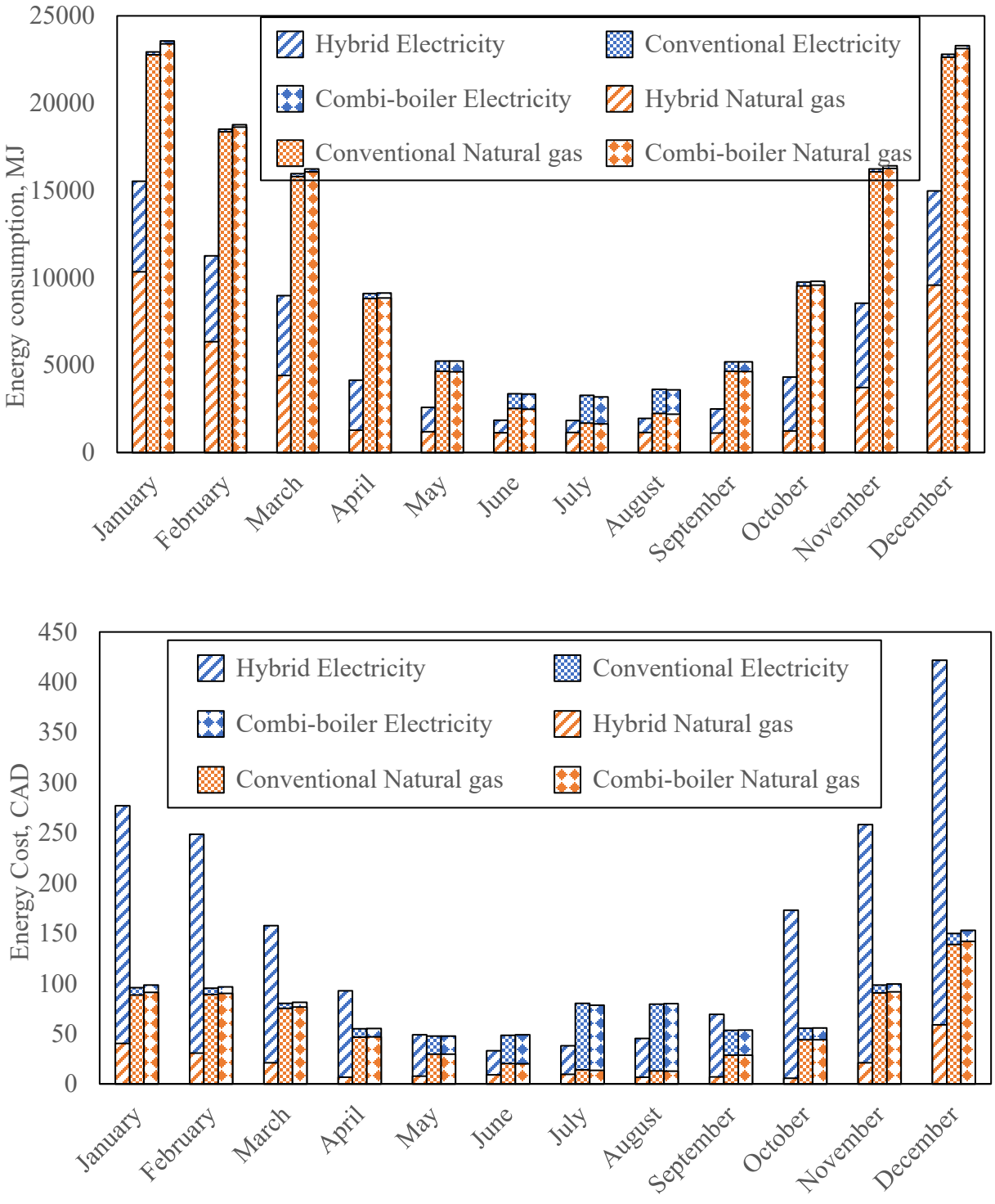

Figure 33. Energy consumption (top) and costs (bottom) comparison of different systems across various months.

Table 16 provides a list of cost parameters for each component of the system that were used in the life cycle cost analysis of this study. The analysis considered a 30-year period based on the period of the residential house mortgage. The initial cost of each component was determined from Table 13 and includes the equipment and labor costs. It was assumed that the replacement cost of each component is the same as the initial cost. The operational energy cost for each year was simulated previously by HOT2000 and includes both electricity and natural gas costs. Since it is impossible to predict the cost of repairs for each component, the maintenance cost includes yearly averaged repair, inspection, filter cleaning, or boiler flushing costs. It was also assumed that the maintenance of the system components includes the maintenance of ductwork. For ease of calculation, it was assumed that the inflation rate is the same as the interest rate. To determine the life cycle cost, LCC, of each system, the following formula was applied:

$$LCC = C_I + C_{OP} + C_M + C_R - RV \tag{4.12}$$

Where:

C_I: Initial costs

C_{OP}: Operational costs

C_M: Maintenance costs

C_R: Replacement costs

RV: Residual values.

And the residual values of components were determined as:

$$RV = C_I \frac{Remaining\ years\ of\ life}{Total\ lifespan} \tag{4.13}$$

Table 16. Cost parameters for each component of the system.

	Equipment	Initial/Replacement cost CAD	Operational energy cost CAD/year	Maintenance cost CAD/year	Lifespan year
Hybrid energy system	TWH (combi-boiler)	7550	1863.44	500	15
	ASHP	7790		300	15
	Ducting	4500		N/A	15
Conventional system	TWH	1950	938.96	200	20
	Natural gas furnace	4100		300	15
	AC	2645		200	20
	Ducting	4500		N/A	15
Combi-boiler system	TWH(combi-boiler)	7550	947.92	500	15
	AC	2645		200	20
	Ducting	4500		N/A	15

Figure 34 shows the 30-year life cycle cost of three different energy systems. The total life cycle cost was analyzed in terms of equipment cost (including initial and replacement cost), operational energy cost (electricity and natural gas), and maintenance cost. The results show that the hybrid system has the highest life cycle cost at 119,583.21 CAD, followed by the conventional system at 73,261.31 CAD and the combi-boiler system at 77,505.11 CAD. Operational energy cost is the highest cost for all three systems, with the highest cost being for the hybrid system due to the relatively expensive electricity rates. The maintenance cost is the lowest portion of the total cost for all three systems, but the hybrid energy system still has a maintenance cost of 20.07% of the total life cycle cost, which is less than the conventional (28.66%) and combi-boiler (27.09%) systems. However, the hybrid energy system's equipment cost is distinct from the conventional and combi-boiler systems, and the total life cycle cost of the hybrid system is considerably higher than that of the conventional and combi-boiler systems, mainly due to operational energy and equipment cost factors.

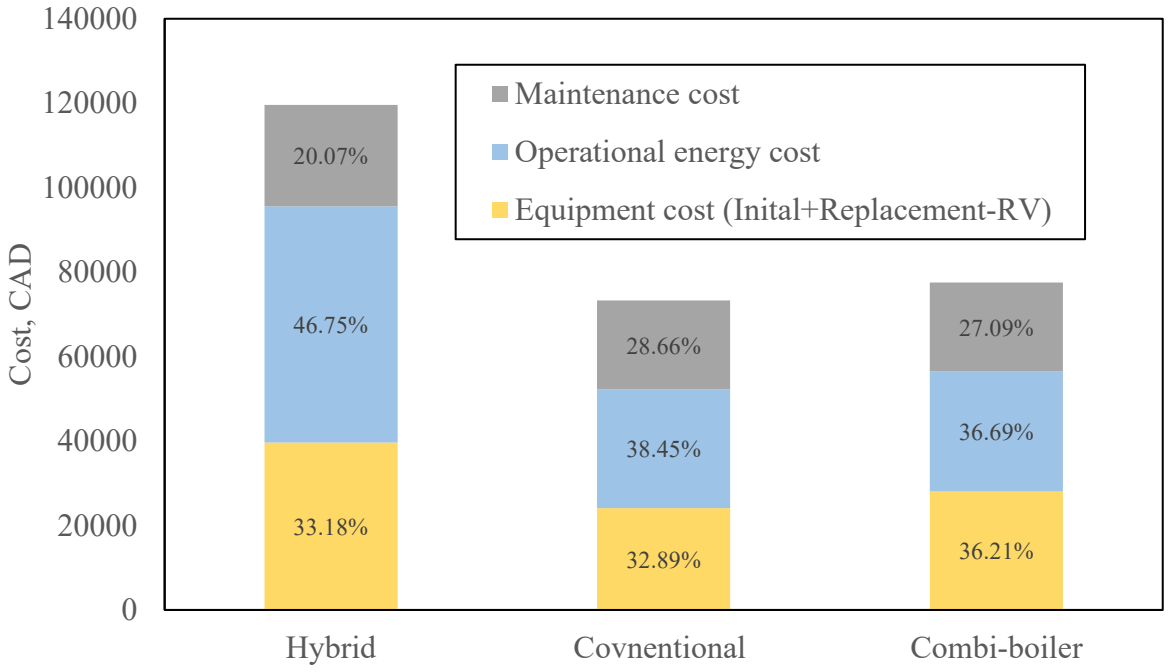

Figure 34. 30-year life cycle cost of three different energy systems.

4.3 Summary

This chapter proposes an approach to compare the performance of a hybrid energy heating system in the field with the HOT2000 building energy simulation software. To predict the actual heating energy consumption of the hybrid energy heating system, a Fully connected feed forward neural network (ANN) was used as the learning algorithm. The model was trained using one month of monitored data, and the results showed that the validation coefficient of variation were 19.89% and 25.43% for natural gas and electricity consumption, respectively.

Based upon the simulation of hybrid energy heating system energy consumption using the HOT2000 building energy simulation software, the simulation showed a relatively large difference with the monitored results of the studied unit. The simulation indicated higher space heating loads and electricity consumption, and lower natural gas consumption. These differences can be attributed to variations in occupancy schedules, thermal stat settings, and differences between the

performance of the system components as specified by the manufacturer and their actual in-situ performance. Furthermore, the differences can also be caused by the differences between default values in the simulation software and the actual conditions of the studied unit.

The Multilayer-perceptron neural network (ANN) model was utilized to estimate the actual energy consumption of the hybrid energy heating system within the HOT2000 simulation environment. The model was trained by inputting the HOT2000 default weather data and corresponding system space heating output, which was determined using linear regression. The ANN model demonstrated improved accuracy in predicting energy consumption as compared to the HOT2000 simulation results. Specifically, the electricity consumption and natural gas consumption were 7.11% and 5.41% higher than the monitored results, whereas the HOT2000 simulation indicated a difference of 236.02% and 59.09%, respectively.

This section also presents a comparative analysis of three residential building energy systems that were modeled using HOT2000, considering both energy consumption and 30-year life cycle cost. The findings indicate that the hybrid energy system is more energy efficient, but due to high local electricity prices, the operational cost of the hybrid energy system is also higher, resulting in a higher life cycle cost. Thus, to optimize the operation of the hybrid energy system, users should primarily operate the air source heat pump (ASHP) for energy savings or mainly operate the boiler for cost savings.

This study highlights the differences between simulation and monitoring in the hybrid energy heating system and proposes a methodology to compare the HOT2000 simulation results and other similar products with default weather files with the actual in-situ performance of the hybrid energy heating system. The findings could also potentially aid HOT2000 and similar products to adjust

their default parameters in the future. Furthermore, the comparative analysis confirms the advantages of the hybrid energy system in terms of energy efficiency but also highlights that there are no cost advantages in terms of energy and 30-year life cycle cost.

CHAPTER 5 CONCLUSION

This thesis aims to analyze the in-situ performance of a hybrid energy heating system, which includes a heat pump and natural gas boiler, installed in a net-zero duplex house in Alberta, Canada, a region with cold climate. The study proposes an approach to compare the in-situ performance of the hybrid energy heating system with the HOT2000 building energy simulation software. Additionally, the study conducts a comparative analysis of the studied hybrid energy heating system, a conventional heating system, and a combi-boiler heating system in terms of energy consumption and cost.

Chapter 1 provides the thesis background, including the description of the hybrid energy system and net-zero duplex house, and defines the research objective.

Chapter 2 reviews the current situation of renewable energy and residential heating energy, discusses the importance of using renewable energy in residential sectors, explores the advantages and disadvantages of existing hybrid energy source heating systems that consume renewable energy, and defines the research gap of the reviewed literatures.

Chapter 3 shows an analysis of a hybrid energy heating system's energy performance in a residential building, including consumption assessment, space heating output, and lessons learned during monitoring. The system exhibited expected behavior, with lower energy consumption in summer and higher consumption in winter. However, issues such as phantom heat, cyclic heating and cooling, and refrigerant leakage were identified, leading to suggestions for improved energy efficiency and operation. The heating performance of the hybrid system was also analyzed, from the heating performance, an economically efficiency control strategy was proposed, including a switching temperature selection chart based on cost ratio of electricity and natural gas. The

proposed control strategy ensures the most favorable energy const during the operation of the system.

Chapter 4 propose a methodology for comparing the performance of a hybrid energy heating system with HOT2000 building energy simulation software. An ANN model was used to estimate the actual energy consumption of the hybrid energy heating system within the HOT2000 simulation environment. The ANN model demonstrated potential improvement of accuracy in HOT2000's prediction of energy consumption as compared to the HOT2000 simulation results. A comparative analysis of three residential building energy systems, considering both energy consumption and 30-year life cycle cost, showed that the hybrid energy system is more energy efficient, but has a higher operational cost, resulting in a higher life cycle cost. This chapter highlights the discrepancies between simulation and monitoring in the hybrid energy heating system and proposes a methodology for comparing the HOT2000 simulation results with the actual in-situ performance of the system, with potential for adjusting default parameters in the future.

The present study is subject to several limitations, which include:

1. Potential errors in sensor measurements,
2. Insufficient indoor set point temperature data.
3. Inadequate data for whole year analysis of the heating system
4. A limited number of experiment houses for comparison
5. Possible inaccuracies in the HOT2000 and ANN models.

To overcome these limitations in future research, the monitoring system can be improved with high-quality sensors to minimize instrument error, and more indoor information such as the thermostat set point temperature and occupancy schedule can be collected. Data collection can be extended to cover an entire year, and the system can be implemented in a greater number of houses

for analysis. Additionally, the average of typical results can contribute to the improvement of the default values of the HOT2000 software. Furthermore, a more detailed investigation of the physical properties and indoor settings (e.g., hot water temperatures) can be conducted to contribute to a more accurate HOT2000 model. Adjusting the inputs and improving data processing can help to enhance the accuracy of the ANN model.

REFERENCES

Abou-Ziyan, H., Ahmed, M., Metwally, M., & Abd El-Hameed, H. (1997). Solar-assisted R22 and R134a heat pump systems for low-temperature applications. *Applied Thermal Engineering, 17*(5), 455-469.

Ahmad, A. S., Hassan, M. Y., Abdullah, M. P., Rahman, H. A., Hussin, F., Abdullah, H., & Saidur, R. (2014). A review on applications of ANN and SVM for building electrical energy consumption forecasting. *Renewable and Sustainable Energy Reviews, 33*, 102-109. doi:https://doi.org/10.1016/j.rser.2014.01.069

Al-Homoud, M. S. (2001). Computer-aided building energy analysis techniques. *Building and Environment, 36*(4), 421-433. doi:https://doi.org/10.1016/S0360-1323(00)00026-3

Amasyali, K., & El-Gohary, N. M. (2018). A review of data-driven building energy consumption prediction studies. *Renewable and Sustainable Energy Reviews, 81*, 1192-1205. doi:10.1016/j.rser.2017.04.095

Bagnasco, A., Fresi, F., Saviozzi, M., Silvestro, F., & Vinci, A. (2015). Electrical consumption forecasting in hospital facilities: An application case. *Energy and Buildings, 103*, 261-270. doi:10.1016/j.enbuild.2015.05.056

Bakirci, K., & Yuksel, B. (2011). Experimental thermal performance of a solar source heat-pump system for residential heating in cold climate region. *Applied Thermal Engineering, 31*(8-9), 1508-1518.

Banister, C. J., & Collins, M. R. (2015). Development and performance of a dual tank solar-assisted heat pump system. *Applied Energy, 149*, 125-132. doi:https://doi.org/10.1016/j.apenergy.2015.03.130

Barnaby, C. S., & Spitler, J. D. (2005). Development of the Residential Load Factor Method for Heating and Cooling Load Calculations. *ASHRAE Transactions, 111*(1).

Bauer, M., & Scartezzini, J.-L. (1998). A simplified correlation method accounting for heating and cooling loads in energy-efficient buildings. *Energy and Buildings, 27*(2), 147-154.

Bilous, I., Deshko, V., & Sukhodub, I. (2018). Parametric analysis of external and internal factors influence on building energy performance using non-linear multivariate regression models. *Journal of Building Engineering, 20*, 327-336.

Chen, J., & Yu, J. (2017). Theoretical analysis on a new direct expansion solar assisted ejector-compression heat pump cycle for water heater. *Solar Energy, 142*, 299-307. doi:10.1016/j.solener.2016.12.043

Chyng, J. P., Lee, C. P., & Huang, B. J. (2003). Performance analysis of a solar-assisted heat pump water heater. *Solar Energy, 74*(1), 33-44. doi:https://doi.org/10.1016/S0038-092X(03)00110-5

Ciulla, G., & D'Amico, A. (2019). Building energy performance forecasting: A multiple linear regression approach. *Applied Energy, 253*, 113500.

D'Amico, A., Ciulla, G., Panno, D., & Ferrari, S. (2019). Building energy demand assessment through heating degree days: The importance of a climatic dataset. *Applied Energy, 242*, 1285-1306.

da Cunha, J. P., & Eames, P. (2018). Compact latent heat storage decarbonisation potential for domestic hot water and space heating applications in the UK. *Applied Thermal Engineering, 134*, 396-406. doi:10.1016/j.applthermaleng.2018.01.120

Da Silva, I. N., Spatti, D. H., Flauzino, R. A., Liboni, L. H. B., & dos Reis Alves, S. F. (2017). Artificial neural networks. *Cham: Springer International Publishing, 39*.
De Rosa, M., Bianco, V., Scarpa, F., & Tagliafico, L. A. (2014). Heating and cooling building energy demand evaluation; a simplified model and a modified degree days approach. *Applied Energy, 128*, 217-229.
De Rosa, M., Brennenstuhl, M., Andrade Cabrera, C., Eicker, U., & Finn, D. P. (2019). An iterative methodology for model complexity reduction in residential building simulation. *Energies, 12*(12), 2448.
Deng, W., & Yu, J. (2016). Simulation analysis on dynamic performance of a combined solar/air dual source heat pump water heater. *Energy Conversion and Management, 120*, 378-387. doi:https://doi.org/10.1016/j.enconman.2016.04.102
Deru, M., Judkoff, R., & Neymark, J. (2002). *Whole-building energy simulation with a three-dimensional ground-coupled heat transfer model*. Retrieved from
Edwards, R. E., New, J., & Parker, L. E. (2012). Predicting future hourly residential electrical consumption: A machine learning case study. *Energy and Buildings, 49*, 591-603. doi:https://doi.org/10.1016/j.enbuild.2012.03.010
Esen, H., Esen, M., & Ozsolak, O. (2015). Modelling and experimental performance analysis of solar-assisted ground source heat pump system. *Journal of Experimental & Theoretical Artificial Intelligence, 29*(1), 1-17. doi:10.1080/0952813x.2015.1056242
Facão, J., & Carvalho, M. J. (2014). New test methodologies to analyse direct expansion solar assisted heat pumps for domestic hot water. *Solar Energy, 100*, 66-75. doi:https://doi.org/10.1016/j.solener.2013.11.025
González, P. A., & Zamarreño, J. M. (2005). Prediction of hourly energy consumption in buildings based on a feedback artificial neural network. *Energy and Buildings, 37*(6), 595-601. doi:10.1016/j.enbuild.2004.09.006
Government of Alberta. (2023). Regulated Rates-Year at a Glance. Retrieved from https://ucahelps.alberta.ca/regulated-rates.aspx
Government of Canada. (2021). Tools for industry professionals. Retrieved from https://www.nrcan.gc.ca/energy-efficiency/homes/professional-opportunities/tools-industry-professionals/20596
Hagan, M. T., & Menhaj, M. B. (1994). Training feedforward networks with the Marquardt algorithm. *IEEE Transactions on Neural Networks, 5*(6), 989-993. doi:10.1109/72.329697
Hou, Z., Lian, Z., Yao, Y., & Yuan, X. (2006). Cooling-load prediction by the combination of rough set theory and an artificial neural-network based on data-fusion technique. *Applied Energy, 83*(9), 1033-1046. doi:10.1016/j.apenergy.2005.08.006
Huang, B. J., & Lee, C. P. (2007). Performance evaluation method of solar-assisted heat pump water heater. *Applied Thermal Engineering, 27*(2), 568-575. doi:https://doi.org/10.1016/j.applthermaleng.2006.06.005
Huang, B. J., Lee, J. P., & Chyng, J. P. (2005). Heat-pipe enhanced solar-assisted heat pump water heater. *Solar Energy, 78*(3), 375-381. doi:https://doi.org/10.1016/j.solener.2004.08.009
HVS Series Variable speed Heat Pump Brochure. (2022). Retrieved from https://hi-velocity.com/en/hvs/Brochure-HVS-Variable-Speed-Heat-Pump-111020.pdf
Jain, R. K., Smith, K. M., Culligan, P. J., & Taylor, J. E. (2014). Forecasting energy consumption of multi-family residential buildings using support vector regression:

Investigating the impact of temporal and spatial monitoring granularity on performance accuracy. *Applied Energy, 123*, 168-178.
Justusson, B. I. (1981). Median Filtering: Statistical Properties. In *Two-Dimensional Digital Signal Prcessing II: Transforms and Median Filters* (pp. 161-196). Berlin, Heidelberg: Springer Berlin Heidelberg.
Kaygusuz, K. l. (1999a). Investigation of a combined solar–heat pump system for residential heating. Part 1: experimental results. *International Journal of Energy Research, 23*(14), 1213-1223.
Kaygusuz, K. l. (1999b). Investigation of a combined solar–heat pump system for residential heating. Part 2: simulation results. *International Journal of Energy Research, 23*(14), 1225-1237.
Klein, K., Huchtemann, K., & Müller, D. (2014). Numerical study on hybrid heat pump systems in existing buildings. *Energy and Buildings, 69*, 193-201. doi:10.1016/j.enbuild.2013.10.032
Kong, X. Q., Zhang, D., Li, Y., & Yang, Q. M. (2011). Thermal performance analysis of a direct-expansion solar-assisted heat pump water heater. *Energy, 36*(12), 6830-6838. doi:https://doi.org/10.1016/j.energy.2011.10.013
Korolija, I., Zhang, Y., Marjanovic-Halburd, L., & Hanby, V. I. (2013). Regression models for predicting UK office building energy consumption from heating and cooling demands. *Energy and Buildings, 59*, 214-227.
Kwok, S. S. K., Yuen, R. K. K., & Lee, E. W. M. (2011). An intelligent approach to assessing the effect of building occupancy on building cooling load prediction. *Building and Environment, 46*(8), 1681-1690. doi:10.1016/j.buildenv.2011.02.008
Landmark Homes. (2023). Retrieved from https://www.landmarkhomes.ca/edmonton/new-luxury-homes/larch12/
Li, F., Zheng, G., & Tian, Z. (2013). Optimal operation strategy of the hybrid heating system composed of centrifugal heat pumps and gas boilers. *Energy and Buildings, 58*, 27-36. doi:https://doi.org/10.1016/j.enbuild.2012.09.044
Li, G. (2018). Parallel loop configuration for hybrid heat pump – gas fired water heater system with smart control strategy. *Applied Thermal Engineering, 138*, 807-818. doi:https://doi.org/10.1016/j.applthermaleng.2018.04.087
Li, G., & Du, Y. (2018). Performance investigation and economic benefits of new control strategies for heat pump-gas fired water heater hybrid system. *Applied Energy, 232*, 101-118. doi:10.1016/j.apenergy.2018.09.065
Li, H., Campana, P. E., Tan, Y., & Yan, J. (2018). Feasibility study about using a stand-alone wind power driven heat pump for space heating. *Applied Energy, 228*, 1486-1498.
Li, Q.-Y., Chen, Q., & Zhang, X. (2013). Performance analysis of a rooftop wind solar hybrid heat pump system for buildings. *Energy and Buildings*, 75-83.
Li, S., Li, S., & Zhang, X. (2015). Comparison analysis of different refrigerants in solar-air hybrid heat source heat pump water heater. *International Journal of Refrigeration, 57*, 138-146. doi:https://doi.org/10.1016/j.ijrefrig.2015.05.008
Li, Y. W., Wang, R. Z., Wu, J. Y., & Xu, Y. X. (2007). Experimental performance analysis on a direct-expansion solar-assisted heat pump water heater. *Applied Thermal Engineering, 27*(17), 2858-2868. doi:https://doi.org/10.1016/j.applthermaleng.2006.08.007

Li, Z., Han, Y., & Xu, P. (2014). Methods for benchmarking building energy consumption against its past or intended performance: An overview. *Applied Energy, 124*, 325-334. doi:https://doi.org/10.1016/j.apenergy.2014.03.020

Liu, Y., Ma, J., Zhou, G., Zhang, C., & Wan, W. (2016). Performance of a solar air composite heat source heat pump system. *Renewable Energy, 87*, 1053-1058.

McCulloch, W. S., & Pitts, W. (1943). A logical calculus of the ideas immanent in nervous activity. *The bulletin of mathematical biophysics, 5*(4), 115-133. doi:10.1007/BF02478259

Natural Resources Canada. (2016). Energy Efficiency Trends in Canada. Retrieved from https://www.nrcan.gc.ca/sites/www.nrcan.gc.ca/files/energy/pdf/trends2013.pdf

Natural Resources Canada. (2017a). Ablout Renewable Energy. Retrieved from https://www.nrcan.gc.ca/our-natural-resources/energy-sources-distribution/renewable-energy/about-renewable-energy/7295#what

Natural Resources Canada. (2017b). Energy Use in the Residential Sector. Retrieved from https://oee.nrcan.gc.ca/publications/statistics/trends/2017/residential.cfm

Natural Resources Canada. (2019a). Residential Sector Canada Table 7: Space Heating Secondary Energy Use and GHG Emissions by Energy Source. Retrieved from https://oee.nrcan.gc.ca/corporate/statistics/neud/dpa/showTable.cfm?type=CP&sector=res&juris=ca&rn=7&page=0

Natural Resources Canada. (2019b). Residential Sector Canada Table 14: Water Heating Secondary Energy Use and GHG Emissions by Energy Source. Retrieved from https://oee.nrcan.gc.ca/corporate/statistics/neud/dpa/showTable.cfm?type=CP&sector=res&juris=ca&rn=14&page=0

Natural Resources Canada. (2020). HOT2000 Climate Map. Retrieved from https://open.canada.ca/data/en/dataset/4672733b-bbb6-4299-a57f-f19ab475ac11

NCB-E Series Combination Boilers Technical Data Sheet. (2022). Retrieved from https://www.navieninc.com/downloads/spec-sheet-ncb-e-series-en

Ozgener, O. (2010). Use of solar assisted geothermal heat pump and small wind turbine systems for heating agricultural and residential buildings. *Energy, 35*(1), 262-268.

Papakostas, K. T., Michopoulos, A. K., & Kyriakis, N. A. (2009). Equivalent full-load hours for estimating heating and cooling energy requirements in buildings: Greece case study. *Applied Energy, 86*(5), 757-761. doi:https://doi.org/10.1016/j.apenergy.2008.10.017

Park, H., Nam, K. H., Jang, G. H., & Kim, M. S. (2014). Performance investigation of heat pump–gas fired water heater hybrid system and its economic feasibility study. *Energy and Buildings, 80*, 480-489. doi:10.1016/j.enbuild.2014.05.052

Ran, S., Li, X., Xu, W., & Wang, B. (2020). A solar-air hybrid source heat pump for space heating and domestic hot water. *Solar Energy, 199*, 347-359.

Sichilalu, S., Tazvinga, H., & Xia, X. (2016). Optimal control of a fuel cell/wind/PV/grid hybrid system with thermal heat pump load. *Solar Energy, 135*, 59-69.

Solar Eenergy Maps Canada. (2020). Retrieved from https://www.energyhub.org/solar-energy-maps-canada/

Solomon, D. M., Winter, R. L., Boulanger, A. G., Anderson, R. N., & Wu, L. L. (2011). Forecasting energy demand in large commercial buildings using support vector machine regression.

Sookoor, T., Holben, B., & Whitehouse, K. (2013). Feasibility of retrofitting centralized HVAC systems for room-level zoning. *Sustainable Computing: Informatics and Systems, 3*(3), 161-171.

Spandagos, C., & Ng, T. L. (2017). Equivalent full-load hours for assessing climate change impact on building cooling and heating energy consumption in large Asian cities. *Applied Energy, 189*, 352-368.

Statistics Canada. (2022, 2022-05-02). Household energy consumption, by type of dwelling, Canada and Provinces.

Sun, X., Dai, Y., Novakovic, V., Wu, J., & Wang, R. (2015). Performance Comparison of Direct Expansion Solar-assisted Heat Pump and Conventional Air Source Heat Pump for Domestic Hot Water. *Energy Procedia, 70*, 394-401. doi:https://doi.org/10.1016/j.egypro.2015.02.140

Treichel, C., & Cruickshank, C. A. (2021a). Economic analysis of heat pump water heaters coupled with air-based solar thermal collectors in Canada and the United States. *Journal of Building Engineering, 35*, 102034. doi:https://doi.org/10.1016/j.jobe.2020.102034

Treichel, C., & Cruickshank, C. A. (2021b). Energy analysis of heat pump water heaters coupled with air-based solar thermal collectors in Canada and the United States. *Energy, 221*, 119801. doi:https://doi.org/10.1016/j.energy.2021.119801

U.S EIA. (2022). Renewable energy explained. Retrieved from https://www.eia.gov/energyexplained/renewable-sources/

U.S. EIA. (2021). International Energy Outlook 2021. Retrieved from https://www.eia.gov/outlooks/ieo/consumption/sub-topic-01.php

Wang, J., Liu, J., Li, C., Zhou, Y., & Wu, J. (2020). Optimal scheduling of gas and electricity consumption in a smart home with a hybrid gas boiler and electric heating system. *Energy, 204*, 117951. doi:https://doi.org/10.1016/j.energy.2020.117951

Westergren, K.-E., Högberg, H., & Norlén, U. (1999). Monitoring energy consumption in single-family houses. *Energy and Buildings, 29*(3), 247-257.

Wind Energy in Canada. (2019). Retrieved from https://www.nrcan.gc.ca/energy/renewable-electricity/wind/7323

Xing-Ping, Z., & Rui, G. (2007). Electrical energy consumption forecasting based on cointegration and a support vector machine in China. *Wseas transactions on mathematics, 6*, 878-883.

Yang, L. W., Xu, R. J., Hua, N., Xia, Y., Zhou, W. B., Yang, T., . . . Wang, H. S. (2021). Review of the advances in solar-assisted air source heat pumps for the domestic sector. *Energy Conversion and Management, 247*, 114710. doi:https://doi.org/10.1016/j.enconman.2021.114710

Youssef, W., Ge, Y. T., & Tassou, S. A. (2017). Effects of latent heat storage and controls on stability and performance of a solar assisted heat pump system for domestic hot water production. *Solar Energy, 150*, 394-407. doi:10.1016/j.solener.2017.04.065

Yun, K., Luck, R., Mago, P. J., & Cho, H. (2012). Building hourly thermal load prediction using an indexed ARX model. *Energy and Buildings, 54*, 225-233. doi:https://doi.org/10.1016/j.enbuild.2012.08.007

Zhang, C., Zhao, X., & Zhou, G. (2011). *The Studying of the Operation Mode of the Solar-Air Dual-Source Heat Pump.* Paper presented at the 2011 Asia-Pacific Power and Energy Engineering Conference.

Zhang, D., Wu, Q. B., Li, J. P., & Kong, X. Q. (2014). Effects of refrigerant charge and structural parameters on the performance of a direct-expansion solar-assisted heat pump system. *Applied Thermal Engineering, 73*(1), 522-528. doi:https://doi.org/10.1016/j.applthermaleng.2014.07.077

Zhao, H.-x., & Magoulès, F. (2012). A review on the prediction of building energy consumption. *Renewable and Sustainable Energy Reviews, 16*(6), 3586-3592. doi:10.1016/j.rser.2012.02.049

Zhu, L., Yu, J., Zhou, M., & Wang, X. (2014). Performance analysis of a novel dual-nozzle ejector enhanced cycle for solar assisted air-source heat pump systems. *Renewable Energy, 63*, 735-740. doi:https://doi.org/10.1016/j.renene.2013.10.030

APPENDICES

Appendix 1 Floor Plans of the Project House

This appendix section shows the construction drawing of the studied duplex house. The floor plan of the main floor can be found in Figure 35 and the floor plan of the basement can be found in Figure 36. The house is facing northwest and has a double car garage attached in the front for each unit, the basement is a daylight basement, fully underground with window wells. Both units contain three bedrooms, one den, two living rooms, one kitchen, and three bathrooms.

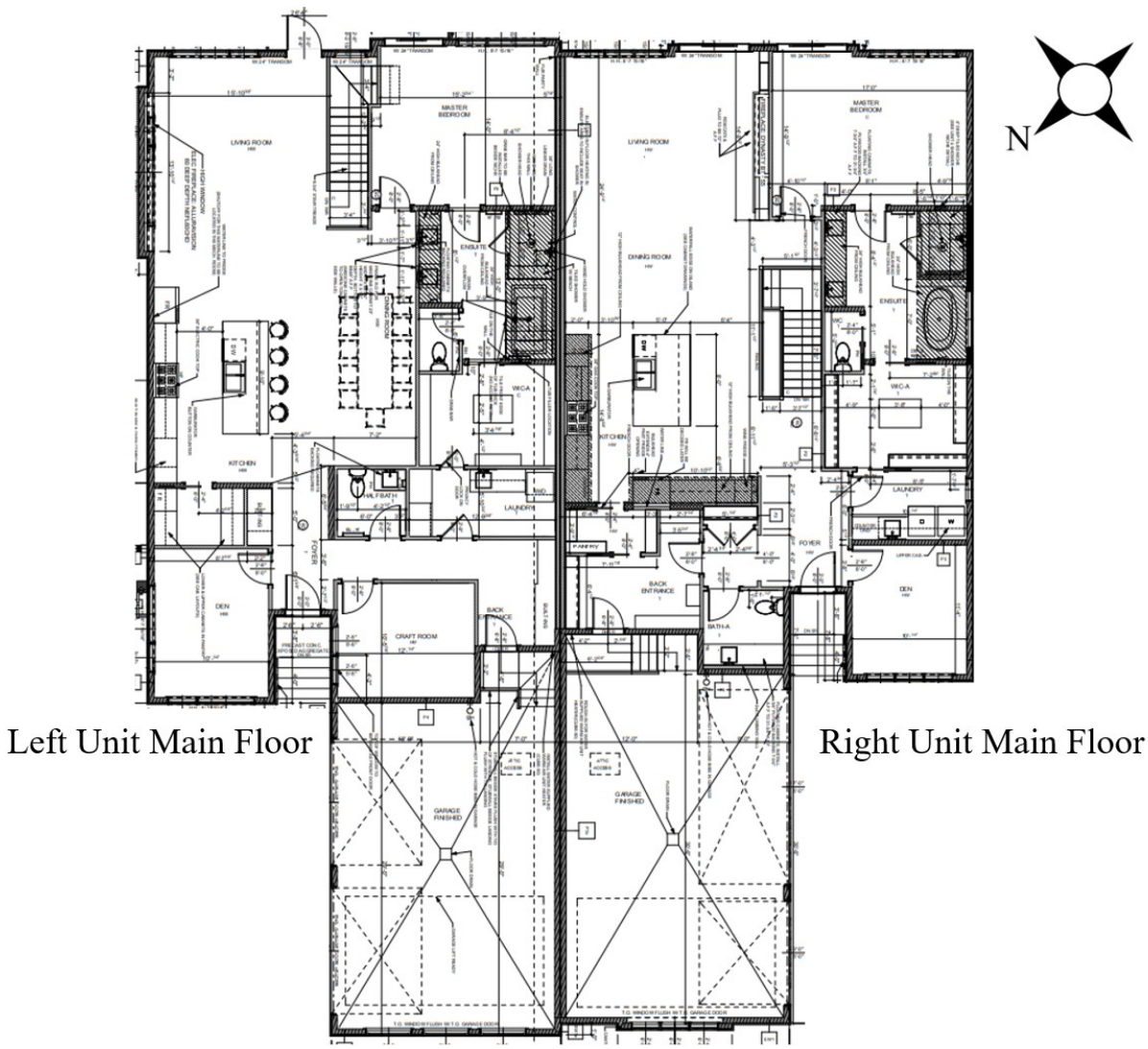

Figure 35. Floor plan of the studied house (main floor).

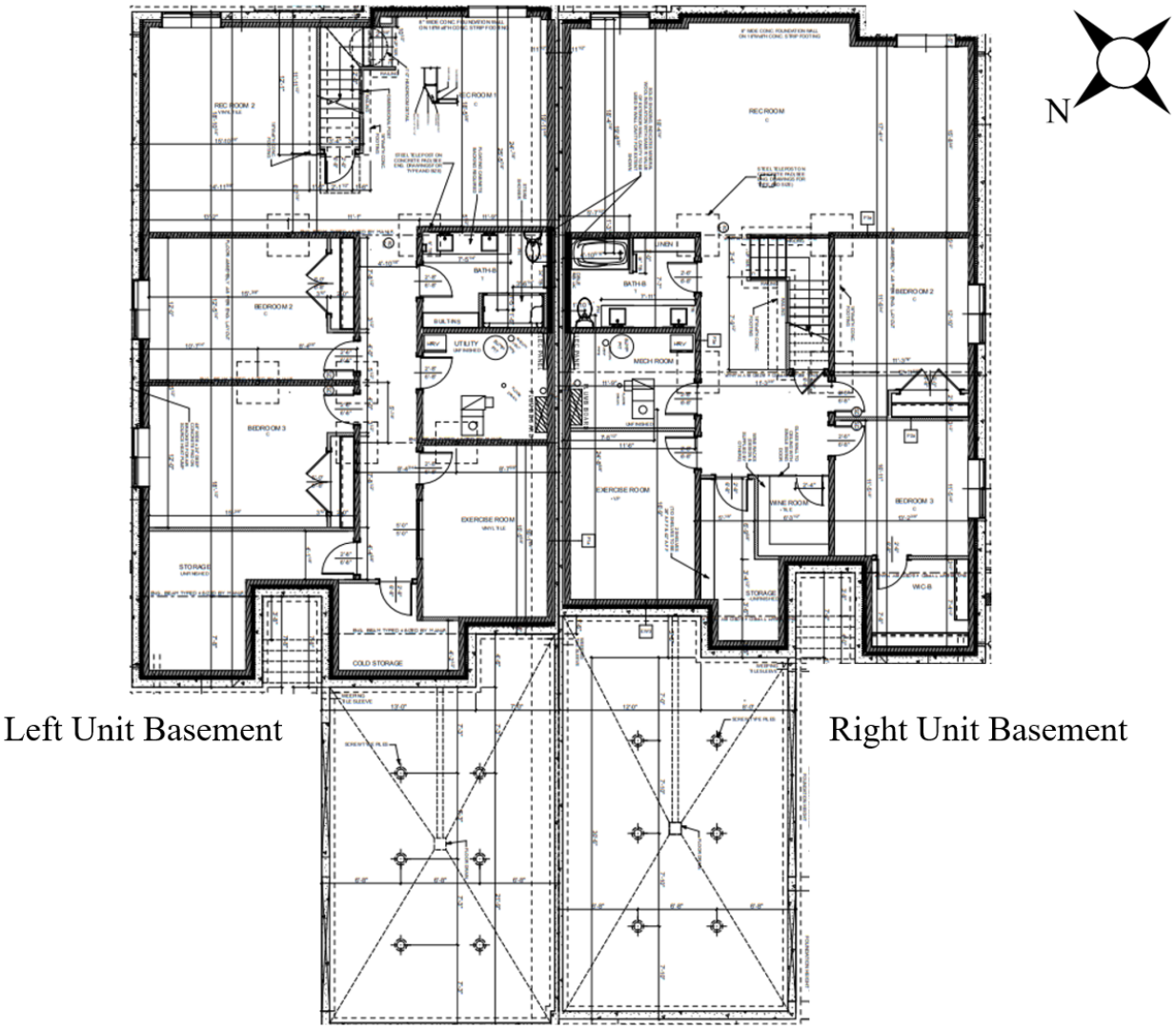

Figure 36. Floor plan of the studied house (basement).

Appendix 2 Specifications of the Hybrid Energy Heating System

This appendix section shows the specifications of the hybrid energy heating system, including the air handling unit (AHU), Heat pump, and the tankless water heater (TWH). For the studied system, the model of the AHU is HE-Z 70, shows in Figure 37, the model of the heat pump is ESP-10, shows in Figure 38 and Figure 39, and the model of the TWH is NCB-240E, shows in Figure 40.

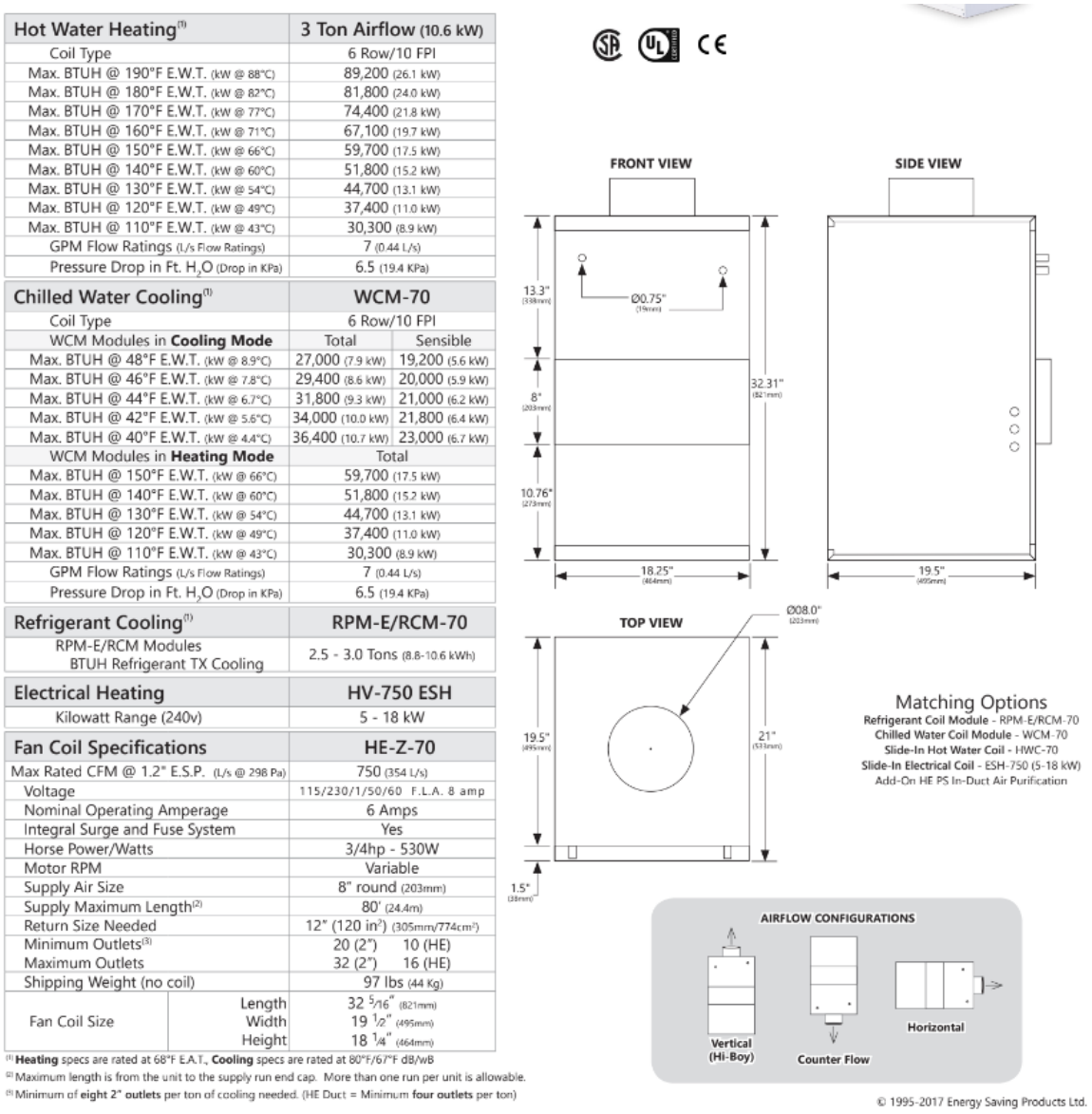

Hot Water Heating[1]	3 Ton Airflow (10.6 kW)	
Coil Type	6 Row/10 FPI	
Max. BTUH @ 190°F E.W.T. (kW @ 88°C)	89,200 (26.1 kW)	
Max. BTUH @ 180°F E.W.T. (kW @ 82°C)	81,800 (24.0 kW)	
Max. BTUH @ 170°F E.W.T. (kW @ 77°C)	74,400 (21.8 kW)	
Max. BTUH @ 160°F E.W.T. (kW @ 71°C)	67,100 (19.7 kW)	
Max. BTUH @ 150°F E.W.T. (kW @ 66°C)	59,700 (17.5 kW)	
Max. BTUH @ 140°F E.W.T. (kW @ 60°C)	51,800 (15.2 kW)	
Max. BTUH @ 130°F E.W.T. (kW @ 54°C)	44,700 (13.1 kW)	
Max. BTUH @ 120°F E.W.T. (kW @ 49°C)	37,400 (11.0 kW)	
Max. BTUH @ 110°F E.W.T. (kW @ 43°C)	30,300 (8.9 kW)	
GPM Flow Ratings (L/s Flow Ratings)	7 (0.44 L/s)	
Pressure Drop in Ft. H_2O (Drop in KPa)	6.5 (19.4 KPa)	
Chilled Water Cooling[1]	**WCM-70**	
Coil Type	6 Row/10 FPI	
WCM Modules in **Cooling Mode**	Total	Sensible
Max. BTUH @ 48°F E.W.T. (kW @ 8.9°C)	27,000 (7.9 kW)	19,200 (5.6 kW)
Max. BTUH @ 46°F E.W.T. (kW @ 7.8°C)	29,400 (8.6 kW)	20,000 (5.9 kW)
Max. BTUH @ 44°F E.W.T. (kW @ 6.7°C)	31,800 (9.3 kW)	21,000 (6.2 kW)
Max. BTUH @ 42°F E.W.T. (kW @ 5.6°C)	34,000 (10.0 kW)	21,800 (6.4 kW)
Max. BTUH @ 40°F E.W.T. (kW @ 4.4°C)	36,400 (10.7 kW)	23,000 (6.7 kW)
WCM Modules in **Heating Mode**	Total	
Max. BTUH @ 150°F E.W.T. (kW @ 66°C)	59,700 (17.5 kW)	
Max. BTUH @ 140°F E.W.T. (kW @ 60°C)	51,800 (15.2 kW)	
Max. BTUH @ 130°F E.W.T. (kW @ 54°C)	44,700 (13.1 kW)	
Max. BTUH @ 120°F E.W.T. (kW @ 49°C)	37,400 (11.0 kW)	
Max. BTUH @ 110°F E.W.T. (kW @ 43°C)	30,300 (8.9 kW)	
GPM Flow Ratings (L/s Flow Ratings)	7 (0.44 L/s)	
Pressure Drop in Ft. H_2O (Drop in KPa)	6.5 (19.4 KPa)	
Refrigerant Cooling[1]	**RPM-E/RCM-70**	
RPM-E/RCM Modules BTUH Refrigerant TX Cooling	2.5 - 3.0 Tons (8.8-10.6 kWh)	
Electrical Heating	**HV-750 ESH**	
Kilowatt Range (240v)	5 - 18 kW	
Fan Coil Specifications	**HE-Z-70**	
Max Rated CFM @ 1.2" E.S.P. (L/s @ 298 Pa)	750 (354 L/s)	
Voltage	115/230/1/50/60 F.L.A. 8 amp	
Nominal Operating Amperage	6 Amps	
Integral Surge and Fuse System	Yes	
Horse Power/Watts	3/4hp - 530W	
Motor RPM	Variable	
Supply Air Size	8" round (203mm)	
Supply Maximum Length[2]	80' (24.4m)	
Return Size Needed	12" (120 in²) (305mm/774cm²)	
Minimum Outlets[3]	20 (2") 10 (HE)	
Maximum Outlets	32 (2") 16 (HE)	
Shipping Weight (no coil)	97 lbs (44 Kg)	
Fan Coil Size — Length	32 5/16" (821mm)	
Fan Coil Size — Width	19 1/2" (495mm)	
Fan Coil Size — Height	18 1/4" (464mm)	

[1] **Heating** specs are rated at 68°F E.A.T., **Cooling** specs are rated at 80°F/67°F dB/wB

[2] Maximum length is from the unit to the supply run end cap. More than one run per unit is allowable.

[3] Minimum of **eight 2" outlets** per ton of cooling needed. (HE Duct = Minimum **four outlets** per ton)

Figure 37. Specification of the air handling unit. ("NCB-E Series Combination Boilers Technical Data Sheet" 2022)

Variable Speed Heat Pump Specifications

System Model	ESP-10		ESP-17	
Outdoor Unit	3 Ton (10.5 kW)		5 Ton (17 kW)	
Capacity Data				
Nominal Cooling Capacity [1) 3)] (Operational Range)	Btu	kW	Btu	kW
	35,500 (6,200-40,900)	10.4 (1.8 - 12.0)	57,300 (6,200-64,800)	16.8 (1.8 - 19)
Nominal Heating Capacity [1) 3)] (Operational Range)	38,200 (6,200-47,700)	11.2 (1.8 - 14.0)	60,400 (6,200-75,000)	17.7 (1.8 - 22)
Air Flow High (l/s)	880		1025	
Air Flow Low (l/s)	200		200	
Electrical Data				
Power Supply	240 Volts - 1 Phase - 50/60 Hz			
Nom. Full Load Amps [2)]	22		30	
Min. Circuit Size (Amps)	25		32	
Electrical Input Cooling (kW) [1)]	3.25		5.3	
Electrical Input Heating (kW) [1)]	3.15		5.2	
ACOP	3.5		3.38	
Sound Pressure (dB) (A) @ 1m	62		63	
Soft Starter	Variable Frequency			
Dimensions				
Outdoor Unit - Length	39" (990 mm)		37" (940 mm)	
Outdoor Unit - Width	14" (356 mm)		15.5" (394 mm)	
Outdoor Unit - Height	38" (965 mm)		54" (1272 mm)	
Outdoor Unit - Weight	155 lbs (70.3 kg)		269 lbs (122 kg)	

NOTES:

1) Capacities are based on A.S.3823.12

2) Full Load Amps taken from Highest Phase

3) Inverter Compressors have the capacity to operate at 40% loading. Capacity modulation is extended by variable indoor airflow. Actual percentage loading will vary depending on application.

DESIGN CONDITIONS:
Cooling 35°C (95°F) DB Outdoor / 27°C (80°F) DB, 19°C (66°F) WB Air Entering Indoor Unit
Heating 7°C (44°F)DB, 6°C (43°F) WB Outdoor/ 21°C (70°F) DB Air Entering Indoor Unit
Operating Range -10°C (14°F) WB to 50°C (122°F) DB
Sound pressure level is influenced by the surrounding, therefore it may vary upon location.

Figure 38. Specification of the heat pump. ("HVS Series Variable speed Heat Pump Brochure," 2022)

HVS-36 Low Temperature Heating Capacities

Indoor Dry Bulb (IDB): 70°F / 21°C Airflow: 750 (250 cfm/Ton) Cooling Coil: RBM-I-70

OD Temp. °F (°C)	BTU/H	Watts	COP
-22 (-30)	8,125	2,485	1.12
-13 (-25)	13,680	2,735	1.26
-4 (-20)	19,080	3,006	1.44
2.3 (-16.5)	20,330	3,167	1.51
5 (-15)	23,580	3,256	1.8
14 (-10)	25,430	3,500	1.98
17 (-8.3)	28,050	3,688	2.1
35 (1.7)	34,440	3,855	2.91
47 (8.3)	36,530	4,035	3.4

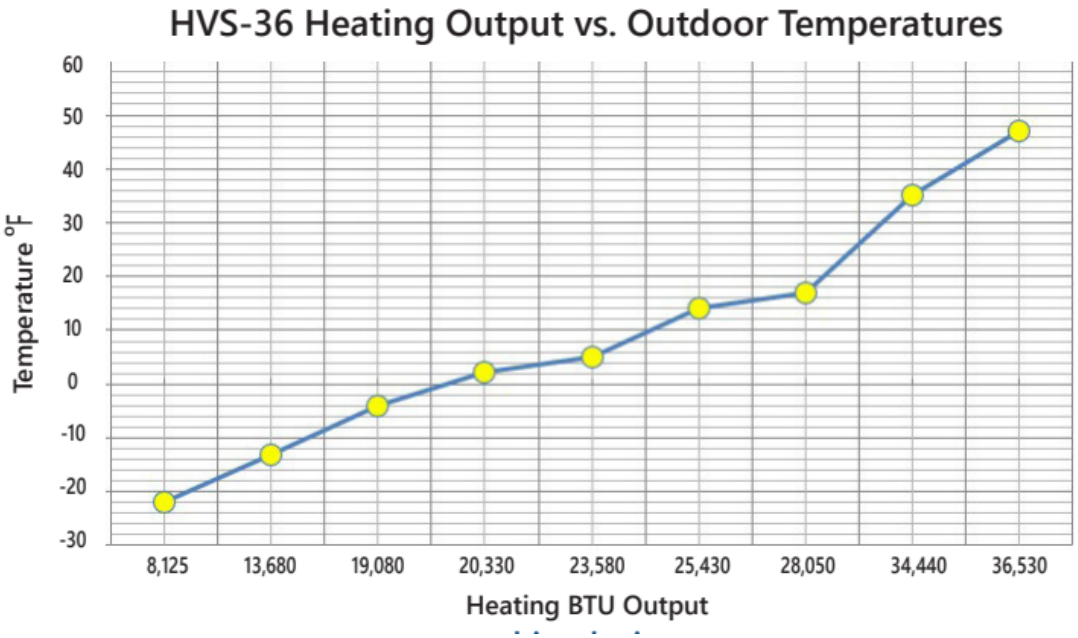

Figure 39. Capacities of the heat pump. ("HVS Series Variable speed Heat Pump Brochure," 2022)

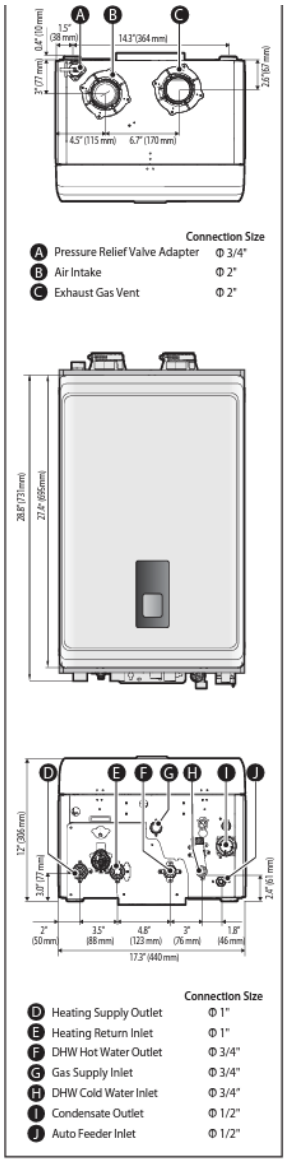

Model Number[1]	Heating Input, MBH		Heating Capacity[2], MBH	Net AHRI Rating, Water[3], MBH	AFUE[2], %	Water Pressure	Water Connection Size (Supply, Return)
	Min	Max					
NCB-150E	12	60	56	49	95.0	12-30 psi	1 in NPT
NCB-180E	14	80	75	65	95.0		
NCB-210E	18	100	94	82	95.0		
NCB-240E	18	120	112	97	95.0		

1 Ratings are the same for Natural Gas models converted to Propane use.
2 Based on U.S. Department of Energy (DOE) test procedures.
3 The NET AHRI Water Ratings shown are based on a piping and pickup allowance of 1.15. Consult Navien before selecting a boiler for installations having unusual piping and pickup requirements, such as intermittent system operation, extensive piping systems, etc.

Specifications

Item		NCB-150E	NCB-180E	NCB-210E	NCB-240E
Gas Input	Space Heating	12,000-60,000 BTU/H	14,000-80,000 BTU/H	18,000-100,000 BTU/H	18,000-120,000 BTU/H
	Domestic Hot Water	12,000-120,000 BTU/H	14,000-150,000 BTU/H	18,000-180,000 BTU/H	18,000-199,900 BTU/H
Flow Rate (DHW)	77°F (43°C) Temp Rise	2.6 GPM (9.8 L/m)	3.4 GPM (12.9 L/m)	4.0 GPM (15.1 L/m)	4.5 GPM (17.0 L/m)
Dimensions		17"(W) x 28"(H) x 12"(D)	17"(W) x 28"(H) x 12"(D)	17"(W) x 28"(H) x 12"(D)	17"(W) x 28"(H) x 12"(D)
Weight		66 lbs (30kg)	74 lbs (34kg)	84 lbs (38kg)	84 lbs (38kg)
Installation Type		Indoor Wall-Hung			
Venting Type		Forced Draft Direct Vent			
Ignition		Electronic Ignition			
Water Pressure (Hydronic/DHW)		12-30 PSI / 15-150 PSI			
Natural Gas Supply Pressure (from source)		3.5"-10.5" WC			
Propane Gas Supply Pressure (from source)		8.0"-13.5" WC			
Natural Gas Manifold Pressure (min-max)		-0.08" WC to -0.34" WC	-0.07" WC to -0.66" WC	-0.05" WC to -0.36" WC	-0.06" WC to -1.2" WC
Propane Gas Manifold Pressure (min-max)		-0.08" WC to -0.30" WC	-0.06" WC to -0.62" WC	-0.1" WC to -0.66" WC	-0.03" WC to -0.98" WC
Minimum Flow Rate (DHW)		0.5 GPM (1.9 L/m)			
Connection Sizes	Heating Supply/Return	1" NPT			
	DHW Inlet/Outlet	3/4" NPT			
	Gas Inlet	3/4" NPT			
	Auto Feeder	1/2" NPT			
	Condensate Outlet	1/2" NPT			
Power Supply	Main Supply	120V AC, 60Hz			
	Maximum Power Consumption	200W (up to 2 amperes)			
Materials	Casing	Cold Rolled Carbon Steel			
	Heat Exchangers	Primary/Secondary Heat Exchanger: Stainless Steel DHW Heat Exchanger: Stainless Steel			
Venting	Exhaust	2" or 3" PVC, CPVC, Approved Polypropylene 2" or 3" Special Gas Vent Type BH (Class II, A/B/C)			
	Intake	2" or 3" PVC, CPVC, Polypropylene 2" or 3" Special Gas Vent Type BH (Class II, A/B/C)			
	Vent Clearances	0" to Combustibles			
Safety Devices	Flame Rod, APS, Gas Valve Operation Detector, Ignition Operation Detector, Water Temperature High Limit Switch, Exhaust Temperature High Limit Sensor				

Figure 40. Specification of the tankless water heater. ("NCB-E Series Combination Boilers Technical Data Sheet," 2022)

Appendix 3 Information of the monitoring devices

This section provides the general information of the monitoring devices, which can be found in Table 17. All the monitoring devices are off the shelf products that can be bought through the PowerWise website.

Table 17. Information of the monitoring devices.

Device	Purpose	Number of devices	Manufacturer	Measurement resolution
Current transformer	Electricity consumption	3	PowerWise	1 A
Gas Meter	Natural gas consumption	1	IMAC System	1 CF
Humidity and temperature sensor	Air humidity and temperature	1	Measurement Specialties	1 %, 1 F
Thermocouple	Air temperature	3	PowerWise	1 F / 1 ˚C
Airflow sensor	Return air flow rate	1	Dwyer	0.01 FPM
BTU meter	Energy consumption	1	ONICON	0.1 kW
SiteSage sPod	Integrate the Modbus sensors with the SiteSage gateway	1	PowerWise	N/A
SiteSage Gateway	Collect, store, and upload data	1	PowerWise	N/A

Appendix 4 Raw Data Examples

This section provides examples of the raw data. Table 18 shows the raw data example of the right unit in minutely interval, and Table 19 shows the raw data ample of the right unit in hourly interval.

Table 18. Monitoring data of the right unit in minutely interval.

Time	Main Power	Heat pump	Mec. Rm	AHU	Voltage	gas meter	Temp garaga heater	Temp after TWH coil	Temp after HP coil	Dewpoint Temp (Td)	RH	Reutrn air Temp	HX inlet flow temperature	HX outlet remote temperature	HX energy rate	TWH heat to AHU Energy Total	volume rate	Return air velocity	Outdoor Temp
2021-11-01 0:00	485	0	85	57	125.2	0	81	76.45	71	43.3	35.5	72.1	51.1	46.8	0	13221.6	0	208.8	
2021-11-01 0:01	485	0	85	57	125.2	0	81	76.45	71	43	35.7	71.4	50.6	46.2	0	13221.6	0	207.2	
2021-11-01 0:02	486	0	86	57	125.3	0	81.1	77.2	71.2	42.9	36.2	70.9	50.1	45.6	0	13221.6	0	214	
2021-11-01 0:03	486	0	86	58	125.4	0	80.9	75.7	70.8	42.3	36	70.5	49.6	45	0	13221.6	0	206.6	
2021-11-01 0:04	487	0	86	59	125.4	0	80.8	74.3	70.5	42	36.4	69.8	49.2	44.4	0	13221.6	0	207	
2021-11-01 0:05	486	0	86	58	125.3	0	80.8	73.5	70.1	41.8	36.5	69.6	48.2	43.2	0	13221.6	0	206.2	
2021-11-01 0:06	441	0	41	58	125.2	0	80.7	72.7	69.9	47.2	45	69.4	47.7	42.7	0	13221.6	0	206	
2021-11-01 0:07	421	0	22	56	125.4	0	80.7	72.3	69.9	47.1	45.2	69.1	47.2	42.1	0	13221.6	0	211.6	
2021-11-01 0:08	422	0	22	56	125.3	0	80.7	71.8	69.9	47	44.9	69.1	46.8	41.6	0	13221.6	0	206.2	
2021-11-01 0:09	387	0	22	23	125.4	0	80.6	71.8	70	43.3	39.1	69.1	46.4	41	0	13221.6	0	0.4	
2021-11-01 0:10	384	0	22	14	125.4	0	80.7	72.1	70.1	43	38.5	69.4	45.5	40.1	0	13221.6	0	0.4	
2021-11-01 0:11	395	0	22	14	125.3	0	80.7	72.3	70.3	42.9	38.2	69.4	45.1	39.6	0	13221.6	0	0.4	
2021-11-01 0:12	389	0	22	14	125	0	80.7	72.5	70.4	42.7	37.9	69.6	44.7	39.2	0	13221.6	0	0.4	-4.4
2021-11-01 0:13	385	0	22	14	125	0	80.6	72.7	70.5	42.7	37.7	69.6	44.3	38.8	0	13221.6	0	0.4	
2021-11-01 0:14	399	0	22	14	125	0	80.6	73	70.6	42.9	37.4	69.8	43.9	38.4	0	13221.6	0	0.4	
2021-11-01 0:15	673	108	163	19	125	0	80.6	73.1	70.7	48.1	45.5	70	46.7	27	8	13221.6	0.7	0.4	
2021-11-01 0:16	2589	1807	240	151	124.7	2	80.5	93.9	72.7	50.9	50.7	70	63.6	55.1	6.8	13221.9	0.7	338.8	
2021-11-01 0:17	2175	1385	235	165	124.8	0	80.6	121.4	80.7	51.6	50.8	70.7	63.5	56.5	5.8	13222	0.7	349.6	
2021-11-01 0:18	2112	1323	234	168	124.8	1	80.7	130.4	85.7	51.7	49.8	71.4	63.9	56.9	5.8	13222.1	0.7	305.4	
2021-11-01 0:19	2205	1423	234	169	124.9	0	80.9	134	88.9	52.6	49.6	72.5	64.5	57.6	5.7	13222.1	0.7	305.8	
2021-11-01 0:20	2228	1454	234	169	125	1	81.1	136.3	91.5	52.7	48.9	73	65.1	58.3	5.6	13222.2	0.7	334.6	
2021-11-01 0:21	2297	1534	225	170	125.1	0	81.2	137.5	93.5	52.3	47.5	73.4	58.6	55.1	2.9	13222.3	0.7	328	
2021-11-01 0:22	2457	1647	224	171	125.1	0	81.3	133	95.6	51.6	45.6	73.9	55.5	52.6	2.4	13222.4	0.7	319.4	
2021-11-01 0:23	1069	371	166	121	125.3	0	81.4	127.5	96.4	49.3	41.7	74.1	53.5	50.7	0	13222.4	0	309.8	
2021-11-01 0:24	430	0	22	13	125.4	0	81.6	124.6	90.7	43.6	33.4	74.1	53.5	50.5	0	13222.4	0	0.4	
2021-11-01 0:25	425	0	22	15	125.5	0	81.5	122.8	87.4	43.5	33.7	73.9	53.3	50.2	0	13222.4	0	0.4	
2021-11-01 0:26	423	0	22	14	125.5	0	81.5	120.5	84.2	43.2	33.3	73.9	52.5	49	0	13222.4	0	0.4	
2021-11-01 0:27	422	0	22	14	125.5	0	81.5	118.4	81.7	42.9	32.8	73.9	51.9	48.3	0	13222.4	0	0.4	
2021-11-01 0:28	422	0	22	14	125.5	0	81.5	116.4	79.9	42.6	32.7	73.6	51.5	47.7	0	13222.4	0	0.4	
2021-11-01 0:29	420	0	22	14	125.5	0	81.4	114.5	78.4	42.4	32.4	73.6	51	47	0	13222.4	0	0.4	
2021-11-01 0:30	421	0	22	14	125.5	0	81.3	112.8	77.2	42.4	32.4	73.6	50.5	46.4	0	13222.4	0	0.4	

Table 19. Monitoring data of the right unit in hourly interval.

Time	Main Power	Heat pump	Mec. Rm	AHU	Voltage	gas meter	Temp garaga heater	Temp after TWH coil	Temp after HP coil	Dewpoint Temp (Td)	RH	Reutrn air Temp	HX inlet flow temperature	HX outlet remote temperature	HX energy rate	TWH heat to AHU Energy Total	volume rate	Return air velocity	Outdoor Temp
2021-11-01 0:00	0.88	0.34	0.106	0.07	125.3	7.24	81.1	101.82	77.56	45.17	38.5	72	52.41	46.92	91.32	793338.57	11.44	158.75	-4.4
2021-11-01 1:00	0.921	0.37	0.108	0.07	125.2	6	81.31	100.88	77.59	44.92	38.3	71.88	52.66	47.59	82.05	793438.77	10.86	155.3	-5
2021-11-01 2:00	1.078	0.5	0.131	0.08	125.1	10	81.55	107.25	79.14	45.33	38.4	72.05	53.95	48.53	144.22	793546.35	16.63	173.91	-5
2021-11-01 3:00	0.94	0.39	0.113	0.07	125.2	7	81.75	104.36	78.92	45.58	38.2	72.7	53.9	48.47	102.42	793658.79	12.88	163.89	-5
2021-11-01 4:00	0.999	0.43	0.12	0.08	125	9	81.75	101.17	77.62	45.33	38.9	71.88	53.5	48.13	137.02	793772.4	14.42	184.7	-5.6
2021-11-01 5:00	1.03	0.46	0.124	0.08	125.2	8	82.06	108.79	80.26	45.8	38	73.1	54.42	49.31	114.74	793893.93	15.2	170.7	-6.1
2021-11-01 6:00	1.391	0.8	0.135	0.08	124.9	9	82.49	113.74	84.27	45.7	38.3	72.83	58.34	51.48	129.14	794016.33	17.31	186.96	-5.6
2021-11-01 7:00	1.157	0.54	0.115	0.07	125.1	7	83.34	104.39	80.54	45.16	37.5	72.79	58.16	50.99	94.73	794124.73	13.65	174.84	-4.4
2021-11-01 8:00	1.189	0.64	0.133	0.08	125.3	8	83.38	113.44	83.5	45.58	37.3	73.44	56.2	50.02	105.07	794234.24	15.41	165.22	-5
2021-11-01 9:00	0.79	0.32	0.114	0.06	125.4	6	82.57	103.57	76.92	43.29	35.6	72.29	52.02	46.63	85.7	794328.52	10.37	141.91	-5
2021-11-01 10:00	0.667	0.1	0.19	0.07	125.6	6	80.13	78.18	67.65	39.66	38.5	65.5	47.68	40.61	75.43	794381.13	7.88	257.74	-3.3
2021-11-01 11:00	0.456	0.06	0.061	0.04	125.3	1	80.15	81.94	72.62	42.47	36.2	70.57	43.73	38.41	12.35	794457.01	2.15	108.3	-1.7
2021-11-01 12:00	0.651	0.17	0.131	0.06	125.1	3	78.56	83.75	72.91	42.1	38.5	68.46	43.65	38.49	54.77	794491.17	5.84	198.13	1.1
2021-11-01 13:00	0.487	0.09	0.077	0.04	124.8	4	76.57	72.13	69.6	41.11	37.8	67.76	33.37	28.89	30.49	794506.05	2.92	104.93	3.3
2021-11-01 14:00	0.959	0.26	0.091	0.05	124.8	3	77.81	92.3	77.26	43.61	36.7	71.54	46.96	42.34	56.09	794556.39	7.19	119.66	5
2021-11-01 15:00	1.401	0	0.05	0.04	125	0	78.01	72.42	70.45	42.37	37.2	69.55	38.18	33.41	0	794589.55	0	102.47	5.6
2021-11-01 16:00	1.418	0	0.05	0.04	125.1	0	75.28	69.96	69.28	42.23	38.9	68.1	27.76	24.79	0	794589.55	0	101.15	5.6
2021-11-01 17:00	1.624	0.18	0.078	0.05	124.7	5	74.48	80.44	72.48	43.58	40	68.94	37.54	34.15	46.01	794608.18	5.07	125.16	4.4
2021-11-01 18:00	1.692	0.19	0.079	0.05	124.5	3	76.71	80.84	73.03	42.12	37.1	69.53	43.1	37.77	40.7	794650.61	5.35	112.85	2.8
2021-11-01 19:00	1.69	0.17	0.079	0.05	124.7	4	77.73	81.87	73.15	43.38	38.7	69.68	45.94	40.45	52.17	794703.63	5.74	135.43	1.1
2021-11-01 20:00	0.766	0.33	0.104	0.07	125	7	78.55	97.82	76.25	44.07	38.5	70.46	49.91	44.27	88.89	794766.86	10.79	150.98	0
2021-11-01 21:00	0.683	0.27	0.093	0.06	124.9	6	79.57	88.59	75.22	43.78	38.3	70.45	50.04	42.99	78.29	794848.36	9.33	148.47	-0.6
2021-11-01 22:00	0.899	0.47	0.099	0.07	125.4	4	80.67	99.22	80.55	44.31	37.2	71.98	53.31	47.54	67.54	794936.6	9.56	155.99	-1.1
2021-11-01 23:00	0.93	0.46	0.124	0.07	124.9	9	81.58	108.39	80.03	44.41	37.5	71.99	55.97	48.03	113.66	795021.97	14.94	161.97	-2.2
2021-11-02 0:00	0.908	0.45	0.122	0.08	124.7	6.2	81.76	106.97	80.18	45.47	37.8	72.88	53.75	49.06	91.03	795126.74	13.6	166.59	-2.2
2021-11-02 1:00	0.813	0.37	0.108	0.07	125	7	81.55	100.81	78.13	44.63	37.6	72.09	51.99	47.02	89	795227.34	12.11	157.25	-2.8
2021-11-02 2:00	0.993	0.51	0.133	0.08	125	10	81.73	108.76	79.24	44.89	38	72.18	54.73	49.17	140.74	795338.09	17.33	177.69	-3.3
2021-11-02 3:00	0.938	0.49	0.115	0.07	125.1	7	81.98	105.79	80.06	45.23	37.3	73	55.42	49.65	88.49	795455.04	11.63	157.32	-4.4
2021-11-02 4:00	1.148	0.66	0.134	0.09	125.3	9	82.39	107.67	81.45	45.45	38.6	72.33	56.61	50.15	129.74	795565.2	17.28	192.28	-5
2021-11-02 5:00	0.943	0.5	0.111	0.07	125	6	82.61	104.26	79.74	45.06	37.2	72.81	55.32	49.22	82.85	795680.51	12.14	171.04	-5.6
2021-11-02 6:00	1.315	0.79	0.163	0.1	124.7	12	83.19	120.14	83.82	46.18	38.1	73.54	59.36	52.08	166.55	795822.6	22.18	198.06	-5.6
2021-11-02 7:00	1.241	0.78	0.119	0.08	124.7	8	83.16	104.48	83.34	45.89	37.8	73.32	55.73	50.88	100.88	795940.14	13.72	186.27	-6.7
2021-11-02 8:00	1.193	0.74	0.129	0.09	125.1	8	83.12	108.31	83.68	44.99	36.9	72.83	55.03	49.88	120.26	796058.61	16.63	186.16	-6.7
2021-11-02 9:00	0.621	0.28	0.098	0.06	125.1	6	82.61	98.65	77.01	44.82	37.6	72.26	52.35	46.91	65.29	796161.91	8.71	150.57	-6.7
2021-11-02 10:00	0.472	0.17	0.079	0.05	125.4	4	80.49	81.65	72.27	43.9	39.5	69.65	46.46	40.47	53.07	796209.84	5.77	139.59	-5.6

Appendix 5 Data Availability Timeline

Figure 41 shows the data availability timeline.

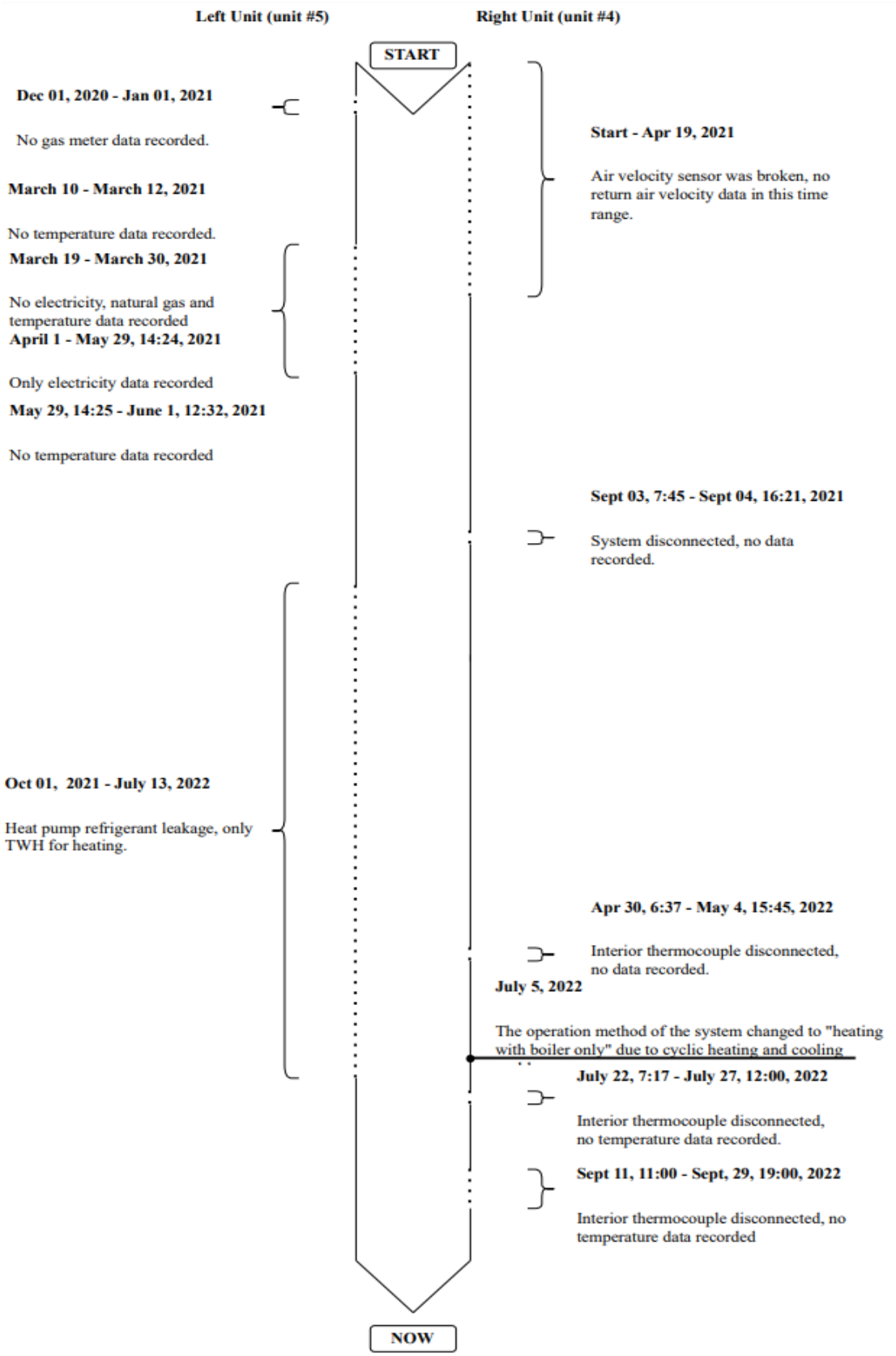

Figure 41. Data availability timeline.

Appendix 6 Programming codes

This section contains examples of the MATLAB codes.

Appendix 6.1 Data interpolation and replacement

Import the data file

```
clear all
data1 = readtable('LP5_20210101_20210116.csv');
data2 = readtable('LP5_20210117_20210131.csv');
data1 = data1(7:end,:);
data2 = data2(7:end,:);
data = [data1;data2];
```

Use linear interpolation to interpolate the hourly exterior temperature into minutely temperature.

```
Tempext = data.(15);
Time = data.(1);


ismissing = isnan(Tempext);
Tempext2 = interp1(Time(~ismissing),Tempext(~ismissing), Time);
data.(15)=Tempext2;
```

Replace NaN using a Moving median with a window of length 5.

```
[numRows1, numCols1] = size(data);


for i = 2 : numCols1-1
    F = fillmissing(data.(i),'movmedian',5);
    data.(i) = F;
end
```

Appendix 6.2 Data filtering and analyzation (Heat pump performance)

Pseudo code for filter out the data to determine the system performance of using heat pump:

If HP is working, and working in a "steady state":

(HP power is not ZERO) & (The power consumption of heat pump in next minute – the power consumption of heat pump in this minute <=5) & (temperature between HX – temperature of return air >=5)

And the supply air temperature is in a constant value:

(Temperature between HX in next minute – temperature between HX in this minute <=0.5)

The MATLAB code can be seen as below:

```
k=1;
m=1;

for i = 1:num_files
    [numRows, numCols] = size(LP4Table.(fldNum(Sookoor et al.)));


     for j = 1 : numRows-1

        if LP4Table.(fldNum{i}.(3)(j) ~= 0 && isnumeric(LP4Table.(fldNum{i}).(10)(j))
            if abs(LP4Table.(fldNum{i}).(3)(j+1) - (LP4Table.(fldNum{i}).(3)(j))) <=
5....
               && abs(LP4Table.(fldNum{i}).(10)(j+1) -
(LP4Table.(fldNum{i}).(10)(j))) <= 0.5....
               && abs(LP4Table.(fldNum{i}).(10)(j) -
(LP4Table.(fldNum{i}).(13)(j))) >=5


                refinedata(k,:)= LP4Table.(fldNum{i})(j+1,:);
                k=k+1;
            end
        end

    end
end
```

The following codes contain the calculation of the heating performance of the system, plotting the diagram, and creating the box plot, is also contain the cooling performance calculation, but this part does not include in this thesis, it may be useful for future analyzation.

```
%% Anayze filtered data

% sort the data file by air velocity
 SortVeldata = sortrows(refinedata,19);

% initial varaibles
Time= SortVeldata{:,1};
Temp_ext=SortVeldata{:,20}; % Exterior temperature
Touthp=((SortVeldata{:,10})-32)*(5/9); % Degreee celsius.
Tinhp=((SortVeldata{:,13})-32)*(5/9); % Degreee celsius.
Whp=(SortVeldata{:,3})*60; % Power consumption of HP  (J/min)
vair=SortVeldata{:,19};  % Air velocity FPM

% Variables assumed constant
rhoair=1.225; % density of air
Cpc=1.02;  % specific heat of air (constant) kJ/kg*K


% Determine Qheat & COP
% Volume flow rate - CFM to m^3/min
% LP4 RH 20” x 10”
Vdot = (25/12)*(9.5/12)*vair*0.0283168; % m^3/min
mdot = Vdot*rhoair;  % Air mass flow rate kg/min.
DT = Touthp-Tinhp; % Temperture difference.
Qheat = 1000*mdot.*DT*Cpc;  % J/min
COP = abs(Qheat)./Whp;
SortVeldata{:,21} = Qheat;
SortVeldata{:,22} = COP;

% Create struct
HeatCool.Heat=table();
HeatCool.Cool=table();


% Step counters
Heatcount=1;
Coolcount=1;

 [numRows2, numCols2] = size(SortVeldata);
 for n=1:numRows2

     if SortVeldata{n,21} > 0 % if Qheat > 0, the system is heating up
         HeatCool.Heat(Heatcount,:) = SortVeldata(n,:);
         Heatcount=Heatcount+1;

     elseif SortVeldata{n,21} < 0 % the system is cooling down
```

```
          HeatCool.Cool(Coolcount,:) = SortVeldata(n,:);
          Coolcount=Coolcount+1;

      end

 end

%screening the unfavorable, outliers, and repeating data (by hand)
writetable(HeatCool.Heat,'LP4heatCOP.csv');
writetable(HeatCool.Cool,'LP4coolCOP.csv');


%% New section after organized the data file for Heat pump
%re-input the orginized data file and plot the result.
HeatCOPtable = readtable('LP4heatCOP.csv');
CoolCOPtable = readtable('LP4coolCOP.csv');

figure
plot(CoolCOPtable.(20),CoolCOPtable.(22),'.')
xlabel('Exterior Temperature, C')
ylabel('Cooling CoP of HP')
legend('Cooling COP')
set(gcf,'color','w')


figure
plot(HeatCOPtable.(20),HeatCOPtable.(22),'r.')
xlabel('Exterior Temperature, C')
ylabel('Heating CoP of HP')
ylim([0 7])
legend('Heating COP')
set(gcf,'color','w')

%% New section for outlier detection
%re-input the orginized data file and plot the result.
HeatCOPtable = readtable('LP4heatCOP.csv');

% sort the data file by air velocity
HeatCOPtable = sortrows(HeatCOPtable,20);

[numRows, numCols] = size(HeatCOPtable);

tempCount = 1;
copCount = 1;
boxtable = table([HeatCOPtable.(20)(1) ; HeatCOPtable.(22)(1)]);

for i = 2 : numRows
    if HeatCOPtable.(20)(i) ~= HeatCOPtable.(20)(i-1)
        if copCount > 4
            tempCount = tempCount + 1;
        end

        boxtable.(tempCount)(1) = HeatCOPtable.(20)(i);
        boxtable.(tempCount)(2) = HeatCOPtable.(22)(i);
```

```
        copCount = 1;
    else
        copCount = copCount + 1;
        boxtable.(tempCount)(1 + copCount) = HeatCOPtable.(22)(i);
    end
end
% replace 0s by NaN
boxtable{2 : height(boxtable), : }(boxtable{2 : height(boxtable), :} == 0) = NaN;

% check last column
if sum(boxtable.(width(boxtable)) > 0) < 5
    boxtable(:, width(boxtable)) = [];
end

figure
for i = 1 : width(boxtable)
    y = boxtable{2 : height(boxtable), i}';
    x = zeros(width(y), 1);
    x(:) = boxtable.(i)(1);
    boxchart(x, y,'BoxFaceColor','blue');
    hold on
end
xlabel('Exterior temperature, C')
ylabel('System heating COP')
set(gcf,'color','w')
hold off
```

Appendix 6.3 Data filtering and analyzation (TWH performance)

The algorithm to filter out the data for determining the system performance of using natural gas in the right unit (with BTU meter):

(Keep the data if BTU meter reading is not ZERO && the supply air temperature increases 5 degree)

The MATLAB codes can be seen as follow:

```
count = 2;
while count <= numRows1

    if data{count,18} > 0 && data{count, 9} - data{count-1, 9} >= 5
        while(data{count,18}>0)
            count = count + 1;
        end

     else
         data{count, 7} = 0;
         data{count, 19} = 0;
         count = count + 1;

    end
end
```

Analyse the system performance while using TWH:

Determine the natural gas consumption and space heating load for TWH

```
% add up the minutely ng data into hourly data
for i = 1:60:numRows1
    k = 1+((i-1)/60);
    data{k,21} = sum(data{i:i+59,7})*1.06; % MJ
end

% Variables assumed constant
rhoair=1.225; % density of air (kg/m^3)
Cpc=1.02;  % specific heat of air (constant) kJ/kg*K


ToutTWH= ((data{:,9})-32)*(5/9); % Degreee celsius.
TinTWH = ((data{:,10})-32)*(5/9); % Degreee celsius.
```

```
vairTWH = data{:,14};  % Air velocity FPM
VdotTWH = (25/12)*(9.5/12)*vairTWH*0.0283168; %m^3/min
mdotTWH = VdotTWH*rhoair;  % Air mass flow rate kg/min.
DTTWH = ToutTWH-TinTWH; % Temperture difference.
QTWH = mdotTWH.*DTTWH*Cpc;  % kJ/min
sumTWH = sum(QTWH)/(10^3) % MJ
```

Calculate the result

```
NGheating = sum(data.(7))*1.06 %MJ
DHW = Totalng-NGheating
```

Appendix 6.4 Training the ANN model.

Following shows the MALTBA code as an example of training the ANN model.

Import the filtered data for training

```
clear all
data = readmatrix('trainingfile2.xlsx');
x = data(:,[2,5]);
y = data(:,[3,4]);
m = data(:,1);
len = length(y);
```

x: input

Hourly heating load of the house @colum2 MJ

Exterior air temperature @colum5 C degree

y:output

1 Natural gas consumption @colum3 MJ

2 Electricity consumption of the heat pump @colum4 MJ

Normalize the features and transform the output

```
y2(:,1) = y(:,1);
y2(:,2) = log(1+y(:,2));

for i=1:2
   x2(:,i) = (x(:,i)-min(x(:,i)))/(max(x(:,i))-min(x(:,i)));
end
xt = x2';
yt = y2';
```

Train an artificial neural network (ANN) and record the performance of the ANN network

```
xt = x2';
yt = y2';
for i = 1:10
    hiddenLayerSize = 6;
    net = fitnet(hiddenLayerSize);
    net.divideParam.trainRatio = 70/100;
    net.divideParam.valRatio = 30/100;
    net.divideParam.testRatio = 0/100;
    [net, tr] = train(net, xt, yt);

    yTrain = net(xt(:,tr.trainInd));
    yTrain(2,:) = exp(yTrain(2,:))-1;

    yTrainTrue = yt(:,tr.trainInd);
    yTrainTrue(2,:) =exp(yTrainTrue(2,:))-1;

    rmse_trainop1(i) = sqrt(mean((yTrain(1,:)-yTrainTrue(1,:)).^2));
    rmse_trainop2(i) = sqrt(mean((yTrain(2,:)-yTrainTrue(2,:)).^2));
    cv_trainop1(i) = sqrt(mean((yTrain(1,:)-
yTrainTrue(1,:)).^2))/mean(yTrainTrue(1,:));
    cv_trainop2(i) = sqrt(mean((yTrain(2,:)-
yTrainTrue(2,:)).^2))/mean(yTrainTrue(2,:));

    yVal = net(xt(:,tr.valInd));
    yVal(2,:) = exp(yVal(2,:))-1;

    yValTrue = yt(:,tr.valInd);
    yValTrue(2,:) =exp(yValTrue(2,:))-1;

    rmse_valop1(i) = sqrt(mean((yVal(1,:) - yValTrue(1,:)).^2));
    rmse_valop2(i) = sqrt(mean((yVal(2,:) - yValTrue(2,:)).^2));
    cv_valop1(i) = sqrt(mean((yVal(1,:) -
yValTrue(1,:)).^2))/mean(yValTrue(1,:));
    cv_valop2(i) = sqrt(mean((yVal(2,:) -
yValTrue(2,:)).^2))/mean(yValTrue(2,:));

    filename = ['qunet',num2str(i)];
    save(filename,'net')
    trname = ['qutr',num2str(i)];
    save(trname,'tr')

end
```

Optimize the number of neurons in the hidden layer

```
xt = x2';
yt = y2';


for k = 1 : 10
    for i = 1:60
        % Defining the architecture of the ANN
        hiddenLayerSize=i;
        net = fitnet(hiddenLayerSize);
        net.divideParam.trainRatio = 70/100;
        net.divideParam.valRatio = 30/100;
        net.divideParam.testRatio = 0/100;

        %Training the ANN
        [net, tr] = train(net, xt, yt);

        % determine the error of the ANN
        yTrain = net(xt(:,tr.trainInd));
        yTrain(2,:) = exp(yTrain(2,:))-1;

        yTrainTrue = yt(:,tr.trainInd);
        yTrainTrue(2,:) =exp(yTrainTrue(2,:))-1;

        rmse_train1(k,i) = sqrt(mean((yTrain(1,:)-yTrainTrue(1,:)).^2));
        rmse_train2(k,i) = sqrt(mean((yTrain(2,:)-yTrainTrue(2,:)).^2)); %RMSE of
training set
        mse_train1(k,i) = mean((yTrain(1,:)-yTrainTrue(1,:)).^2);
        mse_train2(k,i) = mean((yTrain(2,:)-yTrainTrue(2,:)).^2);% MSE of
training set

        yVal = net(xt(:,tr.valInd));
        yVal(2,:) = exp(yVal(2,:))-1;

        yValTrue = yt(:,tr.valInd);
        yValTrue(2,:) =exp(yValTrue(2,:))-1;

        rmse_val1(k,i) = sqrt(mean((yVal(1,:) - yValTrue(1,:)).^2));
        rmse_val2(k,i) = sqrt(mean((yVal(2,:) - yValTrue(2,:)).^2)); %RMSE of
validation set
        mse_val1(k,i) = mean((yVal(1,:) - yValTrue(1,:)).^2);
        mse_val2(k,i) = mean((yVal(2,:) - yValTrue(2,:)).^2);% MSE of validation
set
    end
end

mse_train1_ave = mean(mse_train1,1);
mse_train2_ave = mean(mse_train2,1);
mse_val1_ave = mean(mse_val1,1);
```

```
mse_val2_ave = mean(mse_val2,1);
plot(1:60,mse_train1_ave); hold on;
plot(1:60,mse_val1_ave);
legend('Natural gas training','Natural gas validation')
xlabel('Number of nuerons')
ylabel('MSE'); hold off;
ylim([0 20])


plot(1:60,mse_train2_ave);hold on;
plot(1:60,mse_val2_ave);
legend('Electricity training','Electricity validation')
xlabel('Number of nuerons')
ylabel('MSE'); hold off;
ylim([0 2])
```